NAVAL POSTGRADUATE SCHOOL

MONTEREY, CALIFORNIA

THESIS

INTERANNUAL VARIATIONS IN ARCTIC WINTER TEMPERATURE: THE ROLE OF GLOBAL SCALE TELECONNECTIONS

by

Kathryn A. Parrish

June 2015

Thesis Advisor:	Tom Murphree
Co-Advisor:	David Meyer

Approved for public release, distribution is unlimited

THIS PAGE INTENTIONALLY LEFT BLANK

REPORT DOCUMENTATION PAGE

Form Approved OMB No. 0704-0188

1. AGENCY USE ONLY ***(Leave blank)***	**2. REPORT DATE** June 2015	**3. REPORT TYPE AND DATES COVERED** Master's Thesis

4. TITLE AND SUBTITLE
INTERANNUAL VARIATIONS IN ARCTIC WINTER TEMPERATURE: THE ROLE OF GLOBAL SCALE TELECONNECTIONS

5. FUNDING NUMBERS

6. AUTHOR(S) Kathryn A. Parrish

7. PERFORMING ORGANIZATION NAME(S) AND ADDRESS(ES)
Naval Postgraduate School
Monterey, CA 93943-5000

8. PERFORMING ORGANIZATION REPORT NUMBER

9. SPONSORING /MONITORING AGENCY NAME(S) AND ADDRESS(ES)
N/A

10. SPONSORING/MONITORING AGENCY REPORT NUMBER

11. SUPPLEMENTARY NOTES The views expressed in this thesis are those of the author and do not reflect the official policy or position of the Department of Defense or the U.S. Government. IRB Protocol number ____N/A____.

12a. DISTRIBUTION / AVAILABILITY STATEMENT
Approved for public release, distribution is unlimited

12b. DISTRIBUTION CODE

13. ABSTRACT (maximum 200 words)

To skillfully predict Arctic climate, one must fully understand the conditions influencing Arctic climate on intraseasonal, interannual, and multi-decadal time scales. This study aims to improve climate support to U.S. military operations in the Arctic by exploring the interannual variations in Arctic temperature during the winter. We have found statistically significant and dynamically plausible mechanisms for the variation in January-March (JFM) 850 hectoPascal (hPa) Arctic air temperature (T850, °C). We used JFM Arctic T850 data for 1970–2014 to analyze the associated global scale processes from 75N–90N via time series, composite, correlation, and teleconnection analyses. The patterns and teleconnections revealed in these analyses closely resembled those that have been associated with El Niño-La Niña (ENLN). Correlations between JFM Arctic T850 and ENLN, via the Multivariate El Niño-Southern Oscillation Index (MEI), were statistically significant at lead times of zero to ten months, and showed that the MEI may be a good predictor of JFM Arctic T850. These results indicate a significant potential for the improvement of long-range climate support for U.S. Navy operations in the Arctic.

14. SUBJECT TERMS
Arctic climate, climate system, climate variability, interannual, teleconnection, El Nino-La-Nina, Arctic Oscillation, Pacific-North American, Madden-Julian Oscillation, polar vortex, dynamic warming

15. NUMBER OF PAGES
135

16. PRICE CODE

17. SECURITY CLASSIFICATION OF REPORT	**18. SECURITY CLASSIFICATION OF THIS PAGE**	**19. SECURITY CLASSIFICATION OF ABSTRACT**	**20. LIMITATION OF ABSTRACT**
Unclassified	Unclassified	Unclassified	UU

NSN 7540-01-280-5500

Standard Form 298 (Rev. 2-89)
Prescribed by ANSI Std. 239-18

THIS PAGE INTENTIONALLY LEFT BLANK

Approved for public release, distribution is unlimited

INTERANNUAL VARIATIONS IN ARCTIC WINTER TEMPERATURE: THE ROLE OF GLOBAL SCALE TELECONNECTIONS

Kathryn A. Parrish
Lieutenant, United States Navy
B.S., The Ohio State University, 2006

Submitted in partial fulfillment of the
requirements for the degree of

MASTER OF SCIENCE IN METEOROLOGY

from the

NAVAL POSTGRADUATE SCHOOL
June 2015

Author: Kathryn A. Parrish

Approved by: Tom Murphree
Thesis Advisor

David Meyer
Co-Advisor

Wendell Nuss
Chair, Department of Meteorology

THIS PAGE INTENTIONALLY LEFT BLANK

ABSTRACT

To skillfully predict Arctic climate, one must fully understand the conditions influencing Arctic climate on intraseasonal, interannual, and multi-decadal time scales. This study aims to improve climate support to U.S. military operations in the Arctic by exploring the interannual variations in Arctic temperature during the winter. We have found statistically significant and dynamically plausible mechanisms for the variation in January-March (JFM) 850 hectoPascal (hPa) Arctic air temperature (T850, °C). We used JFM Arctic T850 data for 1970–2014 to analyze the associated global scale processes from 75N–90N via time series, composite, correlation, and teleconnection analyses. The patterns and teleconnections revealed in these analyses closely resembled those that have been associated with El Niño-La Niña (ENLN). Correlations between JFM Arctic T850 and ENLN, via the Multivariate El Niño-Southern Oscillation Index (MEI), were statistically significant at lead times of zero to ten months, and showed that the MEI may be a good predictor of JFM Arctic T850. These results indicate a significant potential for the improvement of long-range climate support for U.S. Navy operations in the Arctic.

THIS PAGE INTENTIONALLY LEFT BLANK

TABLE OF CONTENTS

THIS PAGE INTENTIONALLY LEFT BLANK

LIST OF FIGURES

LIST OF TABLES

LIST OF ACRONYMS AND ABBREVIATIONS

AAO	Antarctic Oscillation
AMJ	April-June
AMS	American Meteorology Society
AN	above normal
AO	Arctic Oscillation
AOI	Arctic Oscillation Index
ASO	August-October
BN	below normal
BonD	Battlespace on Demand
CFSR	Climate Forecast System Reanalysis
CNMOC	Commander Naval Meteorology Oceanography Command
COADS	Comprehensive Ocean Atmospheric Data Set
DJF	December-February
ECMWF	European Centre for Medium-Range Weather Forecasting
EN	El Niño
ENLN	El Niño-La Niña
ENSO	El Niño-Southern Oscillation
ERA-40	Re-Analysis
ESRL	Earth Systems Research Laboratory
FMA	February-April
GCC	Global Climate Change
GPH	geopotential height
hPa	hectoPascal
IR	infrared radiative
JAS	July-September
JFM	January February March
JJA	June-August
LN	La Niña
LRF	long-range forecast
LTM	long-term mean

m	meters
MAM	March-May
MEI	Multivariate El Niño-Southern Oscillation Index
MJJ	May-July
MJO	Madden-Julian Oscillation
NCAR	National Center for Atmospheric Research
NCEP	National Centers for Environmental Prediction
NDJ	November-January
NH	Northern Hemisphere
NN	near normal
NOAA	National Oceanic and Atmospheric Administration
OLR	outgoing longwave radiation
OND	October-December
PNA	Pacific-North American
R1	reanalysis
SAF	surface ice-snow albedo feedback
SAT	surface air temperature
SON	September-November
SSI	spectral statistical interpolation
SSM/I	Special Sensing Microwave/Imager
SST	sea surface or surface skin temperature
T	temperature
U	zonal wind
TEAM	Tropically Excited Arctic Warming Mechanism
Z	geopotential height

ACKNOWLEDGMENTS

I would like to thank my family and friends, especially Ben and Michael, for supporting me throughout my time at the Naval Postgraduate School.

I would also like to acknowledge the NPS faculty, and of course my advisors, Dr. Tom Murphree and Mr. David Meyer, for their expertise and guidance throughout this process.

THIS PAGE INTENTIONALLY LEFT BLANK

I. INTRODUCTION

A. BACKGROUND AND MOTIVATION

The 2014–2030 United States (U.S.) Navy Arctic Roadmap was based on the findings of several revised strategic guidance documents, such as The National Strategy for the Arctic Region, and The Department of Defense Arctic Strategy (U.S. Navy 2014). With such high level national interest geared towards preparing the U.S. military for operations in the Arctic region, the Arctic Roadmap provides the Navy with direction on how to move forward with these preparations. The Arctic Roadmap predicts that in the near-term (present–2020), the demand for additional naval involvement in the Arctic will be low, as the Navy's current capabilities are sufficient in meeting its operational needs (U.S. Navy 2014). In the mid-term (2020–2030), the Arctic Roadmap predicts that the Navy will provide support to Combatant Commanders and U.S. government agencies, and in the far-term (beyond 2030) the Navy may be required to provide routine Arctic support as periods of ice-free conditions increase (U.S. Navy 2014).

Though the Roadmap predicts the Arctic to remain a region of low threat during the near-term, the U.S. has many homeland security-related interests in the Arctic that will persist (U.S. Navy 2014). Arctic warming and the reduction of multi-year sea ice in the Arctic are expected to continue over future decades, and may soon afford the U.S. Navy new opportunities to navigate and operate in the Arctic (U.S. Navy 2014). Predicting Arctic sea ice concentration (SIC) and sea ice extent (SIE), for the purposes of safe operations and navigation, has become crucial to the Navy's mid-term planning period. In order to accurately predict Arctic SIC and SIE, and to plan for future operations in the Arctic region, we need to better understand the Arctic environment and how its climate varies on intraseasonal, interannual, and multi-decadal time scales.

Arctic climate has far-reaching effects around the globe, and the climates of other regions can also alter Arctic climate on varying time scales. A National

Research Council (NRC) publication has explored new and exciting research topics concerning Arctic climate. One of these topics suggests that there is much to be learned about how natural climate variations (e.g., El Niño-Southern Oscillation (ENSO)) and other large scale climate patterns interact with the thermodynamic and dynamic effects of the Arctic (NRC 2014). This topic has gained significant interest in recent years, as rapid Arctic warming has become a new driver in the ocean-atmosphere system (NRC 2014). The NRC also highlights that the changes observed in Arctic climate can rapidly affect multiple interconnected areas within the Arctic and around the globe (NRC 2014). These cause and effect relationships are also known as a teleconnections. When trying to understand or predict changes in Arctic climate (or climate elsewhere), it is imperative to observe global conditions in the ocean-atmosphere system, throughout all seasons. In doing so, teleconnections may be revealed that help to explain how changes in Arctic climate came to be. If we become confident in our understanding of how these changes occur, it may be possible to better predict the timing of these changes.

The purpose of this study is to shed light on the teleconnections affecting winter Arctic climate. In doing so, we have exposed the potential for different oceanic and atmospheric variables, and known modes of climate variability to be used as predictors of interannual variations in Arctic winter temperature. Our study is in line with the objectives put forth in the Arctic Roadmap, and attempts to improve the long-range planning of U.S. Navy operations in the Arctic through an increased understanding of the factors influencing Arctic climate.

The Commander, Naval Meteorology and Oceanography Command (CNMOC) Battlespace on Demand (BonD) concept was developed to describe the concept of operations for providing environmental support to warfighters at short lead times (e.g., 0 to 72 hours). The BonD concept also applies to climate science based long-range support, as highlighted Figure 1. There are four tiers of the BonD concept that explain the flow of environmental data, from collection to warfighter decision-making. Tier zero represents data collection and the

utilization of advanced long-term high-resolution data sets. Our study fits between tier zero and tier one, where the collected data is used for advanced long-lead environmental prediction. At tier two, the information from tiers zero and one is synthesized into advanced long-lead performance surface maps that show how the predicted environment could affect military operations. Finally, advanced long-lead decision support is provided to warfighter decision-makers at tier three, to assist them in making the best operational decisions while mitigating risks to personnel and equipment. Our study analyzed the advanced long-term high-resolution data sets of tier zero in an attempt to uncover teleconnections affecting the interannual variations in Arctic winter temperature. The results of this study, together with further research, may be useful in tiers one through three of the BonD concept.

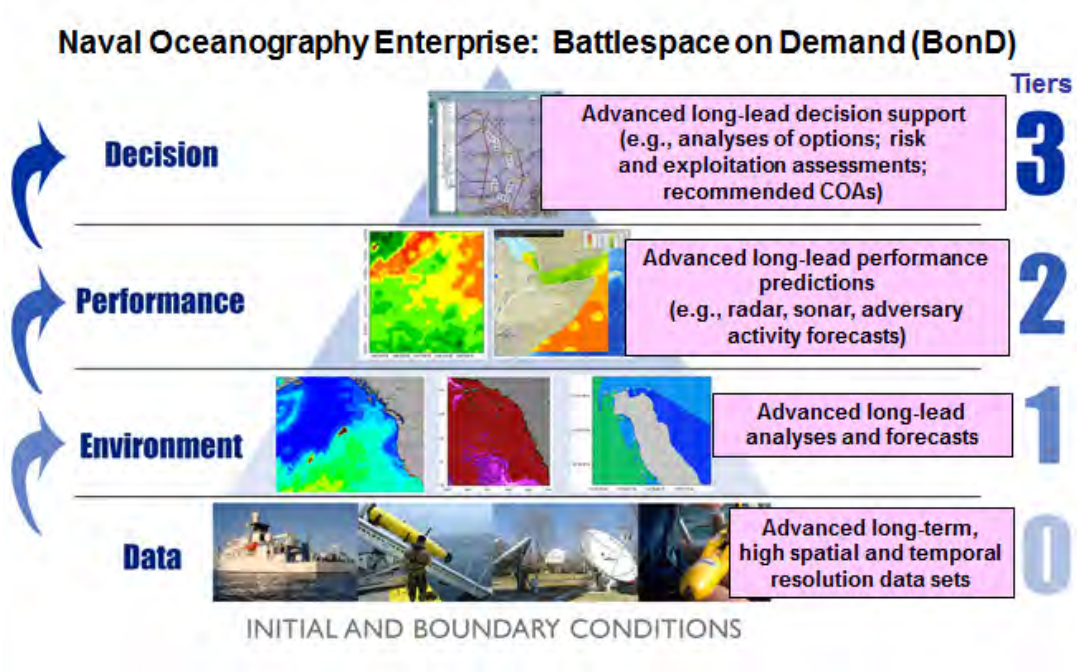

Figure 1. Schematic of the BonD concept of operations developed by CNMOC. Pink boxes indicate the integration of climate science based long-range support for each of the four BonD tiers. Our study fits between tiers zero and one of this concept. Figure adapted from White (2012) for long-range climate support.

B. PRIOR WORK

A number of prior studies have shown that an increased understanding of the climate system can improve climate support for the U.S. Navy (e.g., Stepanek 2006; DeHart 2011). These studies focused on a wide range of predictor-predictand relationships across various regions of the globe. Other studies have focused on the Arctic region in particular (e.g., Stone 2010, Lee 2011a), some of which have investigated the predictor-predictand relationships between known modes of climate variability and Arctic climate, and have shown that lower latitude variations can drive Arctic climate variations. Some of these modes of climate variability have included the El Niño-La Niña (ENLN) the Madden-Julian Oscillation (MJO), the Arctic Oscillation (AO), and the Pacific-North American (PNA) pattern. In light of increased Arctic warming trends, new research has been conducted to uncover the relationships between these trends and midlatitude climate, and the mechanisms behind those relationships (e.g., Francis and Vavrus 2012). These studies have shown that Arctic variations can drive midlatitude variations. The ideas presented in each of these studies have motivated our research.

1. Intraseasonal to Interannual Arctic Climate Variations Can Be Driven by Lower Latitude Variations

A study by Lee et al. (2011b) presented mechanisms for Arctic warming that occurred between the periods of 1958–1977 and 1982–2001. While their study concurs with the generally accepted view that extratropical baroclinic eddies are a main contributor of poleward heat transport, they also present observational evidence that horizontal temperature advection and adiabatic warming (dynamic warming) associated with stationary Rossby (low-frequency, planetary) waves can play an important role in winter Arctic warming (Lee et al. 2011a).

The Lee et al. (2011b) study used the European Centre for Medium-Range Weather Forecasts (ECMWF) Re-Analysis (ERA-40) reanalysis data, and

found that the winter surface warming over the ice-covered Arctic Ocean was due in part to dynamic warming. Downward infrared radiative (IR) flux was found to dominate the warming over ice-free portions of the Arctic Ocean. Through an analysis of the 250 hectoPascal (hPa) flow and tropical convective precipitation, with tropical convective precipitation leading 250 hPa flow by five days, they noticed a decreasing trend in the frequency of negative PNA-like patterns and an increasing trend in positive PNA-like patterns between the two periods. They also noted that two strong El Niño (EN) events during 1982–1983 and 1997–1998 contributed to these trends, and that the corresponding trend in convective precipitation went from below average to above average values in the tropical Indo-western Pacific. By investigating these trends further through linear regression, they found that the increase in convective precipitation was followed three to six days later by the PNA-like trend, and one to two days later by the trend in downward IR flux. The findings of Lee et al. (2011b) suggested that an increase in these trends may happen on intraseasonal time scales, and could account for winter Arctic warming via dynamic warming and downward IR flux. These ideas are in contrast to one of the most prominent explanations of Arctic warming, which is the surface ice-snow albedo feedback (SAF) process, and show that the evidence for this process is mixed (Lee et al. 2011b).

L'Heureux et al. (2008) investigated the role of the positive PNA pattern that accompanied extreme sea ice loss during July-September 2007. Their study found that during this particular year, the PNA pattern created an exceptionally strong anticyclone over the Beaufort and East Siberian seas. It was speculated by Slingo and Sutton (2007), that a growing La Niña (LN) in the eastern tropical Pacific may have contributed to the Artic warming in that case, however L'Heureux et al. (2008) found that it was not likely LN played a significant role in creating this anomalous circulation.

Another study by Lee (2012) tests the Tropically Excited Arctic Warming Mechanism (TEAM) with ENLN, a concept born from Lee et al. (2011b). This more recent study analyzed 13 EN and 13 LN composites from 1957–2001 with

the ECMWF ERA-40 reanalysis data set, and presented evidence that the Arctic surface air temperature (SAT) during December-February was anomalously warm (cold) during LN (EN). It is important to note that SAT in this study is over the Arctic Ocean, and that the Arctic is defined as the region north 66.56N (the Arctic Circle). This study also showed that the LN warming in the Arctic was associated with an increased poleward energy transport in the extratropics, and showed opposite characteristics for EN. Lee argues that the TEAM concept may be able to explain Arctic SAT anomalies associated with ENLN since the total tropical convective heating is more localized in the western tropical Pacific during LN. Consistent with the Lee et al. (2011b) and Lee (2012) TEAM concept, Yoo et al. (2011) found that the convective phase of the MJO, where the convection is enhanced over the western tropical Pacific warm pool, is associated with a warming of the Arctic during the winter. Lee (2012) stresses that ENLN is only one form of tropical variability, and that the TEAM is just one of several processes that may contribute to Arctic warming, which is something we cannot overstress in our study. Lee (2012) also suggests that the Arctic SAT signal associated with ENLN may also include an AO contribution, but does not test that theory in the TEAM study.

L'Heureux and Thompson (2005) studied the seasonally varying signature of ENLN and its relationship to the AO in the Northern Hemisphere (NH), and the Antarctic Oscillation (AAO) in the Southern Hemisphere (SH). Their study concluded that the temporal variability in the AAO is linearly related to fluctuations in the ENLN cycle during the SH summer. However, an analogous relationship was not observed between ENLN and the AO. In contrast, Quadrelli and Wallace (2002) had found that the structure of the NH winter AO *is* in fact influenced by the phase of ENLN. Despite the lack of relationship between the ENLN and the AO of L'Heureux and Thompson (2005), L'Heureux and Higgins (2007) looked at intraseasonal time scales and compared similarities between the MJO and the AO during the NH winter. This study found that the MJO and AO share several analogous features in the global circulation and SAT fields, and

linked the convectively active phase of the MJO to a corresponding shift in the phase of the AO. Their study concluded that there is potential to exploit the relationships between the MJO and the AO to improve sub-seasonal climate forecasts for the U.S. This finding combined with the findings of Lee et al. (2011b), Lee (2012), and Yoo et al (2011) concerning ESNO and Arctic warming, led us to speculate a relationship between ENLN and interannual variations in the Arctic, despite the prior negative findings of L'Heureux and Thompson (2005). We also speculated the potential for a relationship between the AO and winter Arctic warming.

2. Intraseasonal to Interannual Arctic Climate Variations Can Drive Midlatitude Variations

Francis and Vavrus (2012) provided evidence for two mechanisms by which Arctic warming may cause more persistent weather patterns and extreme weather in the midlatitudes. Their study showed that a weakened poleward gradient in 1000–500 hPa thickness slows the eastward progression of the long wave pattern. In response, the amplitude of the wave increases, which weakens the polar vortex and allows for weather conditions to persist and potentially become severe in the midlatitudes. The NH polar vortex is a planetary-scale, middle to high-latitude cyclonic circulation around the NH polar region, extending from the middle troposphere to the stratosphere (American Meteorology Society (AMS) 2014). The polar vortex is strongest during the winter when the pole-to-equator temperature gradient is strongest (AMS 2014). Winter Arctic warming decreases the normal winter pole-to-equator temperature gradient, thereby weakening the polar vortex. A strong (weak) polar vortex is associated with enhanced (decreased) westerlies. A second claim by Francis and Vavrus (2012) is that a northward elongation of ridge peaks in 500 hPa waves occurs, which further increases the potential of slower moving waves. While we agree with these claims, our study investigated further into the possible conditions that lead to Arctic warming which could then lead to changes in the polar vortex as suggested by Francis and Vavrus (2012).

A related study by L'Heureux et al. (2010) examined the negative phase of the AO in 2009 and the extreme effects it had on the NH during June, July, October, and December. The AO accounts for changes in different features of the polar vortex (e.g. pressure, temperature, jet stream strength), and when the polar vortex is strong (weak), the AO tends to be in its positive (negative) state. In December 2009 in particular, a series of cold air outbreaks occurred much like the extreme outbreaks of more recent winters, and were accompanied by extreme negative values of the AO (i.e., an extremely weak polar vortex) (L'Heureux et al. 2010). These studies suggest that teleconnections between the Arctic and midlatitudes do exist.

C. SCOPE OF RESEARCH

1. Research Questions

In our study we researched and explored using advanced climatology data sets and methods to analyze the interannual variations in Arctic winter temperature. It is our hope that the results of this thesis can be used as a basis for further research involving long-range climate support for Arctic operations. This study focused on answering the following questions:

(1) How have Arctic conditions varied on an interannual scale over the last 50 years?

(2) What are the mechanisms underlying Arctic interannual variations?

(3) What are the relationships between Arctic interannual variations and other interannual variations (e.g., ENLN, AO, Indian Ocean Dipole (IOD))?

(4) How might information about these mechanisms and relationships be used to predict Arctic interannual variations?

Please refer to Chapter II, Section B for a discussion of our study limitations and reasons for these limitations.

2. Thesis Organization

To answer our research questions, we conducted an in-depth climate analysis to find possible relationships between interannual Arctic winter temperature and several global scale climate variations.

Chapter II provides: (a) a summary of the data sets and climate indices used in this study; (b) a description of our focus region, period, and variables as well as several reasons for these choices; and (c) the methods and tools used to analyze the influences on Arctic winter temperature. Chapter III provides the results of our tercile categorical analysis, as well as our conditional composite anomaly and correlation analyses. Chapter IV summarizes our results and provides suggestions and options for future research.

THIS PAGE INTENTIONALLY LEFT BLANK

II. DATA AND METHODS

A. DATA SETS

1. NCEP/NCAR Reanalysis

The atmospheric data used in this thesis came from the NCEP/NCAR R1 data set (Kalnay et al. 1996, Kistler et al. 2001). The R1 data set is the result of a global retrospective analysis (i.e., reanalysis) of climate system observations using data assimilation, spectral statistical interpolation (SSI), and dynamical analysis processes that are fixed and applied at each time step. The component data sets used in the R1 data set include: global rawinsonde data, Comprehensive Ocean-Atmospheric Data Set (COADS) surface marine data, aircraft data, surface land synoptic data, satellite sounder data, special sensing microwave/imager (SSM/I) data, and satellite cloud drift winds (Kalnay et al. 1996). This data has a temporal resolution of six hours, with daily and monthly values for January 1948 to present, and long-term mean (LTM) values derived for 1981–2010. The spatial resolution of the R1 data set is 2.5° at 17 standard pressure levels, and 28 sigma levels for the dynamical analysis (Kalnay et al. 1996).

The R1 data set was chosen for our study for several reasons. It is very accessible to the scientific community and is widely used in Arctic research (e.g., Francis and Vavrus 2012, L'Heureux et al. 2009, 2008, Quadrelli and Wallace 2002). This data set has the ability to the capture intraseasonal to multi-decadal climate variations. Also, the NOAA Earth Systems Laboratory (ESRL) website provides user-friendly plotting and analysis tools for the R1 data set, which allowed us to readily conduct an extensive analysis. We chose the R1 data set rather than the Climate Forecast System Reanalysis (CFSR) or other reanalysis data, because: (a) the tools for accessing and analyzing R1 data are better developed; (b) prior comparisons of R1 and CFSR data indicate that the two data sets show very similar large scale spatial and temporal variations in atmospheric

T, heights, and winds. The atmospheric and oceanic R1 variables chosen for our research were 850 hPa air temperature in degrees Celsius (T850, °C), 850 hPa geopotential height in meters (Z850, m), 200 hPa geopotential height (Z200, m), 850 hPa zonal wind in meters per second (U850, ms^{-1}), and 200 hPa zonal wind (U200, ms^{-1}), sea surface or surface skin temperature (SST, °C), and 200 hPa outgoing longwave radiation in Watts per square meter (OLR, W/m^2). We will describe our use of the ESRL plotting and analysis tools in Chapter II, Section C.1.

2. Climate Variation Indices

We investigated relationships between the interannual variations in Arctic air temperature and two global scale atmospheric variations: ENLN, and the AO. To represent ENLN we used the Multivariate El Niño-Southern Oscillation Index (MEI) and for the Arctic Oscillation we used the Arctic Oscillation Index (AOI). Both the MEI and AOI were accessed via the ESRL plotting and correlation tools (ESRL 2015c, 2015d). More information about ENLN can be found at the ESRL website (ESRL 2015a) and in publications by Wolter and Timlin (1993), (1998), and (2011). More information about the AO can be found at the Climate Prediction Center's (CPC) AO website (CPC 2015).

B. FOCUS REGION, PERIOD, AND VARIABLES

1. Focus Region

We chose to focus our attention on the Arctic region, particularly at the higher latitudes of the Arctic. In regards to Arctic warming, Lee (2012) defines the Arctic as extending north of 66.56N (the Arctic Circle), while other studies refer to the Arctic rather vaguely as "high northern latitudes" or simply "the Arctic" (Francis and Vavrus 2012, Francis 2013). We chose to specifically define the Arctic as extending north from 75N at all longitudes. We defined the Arctic this way because the region of the Arctic that lies south of 75N may allow for the mixing of Arctic and midlatitude signals. The polar vortex is commonly observed at 50N-65N, and encompasses the southern boundary of the Arctic. This region

passes through several extratropical eddies (e.g., The Aleutian Low, Icelandic Low) seen in the LTM of January-March (JFM) Arctic Z850 in Figure 2, which encourage interactions between the Arctic and lower latitudes. Figure 3 shows the LTM of JFM Arctic T850, and some of the interactions created by these extratropical eddies. We can see from Figure 3 that the coldest T850 occurs south of 90N over Siberia and east Asia, the Canadian Archipelago and eastern Canada, and Greenland, while the warmest T850 occurs over the western tropical Pacific near the maritime continent, and over tropical landmasses. The northern-most extent of the relatively warm midlatitude air appears to stop south of 75N. Similarly, the relatively warm SSTs in the North Atlantic Ocean (see Figure 10 of Chapter III, Section B) do not appear to extend north of 75N. We decided that our latitude band should not extend south of 75N in order to mitigate these types of interactions between the Arctic and lower latitudes.

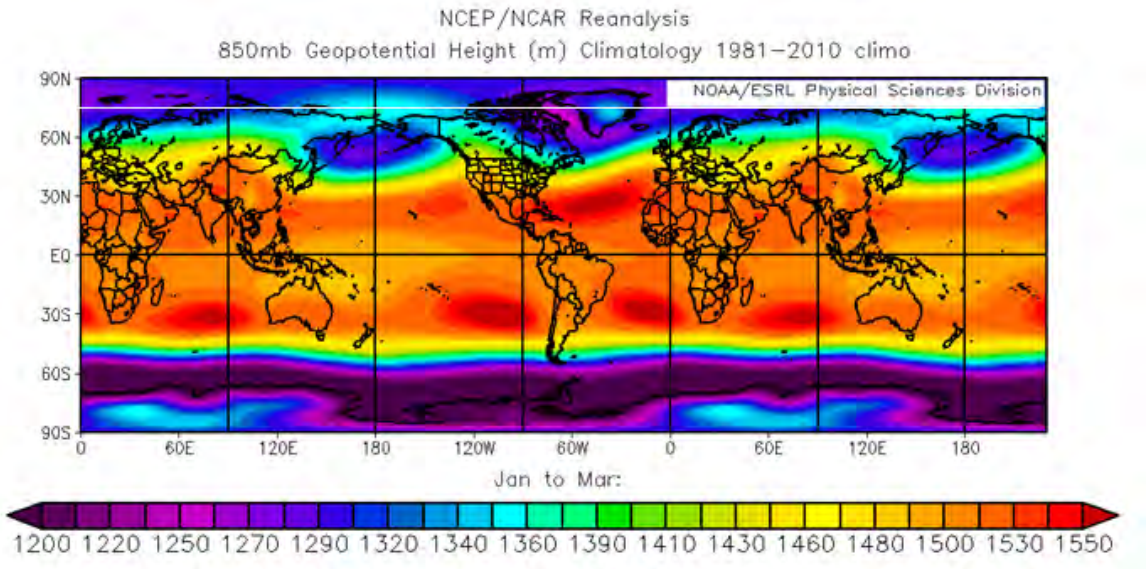

Figure 2. LTM JFM Z850 for 1981–2010. Shows normal Z850 conditions during JFM. The southern boundary of the Arctic (as we have defined it) is at 75N as indicated by the thin white line. Note the locations of extratropical eddies, implied areas of WAA (CAA) and their influence on T850 in Figure 3

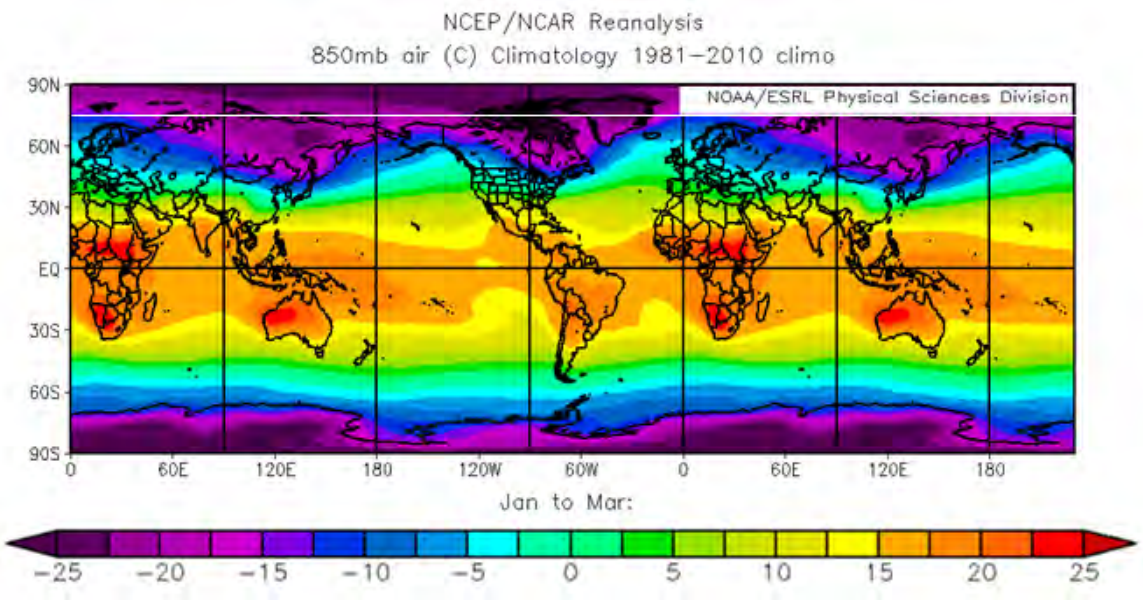

Figure 3. LTM JFM T850 1981–2010. Shows normal T850 conditions during JFM. The southern boundary of the Arctic (as we have defined it) is at 75N as indicated by the thin white line. Note the northward (southward) extensions of warm (cold) air in the midlatitudes.

We created Arctic temperature time series for 75N-90N, as well as other latitude bands including: 70N-90N, 65N-90N, and 65N-75N to make sure that 75N-90N was good representative of T850. We found that the interannual variations in Arctic temperature at the different bands were relatively similar which meant that 75N-90N was a logical choice to represent T850.

Though we focused on the interannual variations in air temperature that occur within the Arctic, it was important for us to look globally when trying to identify teleconnections and anomalous patterns in our composites of atmospheric and oceanic variables. Sometimes conditions in one area of the globe can impact conditions in another area far away. Teleconnections and other anomalous patterns between the tropics and the Arctic quickly became apparent in this study, and led us to focus on signals in the NH. Had we noticed Antarctic signals vice Arctic signals, we would have chosen to focus our attention within the SH.

2. Focus Period

We chose to conduct our analyses for the 45-year period 1970–2014. Ideally we would want to use a study period of as many years as possible, but this study period allowed us to use data from the satellite era, while maintaining a relatively large-sized period for analyzing interannual variations. This 45-year period allowed us to use data that is more representative of current conditions than older data, and also allowed us to use a large sample of ENLN events. We chose to work with the JFM winter season over other seasons because the Arctic is known to have larger impacts on lower latitudes in the winter, which may coincide with the negative phase of the AO (see further discussion of polar vortex and AO impacts on lower latitudes in Chapter 1, Section 2). Similar to Lee (2012), we chose winter because this is also when poleward-propagating Rossby waves are strongest in the NH.

3. Focus Variables

We chose to focus on Arctic T850, but also studied global T850, Z850, Z200 U850, U200, SST, and OLR to help us understand the interannual variations in Arctic T850. Each of these variables also has associated winter ENLN signatures, which have been identified throughout Chapter III. We analyzed temperature at 850 hPa because this level is very representative of the lower troposphere. We investigated other lower tropospheric levels (e.g., surface, 1000 hPa, 700 hPa), and found that these levels showed similar interannual variations in Arctic temperature to the variations seen at 850 hPa. In the remained of this report, we have used *Arctic T* as a shortened version of *winter, or JFM Arctic air temperature at 850 hPa*, unless otherwise noted.

We studied T850 to see how temperatures varied spatially across the globe, in particular the NH. We studied Z850 to help us understand the dynamical mechanisms that may lead to anomalous T850. Analyzing Z850 showed us the lower tropospheric sources horizontal advection, that is, south to

north warm air advection (WAA) and north to south cold air advection (CAA), and the regions where WAA (CAA) and temperature variations occurred.

We studied Z200 as well because Rossby wave trains are more easily identified in the upper troposphere, and because Z200 indicates heat and moisture transport between lower and higher latitudes (cf. Aguado and Burt 2004). The approximate height of the tropopause is also indicated by Z200. Regions where Z850 (Z200) and circulations are approximately centered over each other and qualitatively similar are known as equivalent barotropic regions. Non-equivalent barotropic refers to the vertical structures in which the Z850 and Z200 and their circulations are approximately centered over each other but are qualitatively opposite to each other. The extratropical (tropical) vertical structures are typically referred to as equivalent (non-equivalent) barotropic. These variables were helpful in identifying GPH patterns associated with ENLN.

We also studied U850 and U200 to get a sense of regions where the westerlies are weaker (stronger) than normal, indicating a weak (strong) polar vortex. This was important for identifying exchanges of warm (cold) air between the Arctic and lower latitudes. For further discussion on this topic, see Chapter 1, Section B.2. Cross-section plots of U850 and U200 helped to confirm the strength and location of westerly winds and the polar vortex.

We analyzed SST because the ocean responds slower to changes in temperature than the atmosphere; therefore the SST signatures are very representative of T850 over the ocean (cf. Aguado and Burt 2004). We studied OLR because it connects changes in the ocean and atmosphere, and can show regions of enhanced (suppressed) convection, which are closely linked to warm (cold) SST. Global SST and OLR are also very important to our study because their ENLN signatures could be identified over many parts of the world.

C. CLIMATE ANALYSIS METHODS

1. Tercile Categorical, and Conditional Composite Anomaly Analyses

We constructed a time series for Arctic T (for more information about Arctic T, see Chapter II, Section B.3), using the ESRL website (ESRL 2015d). We then conducted a tercile categorical analysis of this time series (see Figure 4 and Table 2 in Chapter III, Section A). We identified the years in which Arctic T conditions were above normal (AN), near normal (NN), and below normal (BN). We further identified the eight years with the warmest (coldest) Arctic T. We then used the plotting and analysis tools on the ESRL website (ESRL 2015e) to create composite anomalies of global conditions (i.e., our other focus variables) by averaging these conditions during our eight coldest (warmest) years. We were also able to identify the years of our study period in which ENLN events occurred. Based on this information, we created conditional composites by averaging together the warmest (coldest) years of our focus variable that were also years in which LN (EN) events occurred to examine relationships between interannual variations in Arctic T and ENLN.

All composite anomalies in our study were calculated by subtracting the JFM LTM, which used a base period of 1981-2010, from our composite mean of our eight warm (cold) years. The LTM plots helped us to visualize normal conditions during JFM, while the anomalies indicated changes from the normal conditions. It is important to note that the LTM base period does not exactly match our study period 1970-2014. We chose to create composite anomalies for the following reasons:

(1) Composite anomalies of the eight warmest (coldest) years represented the extremes of our focus variables (i.e., roughly 1/6 of our study period).

(2) Composite anomalies showed the averaged anomalies of our focus variables during extreme warm (cold) years.

(3) Compositing eight years, vice a larger (smaller) number of years, allowed for clearer signals in the averaged anomalies.

(4) Composite anomalies were useful in analyzing the patterns and processes that may have contributed to extreme warm (cold) T850

(5) Composite anomalies were used as a benchmark for our correlation analyses

(6) Composite anomalies were useful in identifying teleconnections and possible predictors of Arctic T (e.g., ENLN).

2. Correlation Analyses

We used our composite anomalies as benchmarks for correlating Arctic T with the other focus variables discussed in Chapter II, Section B.3. Table 1 shows the correlation values and corresponding confidence levels for our 45-year study period. The confidence levels in the right column were calculated using a two-tailed hypothesis test for 45 years. For more information on hypothesis testing, see (ESRL 2015 Wilks 2006).

Table 1. Correlation values and corresponding confidence levels for a 45-year period.

Correlation Values for 45 Years	Confidence Levels for 45 Years
0.20	0.81
0.22	0.85
.245	.90
0.294	0.95
0.345	0.975
0.379	0.99
0.41	0.995

We calculated zero lag correlations between area-averaged Arctic T and each of the other focus variables grid point by grid point, everywhere in the world. We also calculated one-, three-, and five-month lag correlations between area-averaged Arctic T and the other focus variables. In each of these correlations, Arctic T lagged the other variables. Certain relationships (explained in Chapter III Section G.) prompted us to calculate zero to ten-month lag correlations between Arctic T and the MEI, with the MEI leading Arctic T. Similarly, we correlated Arctic T with the AO. These correlations helped us to identify teleconnections and possible predictors of Arctic T. Variables and climate indices with the strongest and most significant correlations with Arctic T were identified as possible predictors of Arctic T.

THIS PAGE INTENTIONALLY LEFT BLANK

III. ANALYSIS RESULTS

A. TERCILE CATEGORICAL ANALYSIS

To begin our analysis, we constructed a time series of Arctic T for our study period, 1970–2014 (Figure 4). (Please refer to Chapter II, Section B for more information concerning this focus variable.) It is interesting to note in Figure 4 that the warmest winters are seen in both the early and later portions of our time series, and that the coldest winters occur mainly within the middle portion of our time series. Also of note are the different trends throughout the period. Contrary to prior studies (e.g., Francis and Vavrus 2012), we do not see a distinct warming trend over the past few decades, which could be a result of how we defined the Arctic, and the level of the atmosphere we chose to analyze. Please refer to Chapter IV, Section B for additional limitations to our study and areas for further research. The warming trend in our time series is only clear from approximately 2000–2014. There is also a slight downward trend from approximately 1976–1988, and a near neutral trend during 1988–2000. In each of these trends, and throughout the entire analysis period, large interannual variations in Arctic T occurred. A major goal of this study is to investigate the possible causes of such large interannual variations in Arctic T.

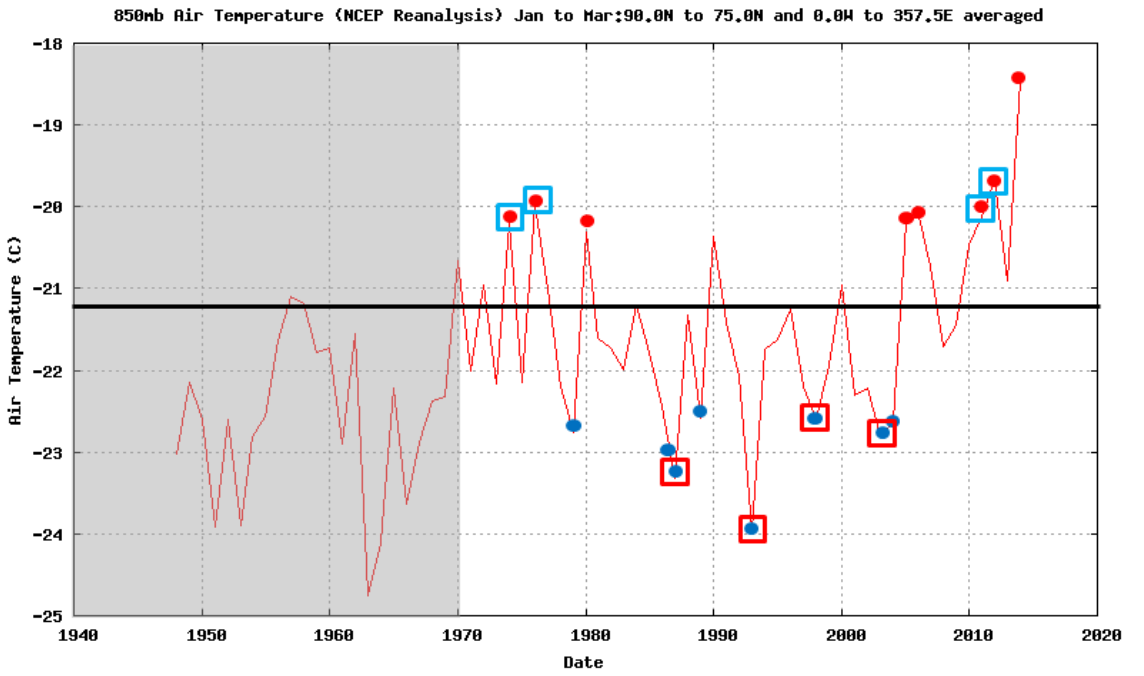

Figure 4. Time series of Arctic T (75N–90N; all longitudes) for 1948 to present. Shows our study period (1970–2014), with pre-1970 years shaded in grey. The bold line indicates the 1970–2014 JFM LTM which is -21.5 degrees. The red (blue) dots indicate the warmest (coldest) years in our time period. The red (blue) squares indicate years in which EN (LN) events occurred during our eight warmest (coldest) years. Note the large interannual variations and distinct upward trend during 2000–2014.

Table 2 separates our 45-year study period, 1970–2014 (see Figure 4), into three terciles, and shows the years in which Arctic T was in the coldest (a), middle (b), or warmest (c) tercile. Table 2 also indicates the state of ENLN in the right column of each tercile, as well as the strength of that state. The general tendency during this period is for the warm winters to be associated with LN, the cold winters to be associated with EN, and the near normal (NN) winters to be associated with neutral ENLN conditions. It is important to note that of our eight warm (cold) years, four of those years included LN (EN) events, and that each of these four EN (LN) events was considered strong. The NN years were dominated by neutral ENLN events.

Table 2. Years in which Arctic T for our 45-year study period, 1970–2014, was in the: (a) lowest tercile, also known as the coldest tercile or below normal (BN) tercile; (b) the middle tercile, also known as the near normal (NN) tercile; (c) the highest tercile, also known as the warmest tercile or above normal (AN) tercile. For each tercile, the years have been ranked from the coldest (at the top) to the warmest (at the bottom). For our 45-year study period, each tercile contains a total of 15 years. For each year, the state of ENLN has been indicated in the right column of each part (EN=El Niño; LN=La Niña; neutral=neither El Niño or La Niña; S=strong; M=moderate; W=weak). The years shaded in red (blue) are the eight coldest (warmest) years used in our study period.

Below Normal		Near Normal		Above Normal	
a. Year	ENLN State	b. Year	ENLN State	c. Year	ENLN State
1993	S-EN	1971	S-LN	2000	S-LN
1987	S-EN	1983	S-EN	1972	Neutral
2003	W to M-EN	1999	S-LN	2013	Neutral
1979	Neutral	1985	W-LN	2007	Neutral
2004	Neutral	1994	Neutral	1970	Neutral
1998	S-EN	1982	Neutral	2010	S-EN
1989	S-LN	2008	S-LN	1990	W-EN
1986	Neutral	1995	M-EN	1980	W-EN
2001	NN to W-LN	1981	Neutral	1974	S-LN
2002	Neutral	2009	W-LN	2005	W-EN
1997	Neutral	1991	Neutral	2006	Neutral
1978	W-EN	1988	W-EN	2011	S-LN
1973	S-EN	1996	Neutral	1976	S-LN
1975	W-LN	1984	Neutral	2012	W-LN
1992	S-EN	1977	Neutral	2014	Neutral

It is important to note that not all of the cold (warm) winters were associated with EN (LN) and that some of the NN winters *were* associated with ENLN. Even so, this distribution of ENLN events among our time period is interesting, and led us to investigate the role that ENLN may play in the interannual variation of Arctic T. ENLN is a well-known climate variation linked to numerous anomalous atmospheric conditions around the globe, and though its relationship with Arctic T may be important, it is also not perfect. There may be several other climate variations that influence interannual variations in Arctic T (see Chapter IV for further discussion).

B. LONG-TERM MEAN (LTM) CONDITIONS

Many of the figures in the remainder of this chapter show maps that repeat information for some longitudes. This repetition was done to facilitate the identification of patterns that extend across many degrees of longitude. (For further descriptions of the focus region, period, and variables discussed in this chapter please refer to Chapter II, Section B.1-B.3 and C.1.)

Figure 5 (also shown in Chapter II, Section B.1) shows the LTM patterns of global JFM T850, and gives a sense of the normal temperature conditions during the NH winter. We can see in Figure 5 that the coldest temperatures occur in the polar and subpolar regions over Siberia and east Asia, the Canadian Archipelago, eastern Canada, and Greenland. The warmest temperatures in the NH are seen across the western tropical Pacific and maritime continent, as well as over Africa and South America. Areas of relatively warm air also appear to extend poleward, just south of the Alaska/Canada border, and Iceland. The largest spatial variations in T850 occur within the midlatitude regions, near the southern-most boundary of the cold air (e.g., over eastern North America and Japan).

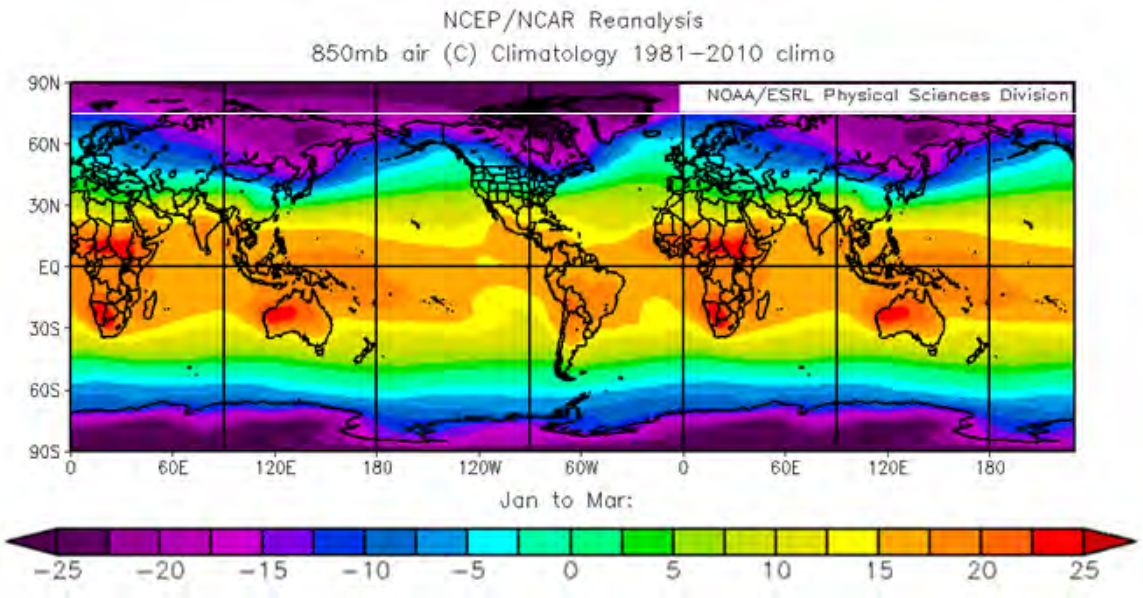

Figure 5. LTM JFM T850 for 1981-2010. Shows normal T850 conditions during JFM. The southern boundary of the Arctic (as we have defined it) is at 75N as indicated by the thin white line. Note the northward (southward) extensions of warm (cold) air in the midlatitudes.

Figure 6 (also shown in Chapter II, Section B.1) shows the LTM patterns of global JFM Z850. This figure gives a sense of the general lower tropospheric circulation patterns that occur during the NH winter, revealing the approximate location of extratropical semi-permanent high and low pressure systems, also known as extratropical eddies. Persistent changes in location, strength, orientation and timing of these eddies are part of important climate variations like ENLN (Murphree 2012c). Low heights are seen across the majority of the Arctic, with exceptionally low heights in the Baffin Bay-Greenland-Iceland region. The extratropical eddies important in our analysis include the Asian High over central Asia, the Aleutian Low in the northern Pacific, the North Pacific-North American High between Hawaii and North America, the Icelandic Low, and the Azores High in the central Atlantic.

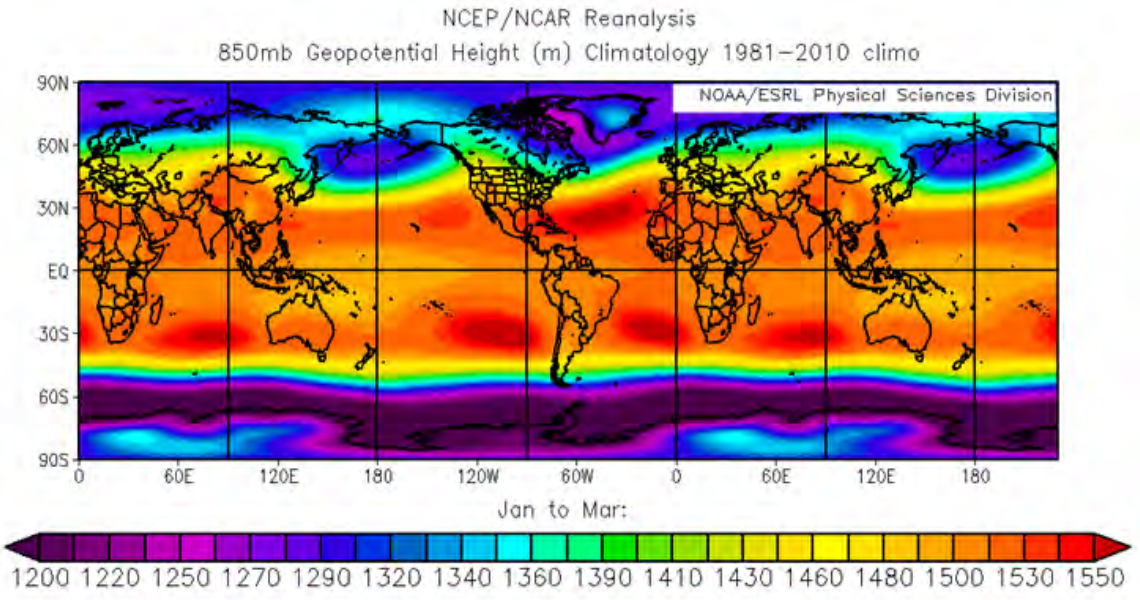

Figure 6. LTM JFM Z850 for 1981–2010. Shows normal Z850 conditions during JFM. Note the locations of extratropical eddies and implied areas of WAA (CAA) and their influence on T850 in Figure 5.

It is important to note that these eddies help to explain north-south flow and the resultant spatial distribution of global T850 seen in Figure 5. For instance, the flow around the Asian High over central Asia in Figure 6, advects cold dry air southward over East Asia in Figure 5. Similarly, the North Pacific-North American High and Icelandic Low advect cold air southward over eastern Canada, while the Aleutian Low and North Pacific-North American High advect warm moist air northward and eastward over the northeast Pacific and western North America. The Icelandic Low and Azores High also advect warm air northward and eastward between Iceland and Scandinavia.

Figure 7 shows the LTM patterns of global Z200 and shows the normal extratopical longwave pattern for JFM. Tropical ridging occurs over the western tropical Pacific, as well as over tropical land masses. The extratropical ridges and troughs are more apparent in the NH midlatitudes than in the SH midlatitudes because the pole-to-equator temperature gradient is strongest (weakest) during winter (summer). The largest height gradients are located between the tropical ridges and extratropical troughs (e.g., over eastern North America and Japan).

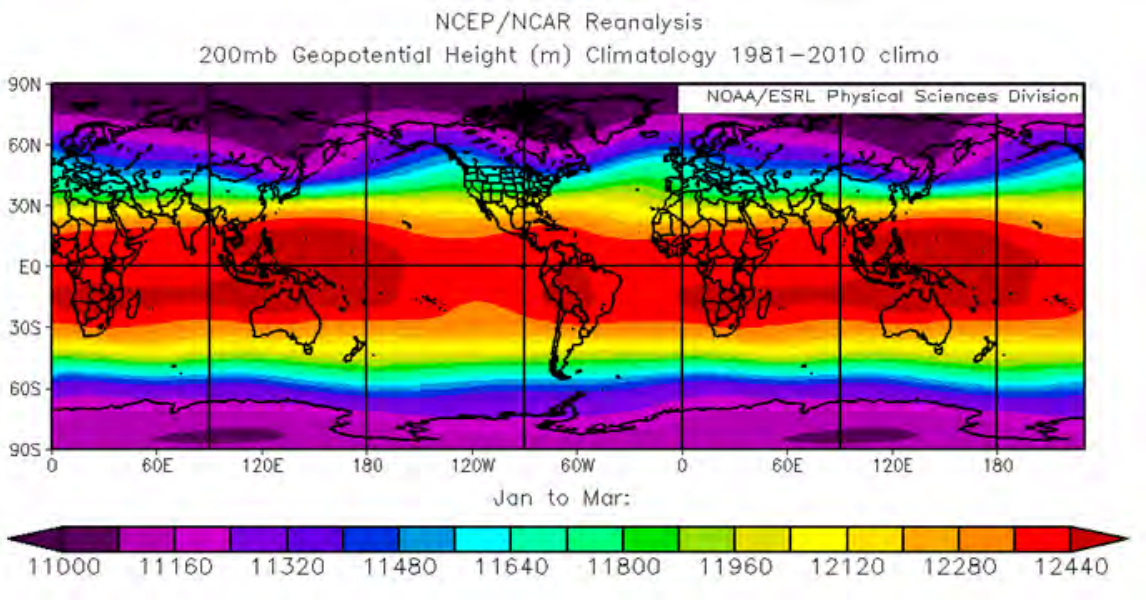

Figure 7. LTM JFM Z200 for 1981–2010. Shows normal Z200 conditions during JFM. Note the locations of extratropical ridges and troughs and the implied areas of WAA (CAA) at low levels.

It is important to explain the relationships between T850, Z850, and Z200, as these relationships are relevant in later results. It makes dynamical sense, from the principles of thermal wind, that strong flow aloft occurs over areas of strong thermal gradients at lower levels. The subtropical jet tends to be strongest over east Asia and Japan during the winter (see Figure 7). The WAA (CAA) induced by the orientation of extratropical eddies in the Z850 field, help to explain the T850 distribution. The WAA (CAA) also works to raise (lower) GPH heights throughout the column, which intensifies the upper level (Z200) ridges (troughs). In the extratropics, where there are ridges (troughs) at upper levels, there tend to corresponding troughs (ridges) at lower levels.

While the LTM patterns of global Z850 help to explain the meridional or north-south flow of air, the U850 (U200) patterns help to explain the horizontal or west-east flow of air in the lower (upper) troposphere. Figures 8 and 9 show the LTM patterns of global JFM U850 and U200, respectively, and reveal the typical locations of westerlies (easterlies) during JFM. In Figure 8 we can see that the regions of strong westerlies vary between 30N-60N. These regions appear

discontinuous, with the strongest westerlies being more apparent over the North Pacific and North Atlantic Oceans, and parts of Eurasia and North America. The regions of strong westerlies between 50N–65N represent the polar vortex. In Figure 9, regions of strong westerlies are more continuous, and the strongest westerlies tend to occur near Japan and southeastern North America. This makes dynamical sense as these are the typical locations for the Subtropical Jet, which is strongest near Japan during the winter.

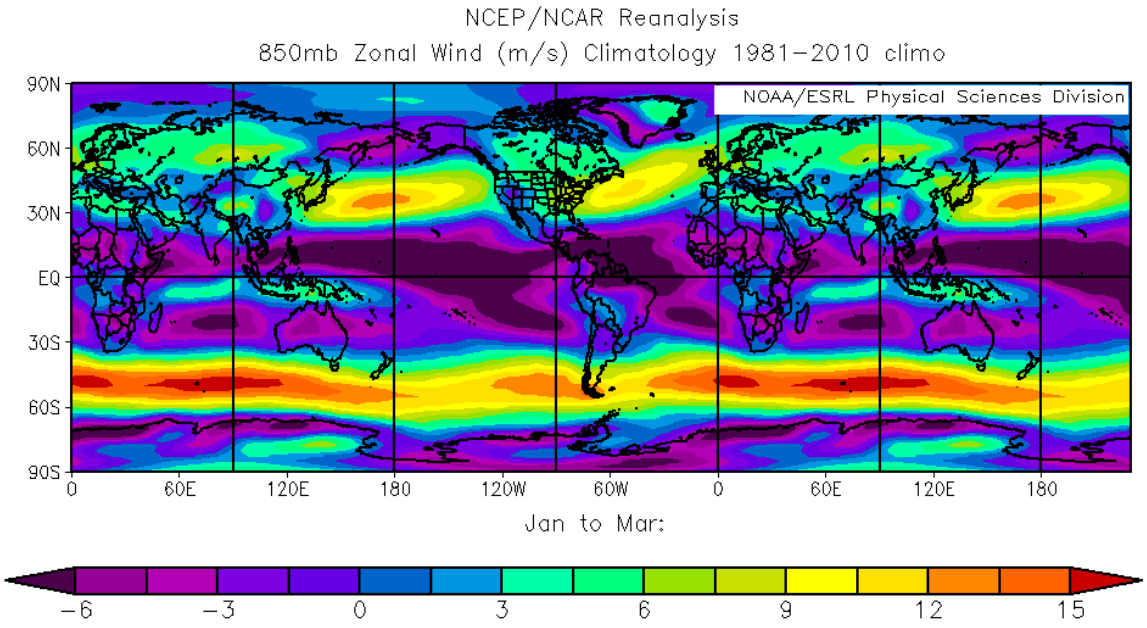

Figure 8. LTM JFM U850 for 1981–2010. Shows normal U850 conditions during JFM. Note the normal locations of strong westerlies (easterlies) in the extratropics (tropics).

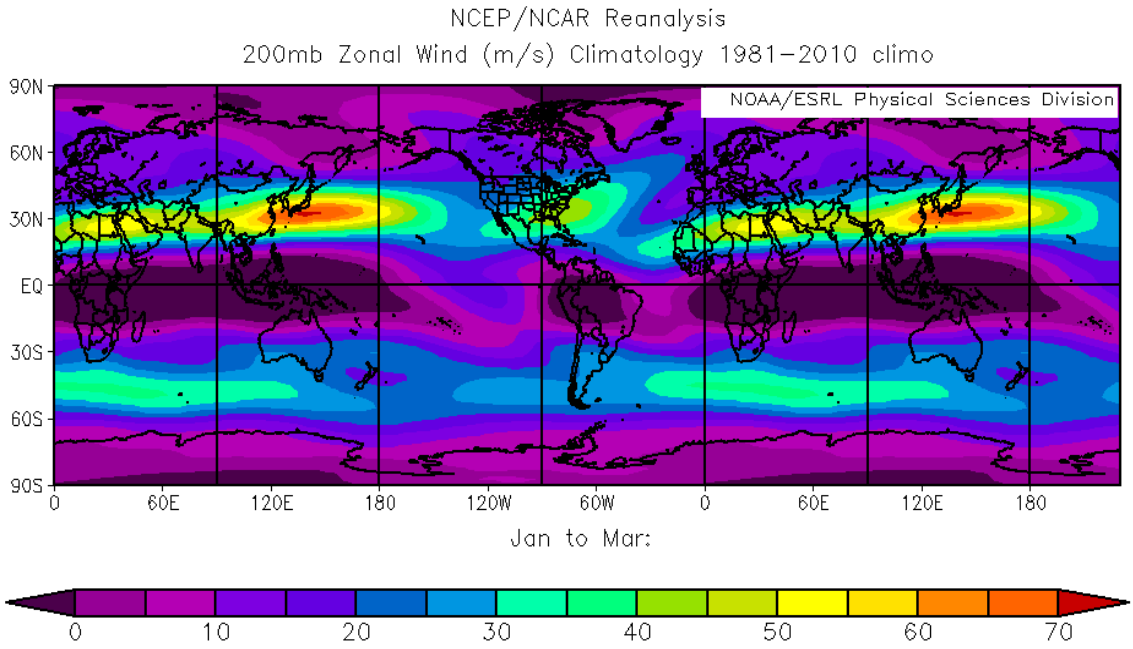

Figure 9. LTM JFM U200 for 1981–2010. Shows normal U200 conditions during JFM. Note the normal locations of strong westerlies (easterlies) in the extratropics (tropics)

Figure 10 shows the LTM patterns of global SST, which are similar to, and closely related to, the LTM T850 patterns over the ocean (Figure 5). The highest SSTs occur in the western tropical Pacific, around the maritime continent (tropical land in between 90E and 160E), and the western tropical Atlantic. Arctic SSTs are exceptionally low north of North America and Greenland. As we touched upon in Chapter II, Section B.3, the regions of relatively warm water in the higher latitudes of the NH (e.g., the northeast Pacific, northeast Atlantic, north of Europe and western Russia) are important in warming the overlying air and in affecting the advection of warm air and sea water into the Arctic. These regions were also important in determining the southern boundary of the Arctic and the poleward extensions of air and sea water from lower latitudes in our study.

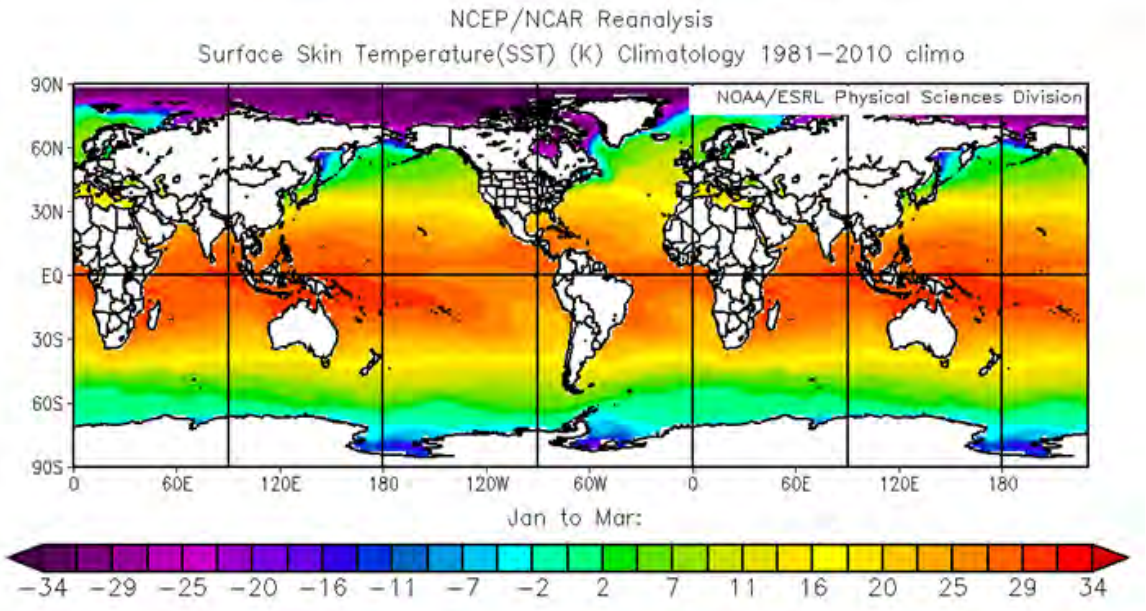

Figure 10. LTM JFM SST for 1981–2010. Shows normal SST conditions during JFM. Note the similar distributions of SST, and T850 in Figure 5, and northward extension of warm SST into the northeast Atlantic.

Figure 11 shows the LTM patterns of global JFM OLR. In the tropics, low OLR indicates deep convection and relatively high latent heating of the atmosphere, and high OLR indicates relatively clear skies and low latent heating of the atmosphere. In the NH winter, OLR is typically low near the maritime continent, due to increased convection from surface convergence and uplift over areas of high SST. OLR is typically high over the central-eastern tropical Pacific in regions of surface divergence and subsiding air.

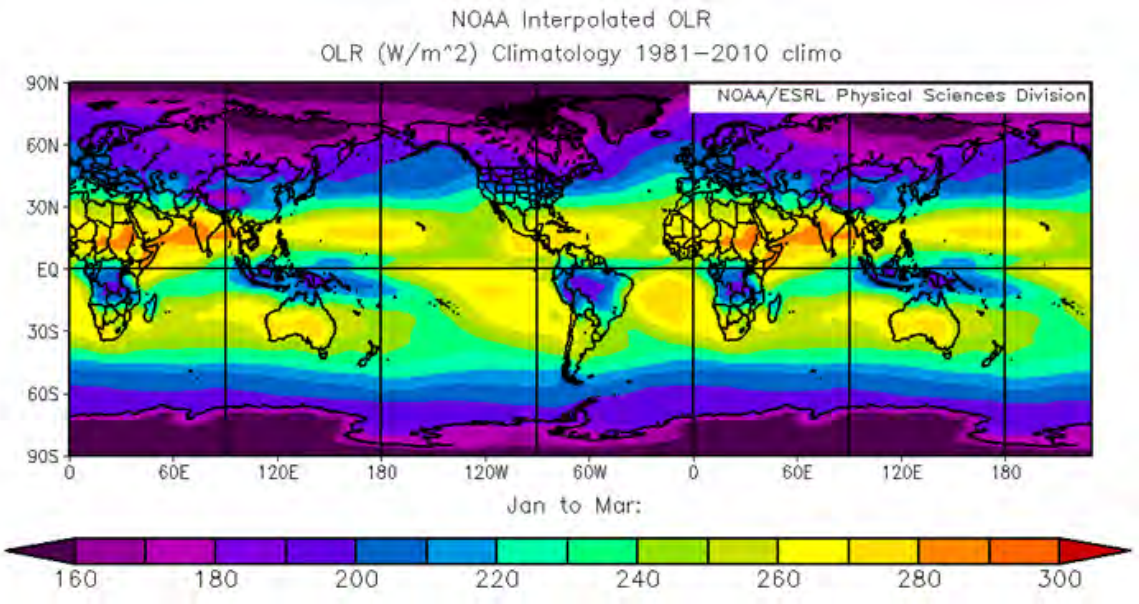

Figure 11. LTM JFM OLR for 1981–2010. Shows normal OLR conditions during JFM. Note the areas of high (low) OLR over the central-eastern (western) tropical Pacific.

C. WARM COMPOSITES

From Table 2, we identified the eight warmest winters, four of which occurred during LN events, and averaged the anomalies for these eight years together to produce anomaly composites for the same variables presented in Figures 5 through 11. Each composite is plotted from 90S-90N at all longitudes using R1 data. These warm composite anomalies help to identify global scale anomalies in atmospheric and oceanic conditions associated with anomalously warm Arctic T.

Figure 12 shows the warm composite anomaly of global JFM T850. From Table 2, we know that three strong LN events, one weak LN event, two neutral events, and two weak EN events occurred during these eight warm winters. In this figure, the Arctic is anomalously warm, especially from 30W to 110E, with an extension of this warm anomaly into the subpolar regions of the North Atlantic (i.e., Baffin Bay-Scandinavia). Weak positive anomalies in the Arctic occurred over from about 150W–90W. These positive anomalies occurred in areas that are normally very cold, indicating that the anomalies weakened the normal T850

conditions in this area. Warm anomalies also occurred over the central North Pacific and southern North America. Cold anomalies occurred over central Asia and Canada, which are areas of normally cold T850. The cold anomalies indicate an intensification of the normal conditions in these areas. The net effect of positive anomalies in the Arctic and negative anomalies in much of the midlatitudes is to weaken the normal horizontal T850 gradient, which weakens the polar vortex.

Many of these T850 anomalies in Figure 12 are similar to the T850 anomalies that tend to occur in the NH winter during LN events (Murphree 2012b, 2014c, ESRL 2015a). These similarities led us to investigate the relationships between Arctic T and ENLN.

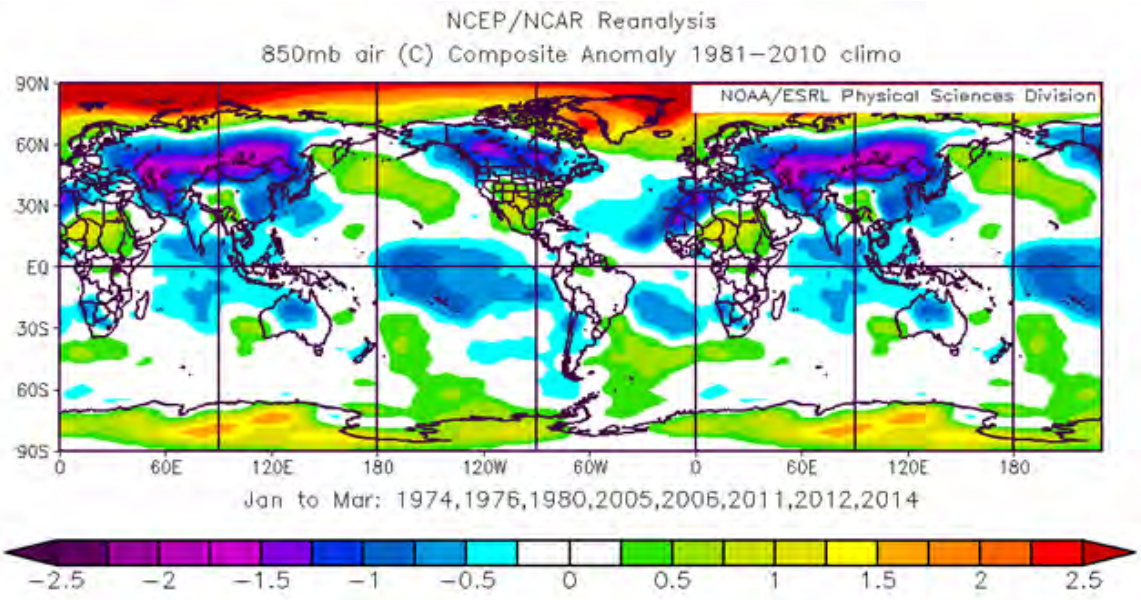

Figure 12. Anomalous JFM T850 for 1970–2014 for warm years. Note the areas of strong (weak) warm anomalies in the Arctic. Also note areas of warm (cold) anomalies in the midlatitudes. Anomalous T850 patterns shown here are similar to those of LN events.

Figure 13 shows the warm composite anomaly of global JFM Z850. Several areas of anomalously high and low heights can be seen when compared

to the Z850 LTM in Figure 6. These anomalous heights reveal circulation patterns that help to produce the T850 anomalies shown in Figure 12. In Figure 13, a weakening of the North Pacific-North American High (Figure 6) and a strengthening of the Icelandic Low may have caused the negative anomalies over much of North America and in the North Atlantic (south of Greenland), while a substantial weakening of the low heights over the Arctic may have caused the positive anomalies over northern Siberia and Scandinavia. We speculate that these areas of positive and negative anomalies in Z850, and implied WAA, may have caused the warm T850 anomalies (Figure 12) from 30W–110E in the Arctic, and in the sub-polar regions of the North Atlantic (Baffin Bay-Scandinavia). This speculation is consistent with the ideas presented in Lee et al. (2011b) concerning the effects of horizontal temperature advection and dynamic warming on winter Arctic warming. The positive anomalies over northern Siberia and Scandinavia may have also produced CAA and the subsequent cold anomalies over much of Eurasia in Figure 12.

Figure 13 also shows that the Aleutian Low may have weakened, as indicated by the positive anomalies in the northern and northeastern Pacific. These positive anomalies and the negative anomalies over North America, and implied CAA, may have produced the cold T850 anomalies (Figure 12) over Canada. The positive anomalies over the northern and eastern Pacific may have also helped to produce the warm T850 anomalies over the Arctic from 150E–90W. It may also be that the CAA which produced the cold anomalies over Canada may have offset some of the WAA which produced the warm Arctic anomalies in Figure 12. This offset could account for the weaker warm anomalies from 50E–90W. A westward shift and slight strengthening of the Azores High in the subtropical Atlantic, and implied WAA, may have produced the warm T850 anomalies over southern North America. It is also necessary to point out that the tropics are dominated by areas of negative Z850 and T850 anomalies. In Figure 13, we also saw evidence of a negative PNA-like pattern, which is a

teleconnection typically associated with LN. This pattern is more easily seen at 200 hPa, and will be discussed further in the anomalies of Figure 14.

Like the T850 anomalies, many of the Z850 anomalies in Figure 12 are similar to the Z850 anomalies that tend to occur in the NH winter during LN events (Murphree 2012b, 2014c, ESRL 2015a). These similarities led us to investigate the relationships between Arctic T and ENLN

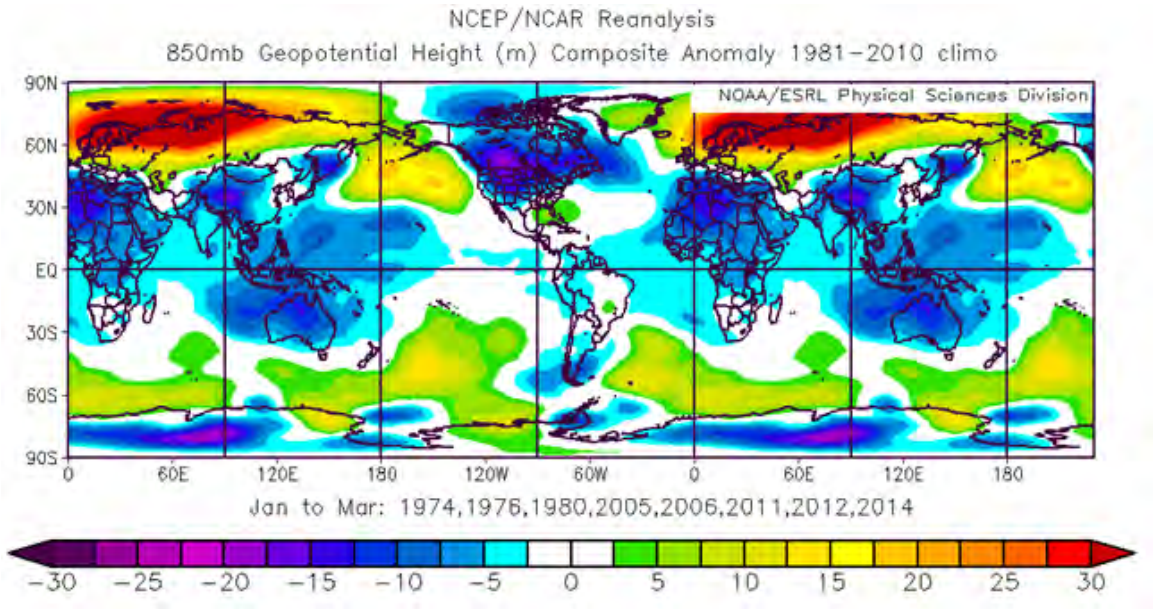

Figure 13. Anomalous JFM Z850 for 1970–2014 for warm years. Note the areas of positive (negative) anomalies throughout the Arctic and midlatitudes. The implied WAA (CAA) induced by these anomalies may have helped to produce the warm (cold) anomalies of T850 in Figure 12.

Figure 14 shows the warm composite anomaly of global JFM Z200. In comparing Figures 13 and 14, extratropical (tropical) vertical structures appear to be equivalent (non-equivalent) barotropic. We identified a possible PNA pattern in Figure 13. This pattern shows up nicely in Figure 14, and is indicated by the alternating negative and positive anomalies in Z200 (the Low near Hawaii, the High over the northern Pacific, the Low over Canada, and the weak High over the southeastern U.S.). This figure shows the negative phase of the PNA, which is

associated with the tropical cooling in Figure 12. Positive PNA patterns typically occur during EN events. These PNA patterns are teleconnections that typically occur during LN events (Murphree 2014c) and led us to investigate possible relationships between Arctic T and ENLN.

In Figure 14, alternating anomalies arch northward and eastward from the northern Pacific to Southeast Asia (the High over the northern Pacific, the Low over Canada, the High north of western Siberia, the Low over Eurasia, and the High over Southeast Asia), and resemble a Rossby wave train. The negative PNA pattern and wave train appear to constructively interfere with each other, which may also account for these strong height anomalies. The positive anomalies north of western Russian and the negative anomalies over central Asia may have induced an easterly component to the U200 field over northern Eurasia (see Figure 16), which indicates a possible weakening of the polar vortex. Consistent with Hoskins and Karoly (1981), and Lee et al. (2011b), we speculated that the anomalous stationary Rossby wave train may have been triggered by increased localized tropical convection in the western Pacific. This process may be related to high latitude warming that occurs over interannual time scales (cf. Serreze et al. 2000). Our speculations possibly refute those of Tang et al. (2013) that relate the change in winter atmospheric circulation to sea ice loss.

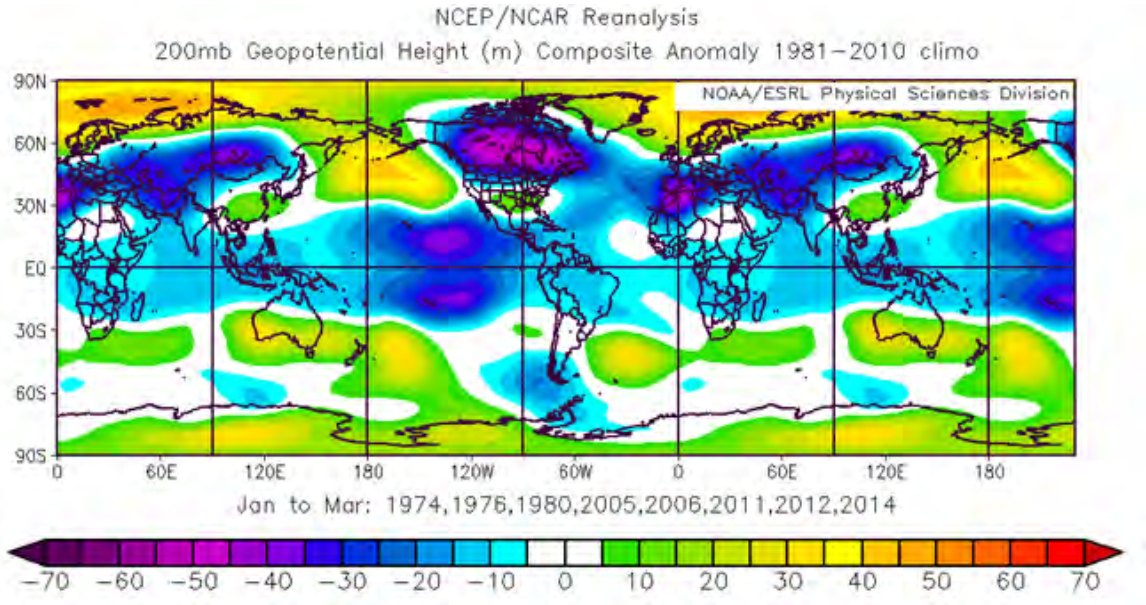

Figure 14. Anomalous JFM Z200 for 1970–2014 for warm years. Note the negative PNA pattern originating east of Hawaii, and the anomalous stationary wave train originating in the northern Pacific.

Figure 15 (16) shows the warm composite anomaly of global JFM U850 (U200) and areas of anomalous westerlies (Compare to the LTM in Figure 8(9)). The negative anomalies over Eurasia and Canada indicate a weakening of the westerlies, which may indicate a weakening of the polar vortex. (See Chapter I, Section C.1, and Chapter II, Section B.3 for more information on the polar vortex.) A weakening of the polar vortex may have resulted from a decrease in the pole-to-equator thermal gradient caused by the Arctic warming seen in Figure 12. A weak polar vortex may have allowed for the southward flow of cold air that resulted in cold T850 anomalies over central Asia and Canada (Figure 12). Our findings are consistent with Francis and Vavrus (2012), which suggest that the slower progression of upper-tropospheric waves (here the polar vortex) caused by Arctic warming, could cause associated weather patterns in the midlatitudes to be more persistent. We disagree however, with their claim that the surface ice-snow albedo feedback process may account for recent Arctic warming.

We have also found evidence (not shown) that the portion of the polar vortex over the northern Pacific may have shifted slightly northward, while the portion of the polar vortex over North America may have shifted slightly southward. It is unclear whether a northward or southward shift of the polar vortex had occurred over Eurasia. The tropical to subpolar anomalies in Figure 15 (16) are consistent with LN U850 (U200) anomalies.

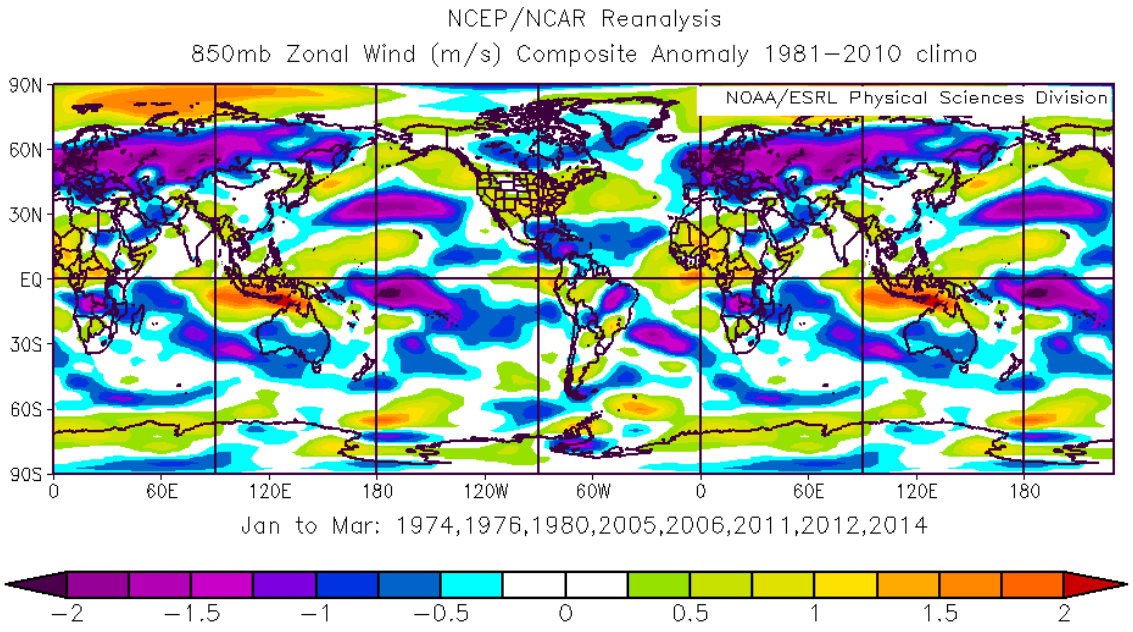

Figure 15. Anomalous JFM U850 for 1970–2014 for warm years. Note the negative anomalies over Eurasia and Canada. These anomalies indicate a weakening of the polar vortex due to the Arctic warming shown in Figure 12.

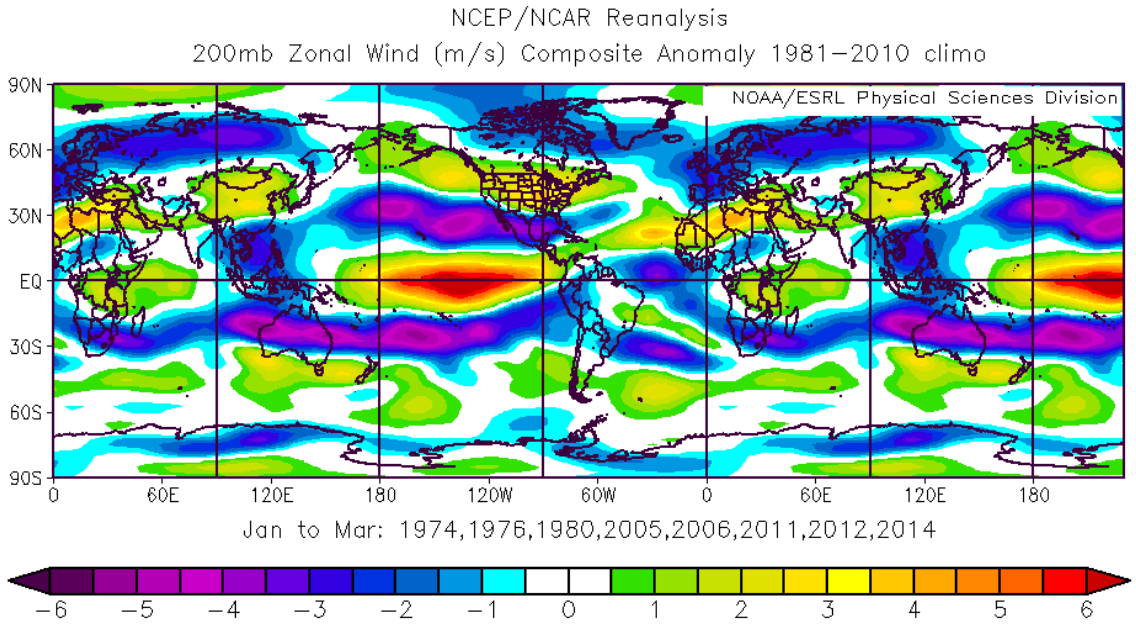

Figure 16. Anomalous JFM U200 for 1970–2014 for warm years. Note the negative anomalies over Eurasia and northern Canada. These anomalies indicate a weakening of the polar vortex due to the Arctic warming shown in Figure 12.

Figure 17 shows the warm composite anomaly of global JFM SST. Arctic SST is anomalously warm at all longitudes from 75N-90N, with southward extensions of warm water into the North Atlantic (Baffin Bay-northeastern U.S. coast-Scandinavia). Other regions of anomalously high SST are located in the northern and southern Pacific Ocean, and near the maritime continent in the western Pacific. Areas of anomalously cold SSTs extend across the central-eastern tropical Pacific, and Indian Oceans, and also along the west coasts of North and South America.

The SST patterns of Figure 17 are similar to the T850 patterns in Figure 12. (See Chapter II, Section B.3 for more information on this relationship.) These patterns also bear a strong resemblance to the SST patterns associated with LN events (Murphree 2014c). The strong positive anomalies in the Arctic Ocean and the strong negative anomalies in the central-eastern tropical Pacific suggest the possibility of a negative correlation between the SSTs in these regions, and likewise, a positive correlation between SSTs in the Arctic and the northern and

southern Pacific. This further suggests that a negative correlation exists between central-eastern tropical SST and Arctic T, and likewise a strong positive correlation between northern and southern Pacific SST and Arctic T. These results support our speculation that ENLN may contribute to interannual variations in Arctic T.

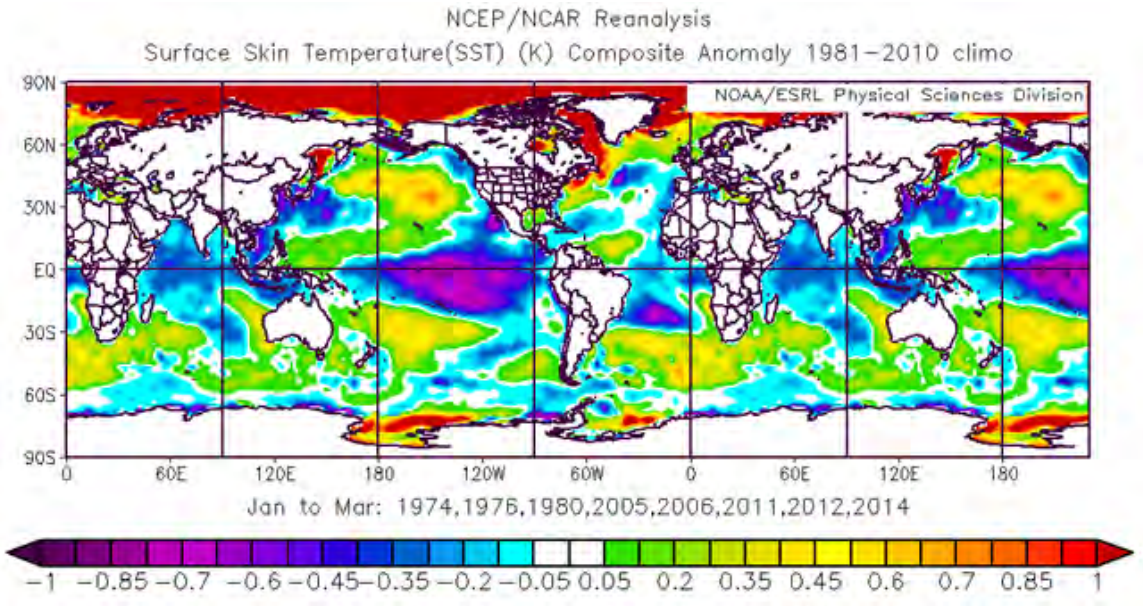

Figure 17. Anomalous JFM SST for 1970–2014 for warm years. Note the strong warm anomalies across the Arctic and the warm (cold) anomalies in the Pacific, Atlantic and Indian Oceans, and their similarities to T850 anomalies in Figure 12. Also note the similarities in these SST patterns, especially in the tropical Pacific and Indian Ocean, to SST patterns associated with ENLN.

Figure 18 shows the warm composite anomaly of JFM 200 hPa OLR. There are positive anomalies across much of the NH, north of the tropics, especially north of Siberia and western Russia. This positive anomaly makes dynamical sense because it occurred in a region of positive Z200 anomalies, and areas of high pressure are associated with high OLR and clear skies. The strongest OLR anomalies occur throughout the tropics. We can infer from these negative (positive) OLR anomalies that enhanced (suppressed) convection, and cloudy (clear) skies occurred over the western (central-eastern) tropical Pacific.

The anomalies in this figure are consistent with the corresponding anomalies seen in Figure 17 for SST, and the results of Lee (2011a, 2011b, 2012) related to tropical convection.

Lee (2012) suggests that there are two prominent internal processes that can stir the tropical atmosphere through convective heating: the MJO and ENLN, which is also consistent with Yoo et al. (2011), and the idea that convection over the western tropical Pacific warm pool is associated with a warming of the Arctic during the winter. The MJO is observed over seasonal to intraseasonal (S2S) time scales, and is related to patterns in OLR (Murphree 2014c). We speculate that analogous relationships may occur on interannual time scales (cf., L'Heureux and Higgins 2010). This speculation, and the anomalous warmth in the Arctic shown in Figure 12 which may have resulted from anomalous WAA inferred from Figure 13, help support the findings of Lee et al. (2011b). Their findings suggested that anomalous upper-tropospheric circulations in response to external forcing (tropical convective heating over the Indian and western Pacific Oceans), can bring about NH winter Arctic warming, by dynamical processes (Lee et al. 2011b).

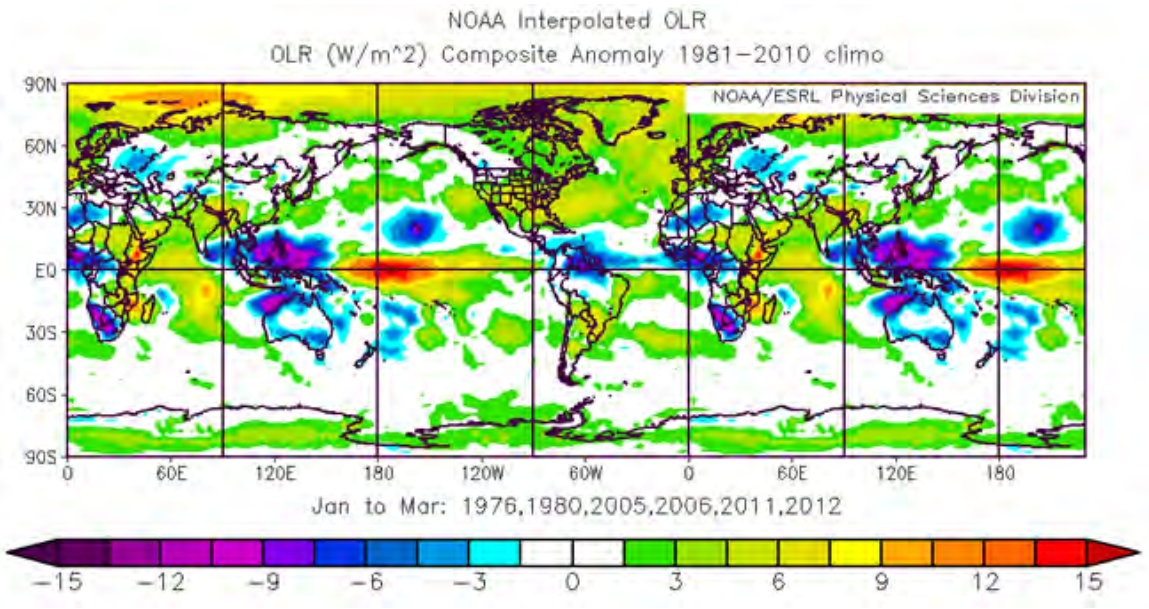

Figure 18. Anomalous JFM OLR for 1970–2014 for warm years. Note the positive anomalies across the Arctic Ocean, especially north of Siberia and western Russia. Note the strong negative (positive) OLR values in the western (central-eastern) tropical Pacific. The inferred convection patterns over the tropical Pacific and Indian Oceans are similar to those associated with LN.

Figure 19 is a comparison of the Z850 anomalies for the four warm years in Table 1 which were also LN years (warm/LN), and the original warm composite of eight years (same as Figure 13). The warm/LN anomalies in the top panel are in relatively similar locations as the anomalies in the bottom panel, however they are stronger. This difference was expected since not all of the eight warm years were characterized by LN conditions, and suggests that LN may have had an impact on Z850 in our eight warm years. The negative anomalies over North America are much stronger in the top panel than they are in the bottom panel, and are also seen over Greenland, and in the higher latitudes of the Arctic (approximately north of 80N) at all longitudes. These stronger negative anomalies for warm/LN may have allowed for an increase in WAA through the Greenland Sea area into the Arctic during these four years. This comparison suggests that during winter LN years, the Arctic is likely to be anomalously warmer that it would otherwise be without a LN present. Though the composites

in Figure 19 show that T850 may be associated with EN conditions, their differences help to show how EN is not the only climate variable affecting T850 in our composite of eight cold years.

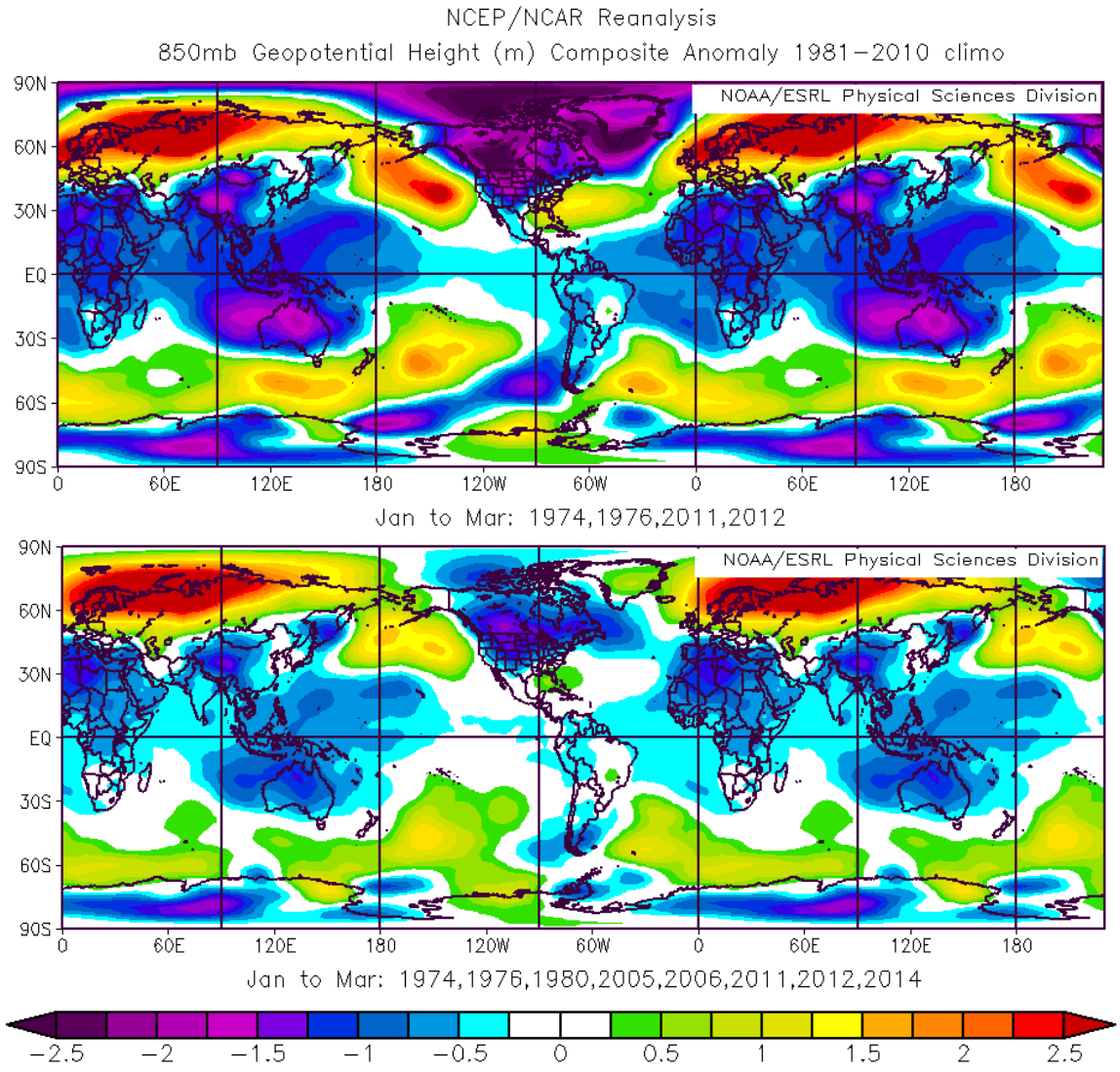

Figure 19. Anomalous JFM Z850 for 1970–2014 for: (top panel) four of the eight warm years in which LN events occurred; (bottom panel) eight warmest years of our study period, same as Figure 13. Note the stronger anomalies in the top panel, especially the negative anomalies over North America, Greenland, and the higher latitudes of the Arctic.

Figures 44 through 49, of the Appendix, show similar comparisons to those in Figure 19, but for the rest of our focus variables. In each of these figures, the warm/LN anomalies in the top panels were in relatively similar geographic locations as the anomalies in the original composites of our eight warm years, but were stronger. These similar yet stronger anomalies in the top panels were expected and show that the four LN events had an impact on each of the focus variables for our eight warm years, and that a relationship exists between ENLN and Arctic T.

D. COLD COMPOSITES

Similar to the methods used in Chapter III, Section C, we identified the eight coldest winters, four of which occurred during EN events, and averaged the anomalies for these eight years together to produce anomaly composites for our focus variables. These cold composite anomalies help to identify global scale anomalies in atmospheric and oceanic conditions associated with anomalously cold Arctic T.

Figure 20 shows the cold composite anomaly for JFM T850. From Table 2, we know that three strong EN events, one weak-moderate EN event, three neutral events, and one LN event occurred during these eight cold winters. In this figure, the Arctic is anomalously cold, especially from 0 to 150E. Cold Arctic anomalies are also seen over Canada, especially over the Canadian Archipelago. Weak negative anomalies in the Arctic occurred from about 170E to 120W. The negative anomalies occurred in areas that are normally very cold, indicating that the anomalies strengthened the normal T850 conditions in these areas. Weak cold anomalies also occurred over western Eurasia, and the central and western North Pacific. Warm anomalies occurred over central-eastern Asia and the Bering Strait in the NH, and indicate a weakening of the normal conditions in these areas. The net effect of negative anomalies in the Arctic and positive anomalies in parts of the sub-polar regions and midlatitudes, is to

strengthen the normal horizontal T850 gradient, which strengthens the polar vortex.

Some of these T850 anomalies in Figure 20, though weak, tend to occur in the NH during EN events. (Murphree 2012b, 2014c, ESRL 2015a). Like the warm composites of the previous section, these similarities let us to investigate the relationships between Arctic T and ENLN.

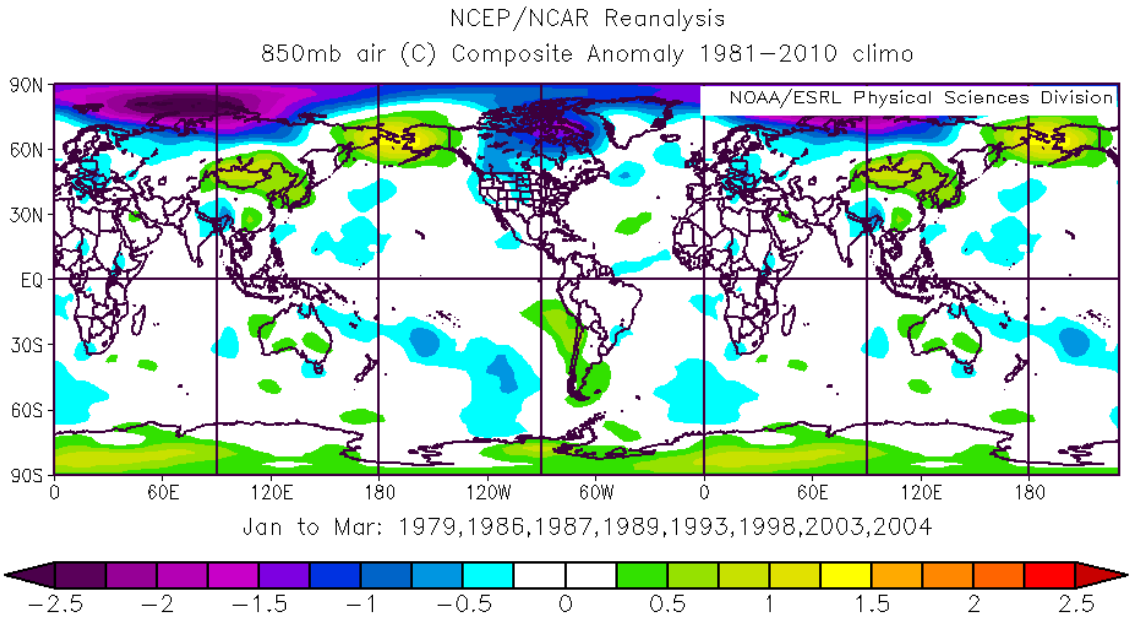

Figure 20. Anomalous JFM T850 for 1970–2014 for cold years. Note the areas of strong (weak) cold anomalies in the Arctic. Also note areas of warm (cold) anomalies in the midlatitudes. Anomalous T850 patterns shown here are similar to those of EN events.

Figure 21 shows the cold composite anomaly of global JFM Z850. In comparison to the LTM of Z850 in Figure 6, there are several areas of anomalously high and low heights. These anomalous heights revealed circulation patterns that helped produce the T850 anomalies in Figure 20. In Figure 21, the negative anomalies over Baffin Bay and Greenland indicate a strengthening of the Icelandic Low. These negative anomalies and the positive anomalies over Canada, and implied CAA, may have produced the cold T850 anomalies over

North America in Figure 20. The area of strong negative anomalies from about 60E to140E indicate a strengthening of the low heights over the Arctic in the Z850 LTM (Figure 6), and may be responsible for the cold T850 anomalies over the Arctic, north of Siberia. These negative Z850 anomalies and the positive anomalies over Scandinavia, and implied CAA, may have produced the cold T850 anomalies over parts of western Eurasia in Figure 20. The positive Z850 anomalies over Alaska and negative anomalies from 60E to 140E, and implied WAA into the Arctic, may have caused the cold T850 anomalies in the Arctic to be weak from 170E to 120W. The negative Z850 anomalies over the northeast Pacific indicate a strengthening of the Aleutian Low. The implied WAA on the eastern side of the Aleutian Low may have caused the warm T850 anomalies over the Bering Strait, while the implied CAA on the western side of the Aleutian Low may have caused the weak cold anomalies in the central and western North Pacific. The positive Z850 anomalies over Southeast Asia, and implied WAA, may have produced the warm T850 anomalies over central-eastern Asian in Figure 20.

Some of these Z850 anomalies in Figure 20, though weak, tend to occur in the NH during EN events, and led us to investigate the relationships between Arctic T and ENLN (Murphree 2012b, 2014c, ESRL 2015a).

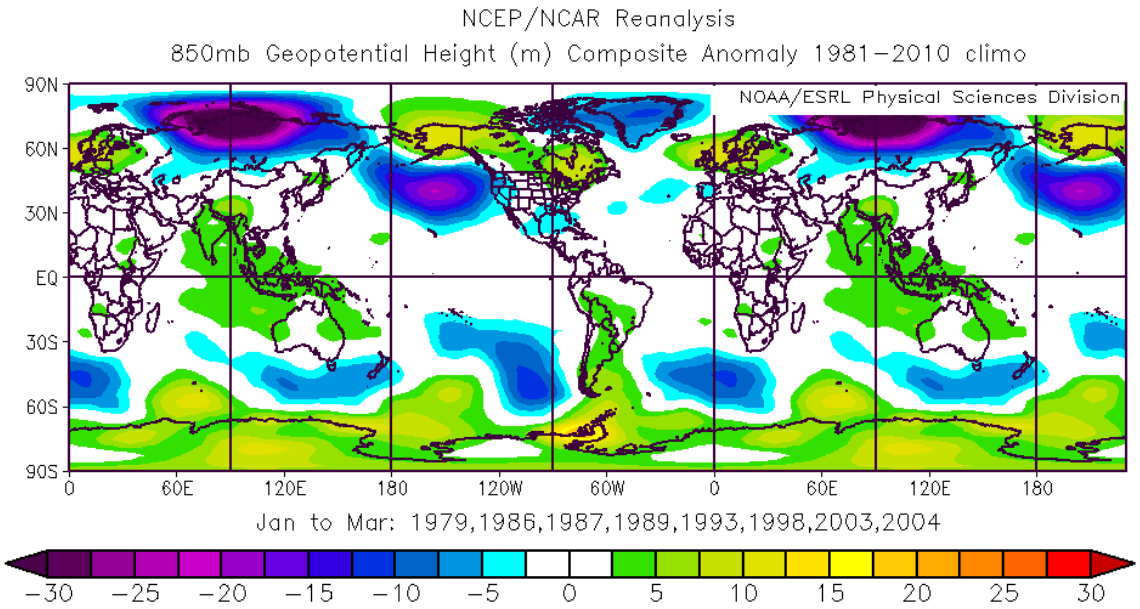

Figure 21. Anomalous JFM Z850 for 1970–2014 for cold years. Note the areas of positive (negative) anomalies throughout the Arctic and midlatitudes. The implied WAA (CAA) induced by these anomalies may have helped to produce the warm (cold) anomalies of T850 in Figure 20.

Figure 22 shows the cold composite anomaly of global JFM Z200. Comparing Figures 21 and 22, the extratropical (tropical) vertical structures appear to be equivalent (non-equivalent) barotropic, much like the warm composites had been, but opposite in sign. We identified a possible PNA-like pattern in Figure 22, which is indicated by the alternating positive and negative anomalies (the High near Hawaii, Low in the northeast Pacific, High over the Bering Strait, Low over the Canadian Archipelago, and weak High over southeast Canada). This pattern shows the positive phase of the PNA, which is normally associated with tropical warming. We do not see positive T850 anomalies in the tropics in Figure 20, however there are warm anomalies near the west coast of South America. Warm T850 anomalies in this area, and positive PNA patterns like the one in Figure 22, typically occurs during EN events, and led us to investigate possible relationships between winter Arctic T and ENLN (Murphree 2014c).

Similar to the wave train of Figure 14 of the warm composite, but opposite in sign, Figure 22 shows alternating anomalies that arch eastward and southward from the Bering Strait to Southeast Asia (the High over the Bering Strait, the Low over the Canadian Archipelago and Greenland, the High between Iceland and Scandinavia, the low over the Arctic and northern Siberia, the High over central-eastern Asia, and the Low over Southeast Asia), and resemble a Rossby wave train. The positive PNA pattern and wave train appear to constructively interfere with each other, which may also account for these strong height anomalies. Like the warm Z200 composite in Figure 14, we speculate that the Rossby wave train may have been triggered by localized tropical convection. However, we suspect the convection may have originated over the central-eastern tropical Pacific, vice the western Pacific because of the possible association with EN.

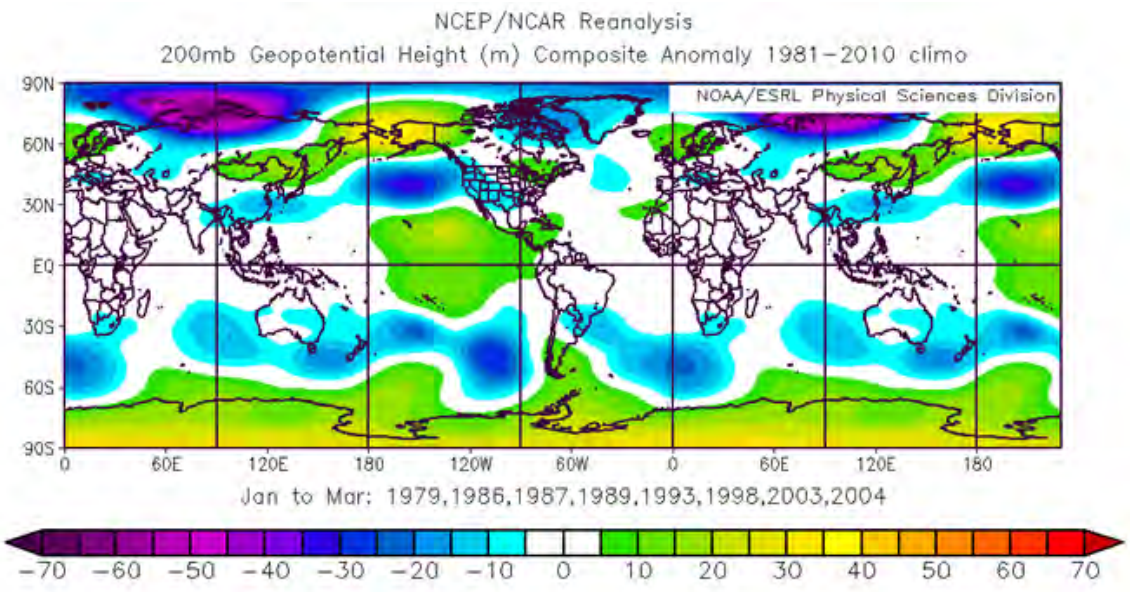

Figure 22. Cold composite anomaly of global Z200 for cold years. Note the positive PNA pattern originating east of Hawaii, and the stationary anomalous Rossby wave train from the Bering Strait, and arching eastward and southward toward Southeast Asia.

Figure 23 (24) shows the cold composite anomaly of global JFM U850 (U200), and areas of anomalous westerlies (Compare to the LTM in Figure 8 (9)). The anomalies in Figure 23 (24) are centered in locations similar to the anomalies of zonal wind in Figure 15 (16) for the warm years, however they are opposite in sign.

The positive anomalies over Eurasia and eastern Canada indicate a weakening of the westerly's, which may indicate a strengthening of the polar vortex. A strengthening of the polar vortex may have resulted from an increase in the pole-to-equator thermal gradient caused by the net Arctic cooling seen in Figure 20. A strong polar vortex may have allowed cold Arctic air to remain in the Arctic region, especially north of 75N. When the polar vortex is strong, interactions between the Arctic and midlatitudes is less apparent, which could account for the weaker T850 anomalies in Figure 20 when compared to the anomalies in Figure 12.

We have also found evidence (not shown) that the portion of the polar vortex over the northern Pacific may have shifted slightly northward, while the portion of the polar vortex over North America may have shifted slightly southward. It is unclear whether a northward or southward shift of the polar vortex had occurred over Eurasia. The tropical to subpolar anomalies in Figures 23 (24) are consistent with EN U850 (U200) anomalies

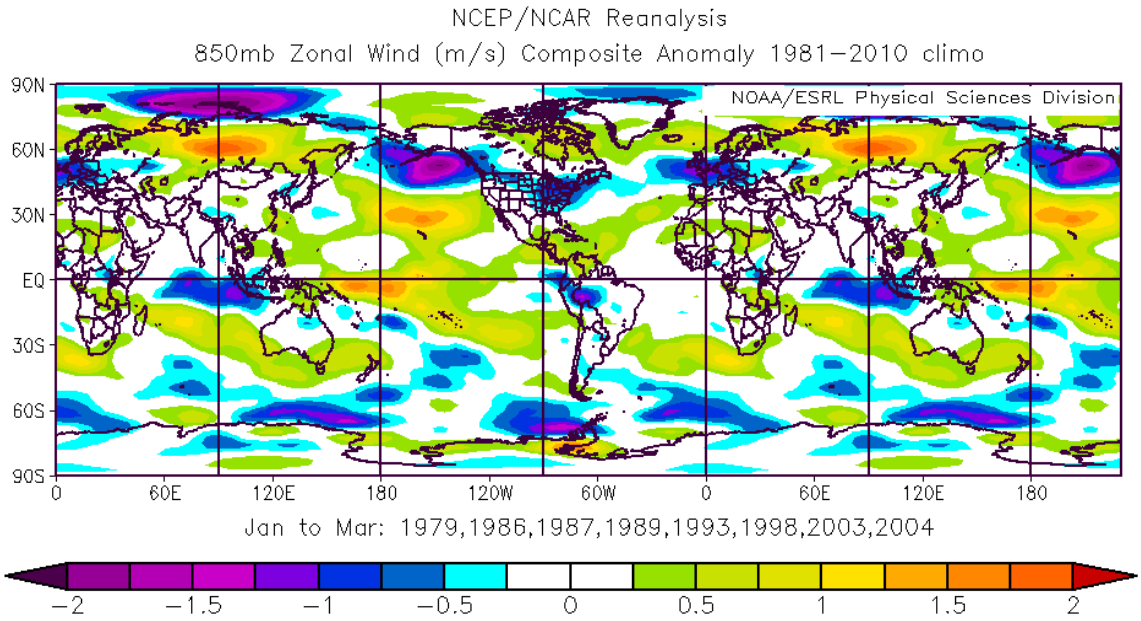

Figure 23. Anomalous JFM U850 for 1970–2014 for cold years. Note the positive anomalies over Eurasia and eastern Canada. These anomalies indicate a strengthening of the polar vortex due to the Arctic cooling shown in Figure 20.

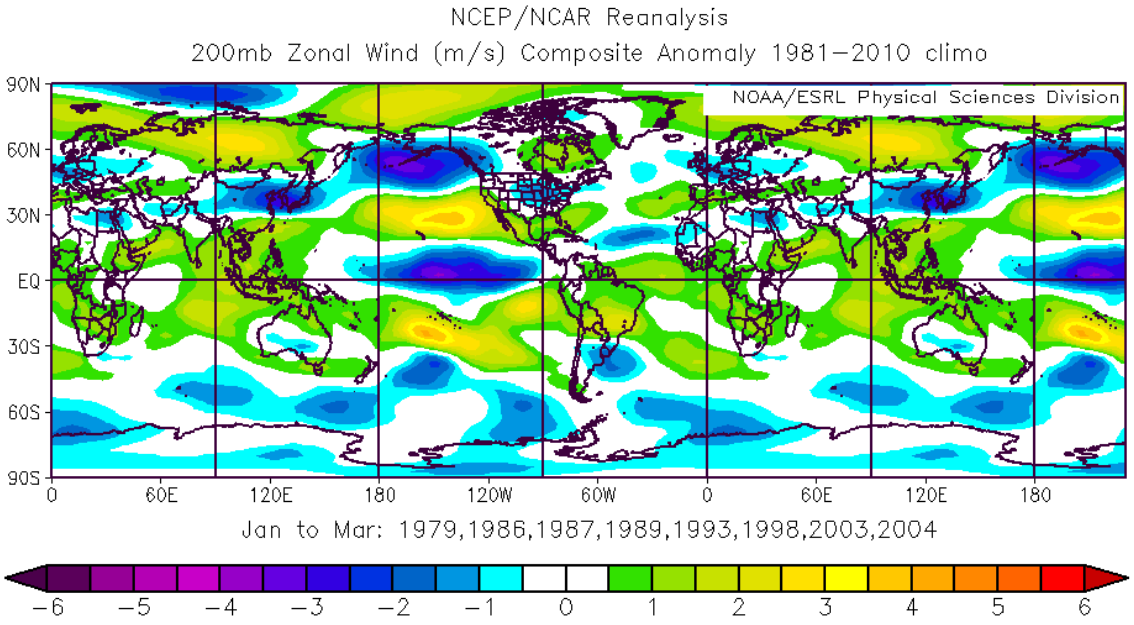

Figure 24. Anomalous JFM U200 for 1970–2014 for cold years. Note the positive anomalies over Eurasia and eastern Canada. These anomalies indicate a strengthening of the polar vortex due to the Arctic cooling shown in Figure 20.

Figure 25 shows the cold composite anomaly of global SST. Arctic SST is anomalously cold at all longitudes from 75N–90N however the coldest anomalies extend from 90N southward to the northern Siberia coast, and west coast of Iceland. Weak cold anomalies extend southward around Scandinavia. Other regions of anomalously cold SST are located in the northern and southern Pacific Ocean, the central North Atlantic and tropical Atlantic, the Indian Ocean, and near the maritime continent in the western Pacific. Areas of anomalously warm SSTs are located in the sub-polar regions (Bering Strait, southern Baffin Bay-Greenland). Other areas of warm SSTs extend across the central-eastern tropical Pacific, and Indian Oceans, and also along the northern west coast of South America.

The SST patterns in Figure 25 are similar to the T850 patterns in Figure 20 (see Chapter II, Section B.3 for more information on this relationship). Some of these patterns, especially those in the Pacific and Indian Oceans, bear a strong resemblance to the SST patterns associated with EN events (Murphree 2014c). The strong negative anomalies in the Arctic Ocean and strong positive anomalies in the central-eastern tropical Pacific suggest a possible negative correlation between the SSTs in these regions, and suggest that a weak negative correlation may exist between tropical SST and Arctic T850 during cold Arctic winters. These relationships could suggest that ENLN may contribute to internal variations in Arctic T.

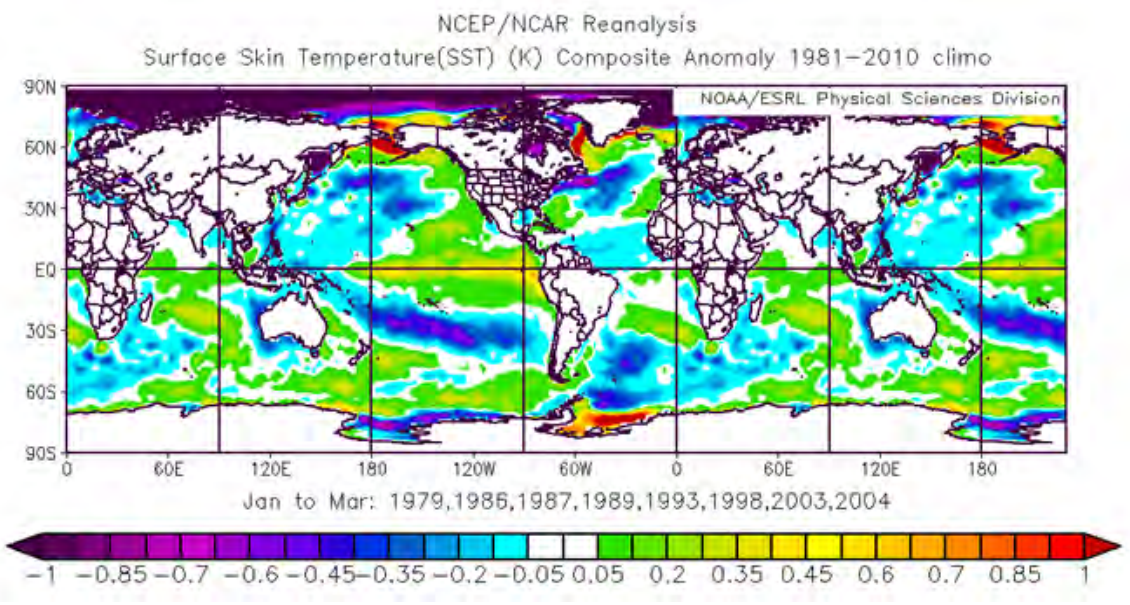

Figure 25. Anomalous JFM SST for 1970–2014 for cold years. Note the strong cold anomalies across the Arctic and the warm (cold) anomalies in the Pacific, Atlantic and Indian Oceans, and their similarities to T850 anomalies in Figure 20. Also note the similarities in these SST patterns, especially in the tropical Pacific and Indian Ocean, to SST patterns associated with ENLN.

Figure 26 shows the cold composite anomaly of global JFM 200 hope OLR. There are weak positive anomalies across much of the NH, however there are negative anomalies over the Arctic, especially over the Arctic Ocean north of Siberia and western Russia. This area of negative anomalies makes dynamic sense because it occurred in a region of negative Z200 anomalies, and areas of low pressure are associated with low OLR and cloudy skies. The strongest OLR anomalies occur throughout the tropics. We can infer from these negative (positive) OLR anomalies that enhanced (suppressed) convection, and cloudy (clear) skies occurred over the central-eastern (western) tropical Pacific. The anomalies in this figure, like the warm composite anomalies in Figure 17, are consistent with the corresponding SST anomalies, and the results of Lee (2011a, 2011b, 2012) related to tropical convection. The patterns in the OLR anomalies of Figure 26 show patterns similar to the OLR anomalies associated with ENLN, and suggest a relationship between ENLN and Arctic T.

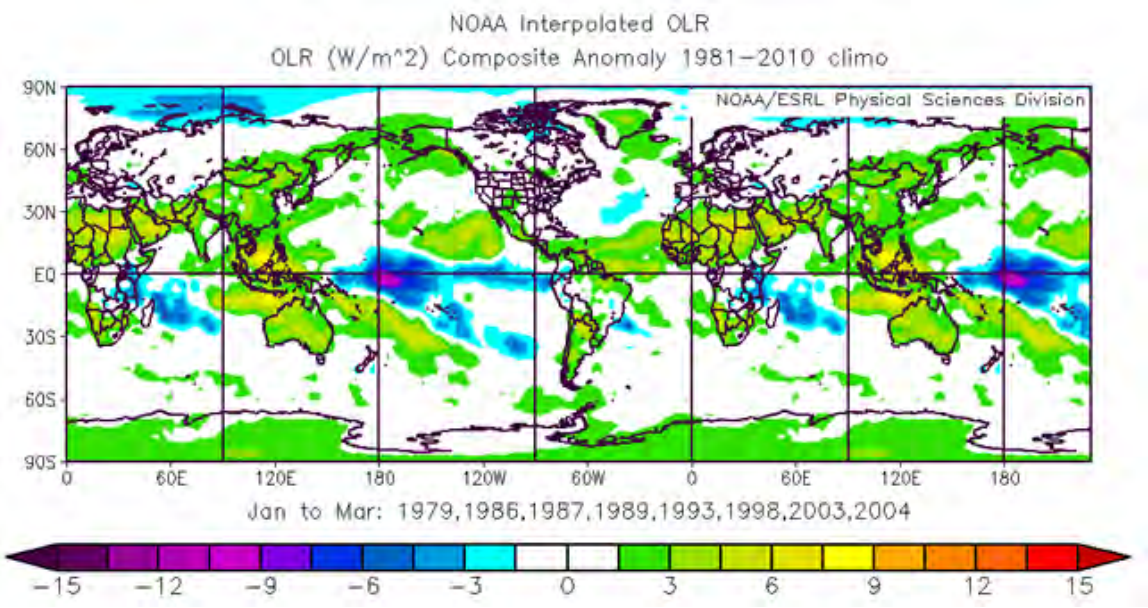

Figure 26. Anomalous JFM OLR for 1970–2014 for cold years. Note the negative anomalies across the Arctic Ocean, especially north of Siberia and western Russia. Note the strong negative (positive) OLR values in the central-eastern (western) tropical Pacific. The inferred convection patterns over the tropical Pacific and Indian Oceans are similar to those associated with EN.

As we did with the warm /LN composites of Chapter III, Section 2, we also created cold/EN composites and compared them to the original cold composites for our eight cold years. These comparisons show the possible impact EN might have on the eight coldest winters of our study period. Figure 27 is a comparison of the T850 composite for the four cold/EN years (top panel) to the original cold composite from Figure 20 (bottom panel). The anomalies in the top panel are in similar locations as the anomalies in the bottom panel but appear stronger, especially throughout the Pacific and Atlantic Oceans. This was expected because not all of the eight cold years were characterized by EN conditions. We also noticed that the positive anomalies over Alaska extend eastward and southward across Canada in the top panel, however the T850 anomalies across Canada in the bottom panel is anomalously cold.

Though these composites reveal T850 distributions that may be associated with EN conditions, their differences help to show that EN is not the

only climate variation affecting T850 in our composite of eight cold years. This comparison also suggests that during winter EN years, the Arctic is likely to be anomalously colder than it would otherwise be without an EN present. As expected, the Z850 anomalies that helped to produce the T850 anomalies in Figure 27 were also stronger for cold/EN years when compared to the original composite for our eight cold years. (See Figure 47 of the Appendix for this comparison.)

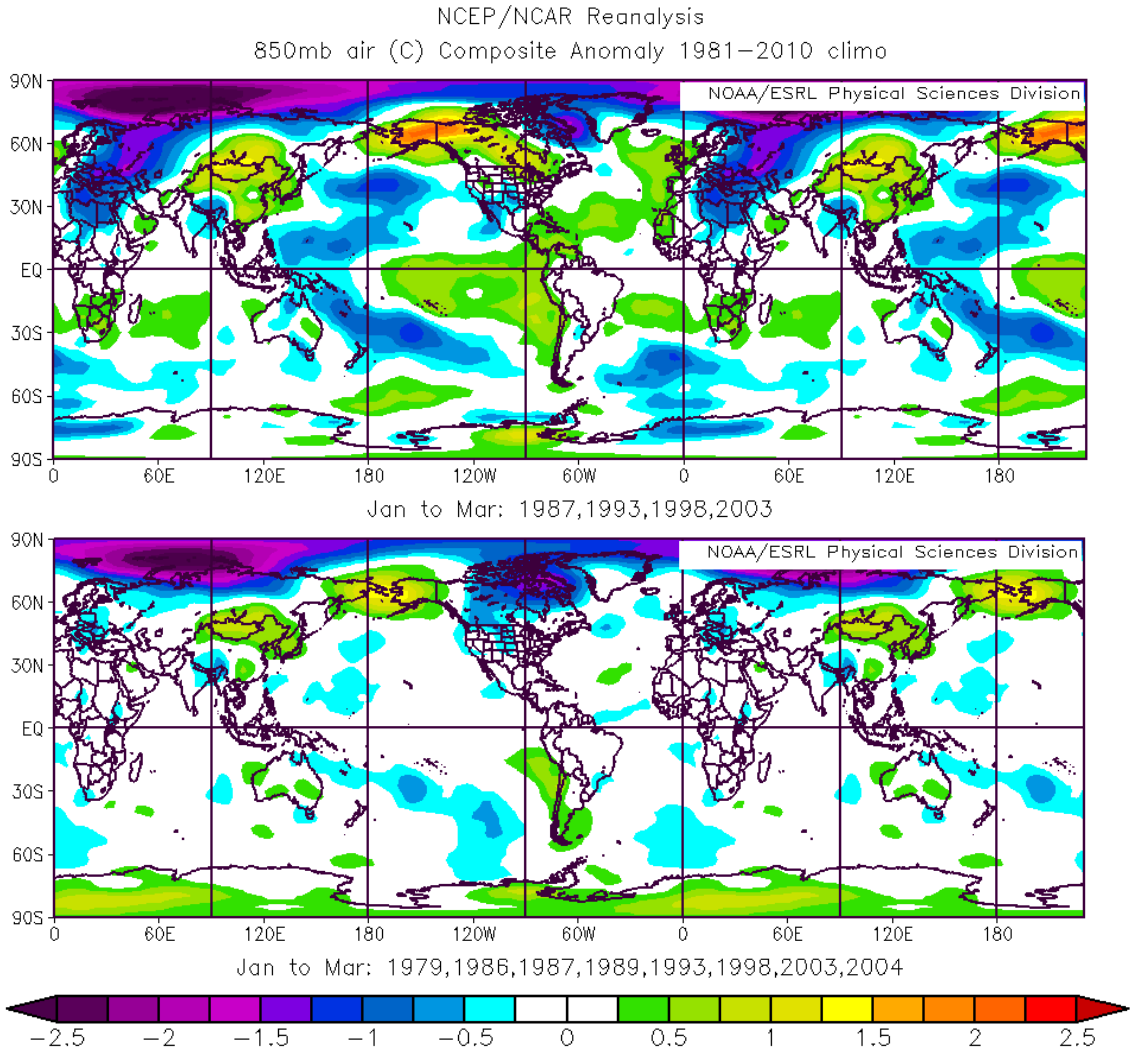

Figure 27. Anomalous JFM Z850 for 1970–2014 for: (top panel) four of the eight cold years in which EN events occurred; (bottom panel) eight coldest years of our study period, same as Figure 20. Note the stronger anomalies in the top panel, especially the positive anomalies over Alaska and Canada, Greenland, and lack of strong anomalies throughout the Pacific and Atlantic Oceans.

Figures 50 through 55, of the Appendix, show similar comparisons to Figure 27 but for the other focus variables. In each of these figures, the cold/EN anomalies in the top panels were in relatively similar geographic locations as the anomalies in the original composites of our eight cold years, but were stronger. These similar yet stronger anomalies in the top panels were expected and show that the four EN events may have had an impact on each of the focus variables for our eight cold years, and suggest a relationship between ENLN and Arctic T.

E. WARM VS. COLD COMPOSITES

Thus far we have analyzed the warm winter and cold winter composite anomalies separately. By comparing the warm and cold composites to each other, we would reasonably expect to see anomalies in relatively similar locations, but opposite in value if there is an association to ENLN. By opposite we mean that at the relatively the same location, anomalies should be positive (negative) for the warm (cold) composites, and vice versa. Areas of opposite anomalies make sense because anomalous conditions associated with LN tend to opposite to anomalous conditions associated with EN

Figure 28 compares the composite anomalies of T850 for the eight warm years (top panel) to the anomalies of T850 for the eight cold years (bottom panel). Figure 29 shows a similar comparison, but for SST instead of T850. We chose to show these two figures because of the relationships between T850 and SST discussed in Chapter II, Section B.3. Figures 56 through 60, of the Appendix, show similar comparisons of the warm (cold) year composite anomalies for the rest of the focus variables.

In Figure 28, the Arctic is anomalously warm (cold) in the top (bottom) panel. Warm (cold) anomalies seen in the midlatitudes over Eurasia are strong (weak) in the top (bottom) panel. Warm (cold) anomalies over the northern and southern Pacific Ocean and parts of the west coast of North America are strong (weak) in the top (bottom) panel. The patterns in T850 in both panels resemble patterns associated with ENLN (see Chapter III, Section C-D). We suspect that

these areas of opposite anomalies suggest that the four LN (EN) events which occurred during our eight warm (cold) winters may have influenced Arctic T. We further suspect that the stronger anomalies in the top panel show that LN may have a larger impact on Arctic T than EN.

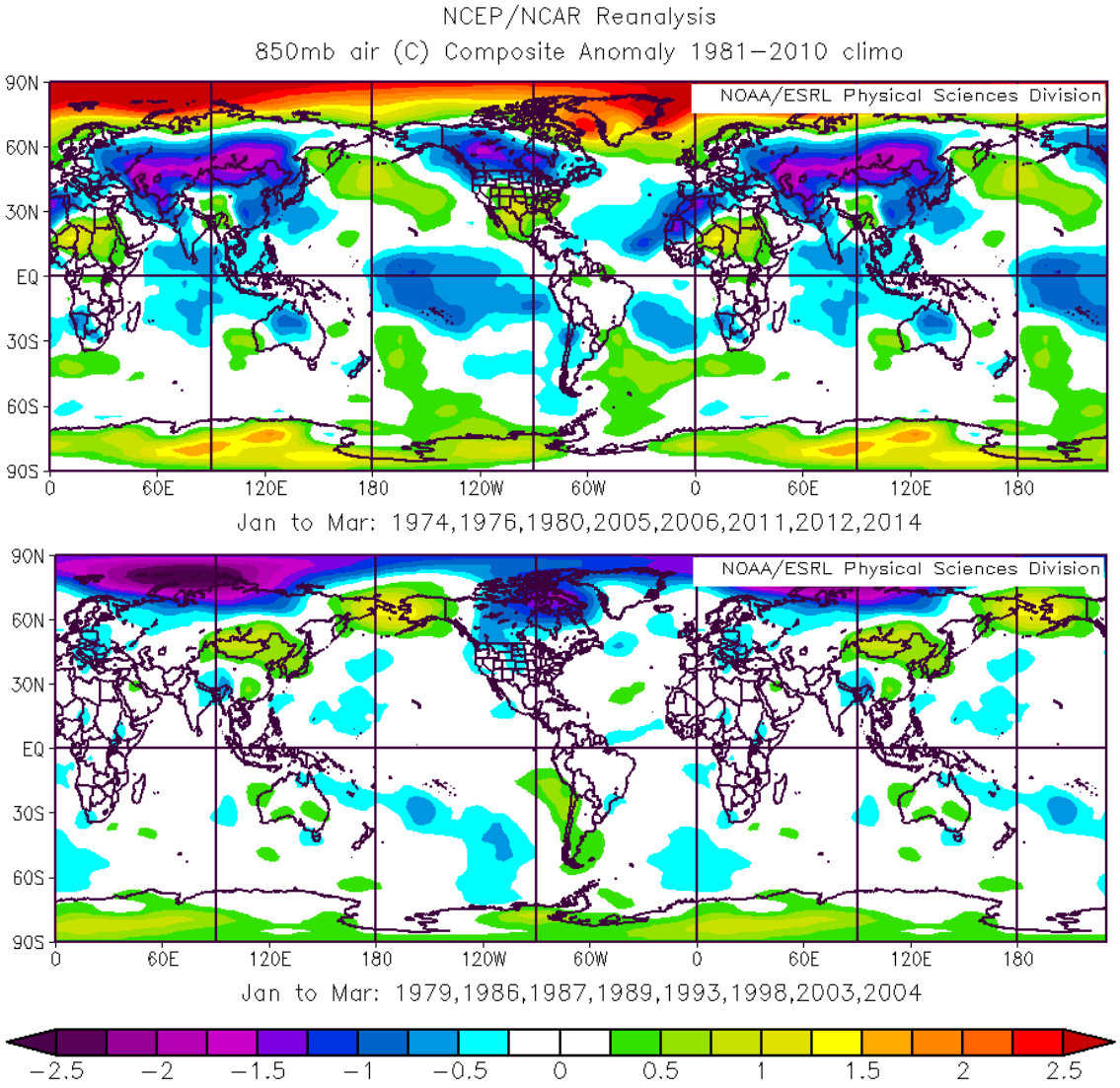

Figure 28. Comparison anomalous JFM T850 for warm and cold years. The top panel shows the anomalies in T850 that occurred during our eight warm years. The bottom panel shows the anomalies in T850 that occurred during our eight cold years. Note the opposite anomalies and their differences in strength. The top (bottom) panel reveals LN (EN) conditions throughout the midlatitudes, subtropics, and tropics.

Similar to the results seen in Figure 28, Figure 29 shows that the Arctic SSTs are anomalously warm (cold) in the top (bottom) panel. Strong LN (EN) SST signatures can also be seen in this figure throughout the Indian Ocean, Pacific Ocean, and Atlantic Ocean in the top (bottom) panel (cf. Murphree 2014c).

The results shown in Figures 28 and 29 suggest possible negative correlations between ENLN and Arctic T. It is important to note that not every area in the warm (cold) composites of Figures 28 and 29 show opposite anomalies. For example, SST anomalies near the Bering Strait and the southern portions of Baffin Bay in Figure 29 do not appear to be opposite. It is hard to tell from our analysis what is influencing these anomalies. These discrepancies tell us that other conditions besides those associated with ENLN may be influencing SST in these regions, and may also be influencing Arctic T. These need to be explored in future research.

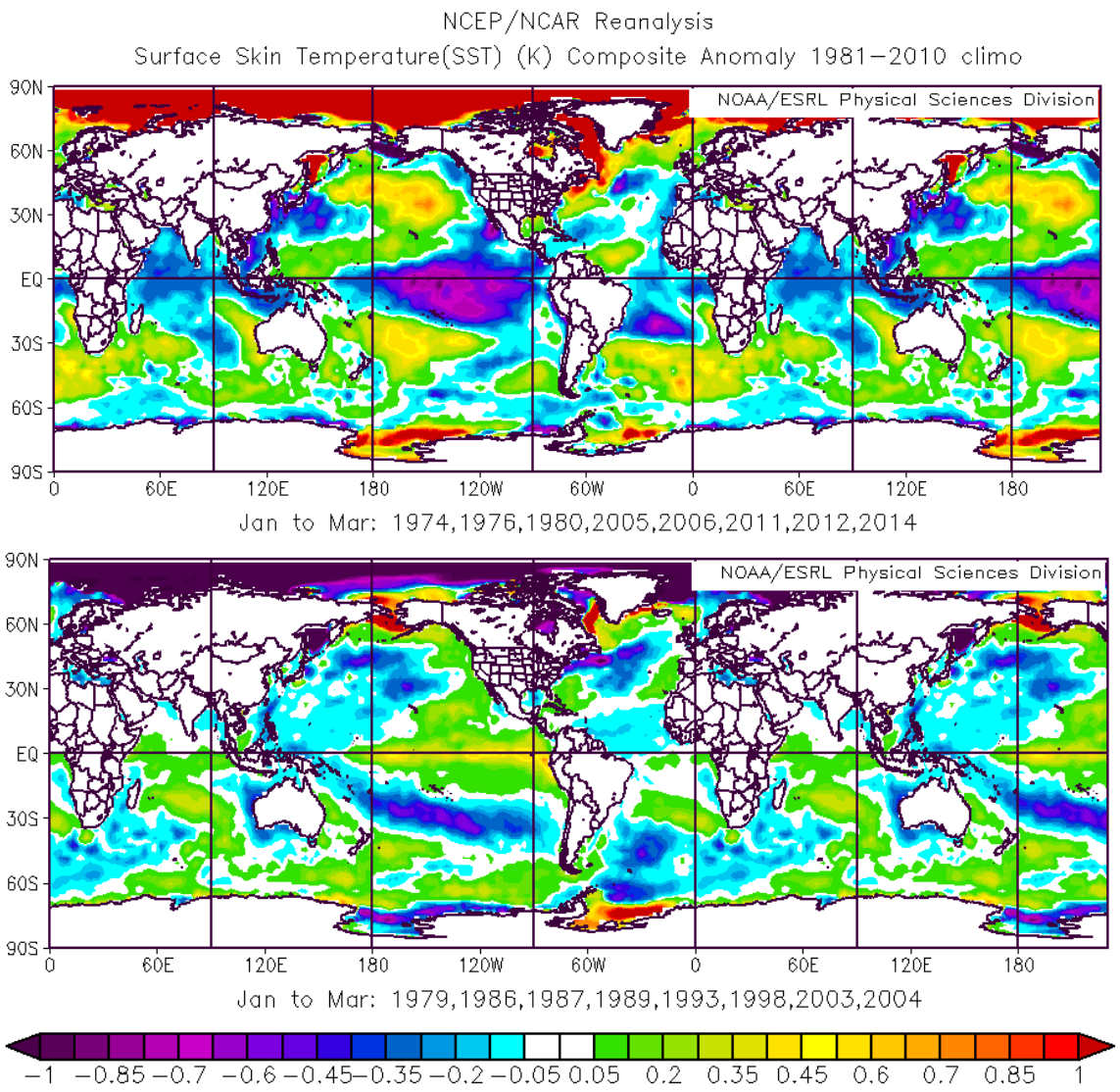

Figure 29. Comparison of anomalous JFM SST for warm and cold years. The top panel shows the anomalies in SST that occurred during our eight warm years. The bottom panel shows the anomalies in SST that occurred during our eight cold years. Note opposite anomalies and their differences in strength. The top (bottom) panel reveals warm (cold) Arctic SSTs, and strong (weak) LN (EN) conditions throughout the midlatitudes, subtropics, and tropics.

F. ZONAL WIND CROSS-SECTION COMPOSITES

Figures 30 through 35 are a series of zonal wind cross sections for our eight warm (cold) years, warm/LN (cold/EN) years, and the eight years in which the strongest LN (EN) events occurred during our study period 1970-2014. These cross section plots confirm our results from Chapter III, Section C regarding the strengthening (weakening) of the polar vortex during the eight coldest (warmest) years of our study period. A cross section for the JFM LTM of zonal wind can be seen in Figure 61 of the Appendix. Please refer to this figure when comparing the following zonal wind anomalies to normal conditions.

In Figures 30 and 31, the large area of negative anomalies surrounding 60N indicates a weakening of the westerlies in this region throughout the troposphere, which suggests a weakening of the polar vortex. Evidence of these weak westerlies were also shown in Figures 15 (16) in Chapter III, Sections C. It is important to note that this negative anomaly is strongest for the composite of eight warm years in Figure 30. This anomaly has weakened in the warm/LN composite (Figure 31), and further weakened in the composite of the years in which the eight strongest LN events occurred (Figure 32). These composites suggest a relationship between LN and a weak polar vortex.

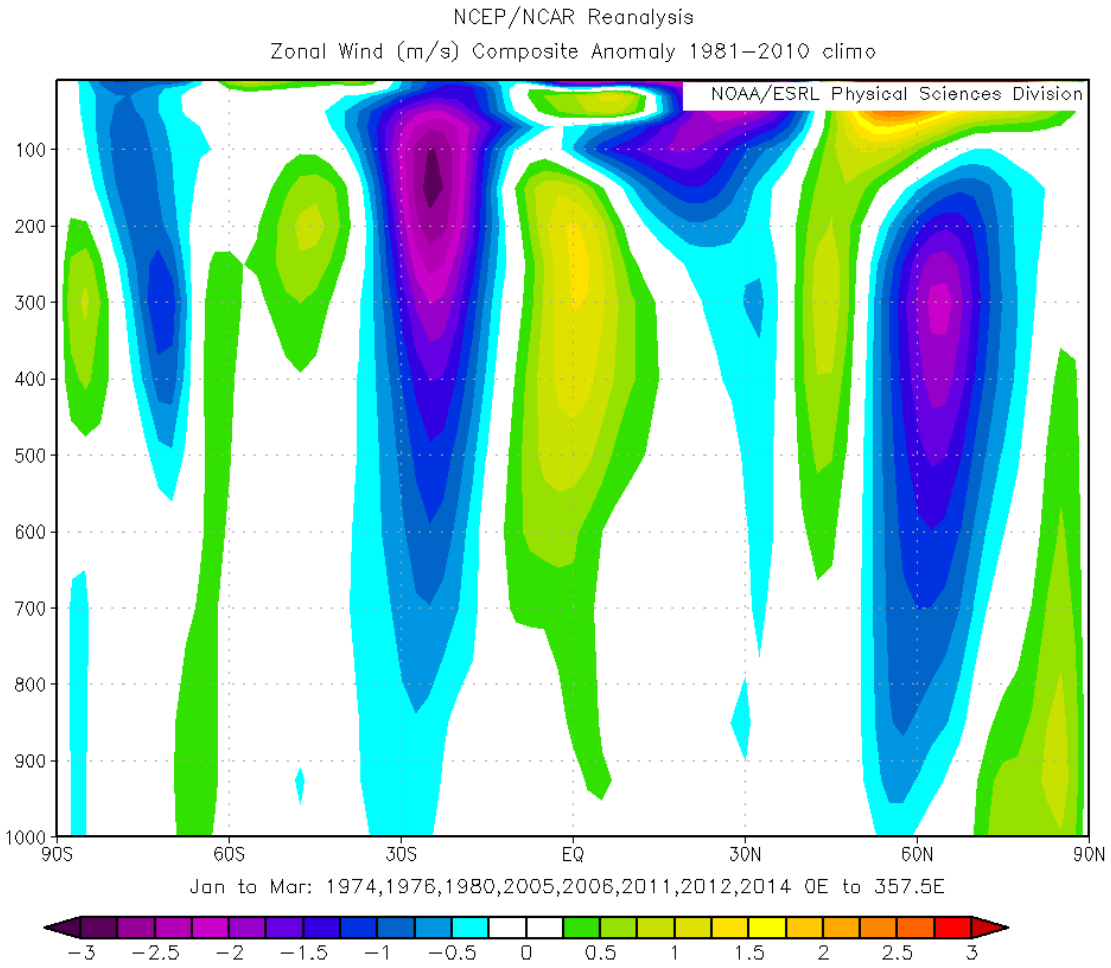

Figure 30. Cross section of anomalous JFM zonal wind from 1000 hPa to 100 hPa for warm years. Note the strong negative anomalies from about 55N to 70N. These anomalies indicate a weakening of the polar vortex.

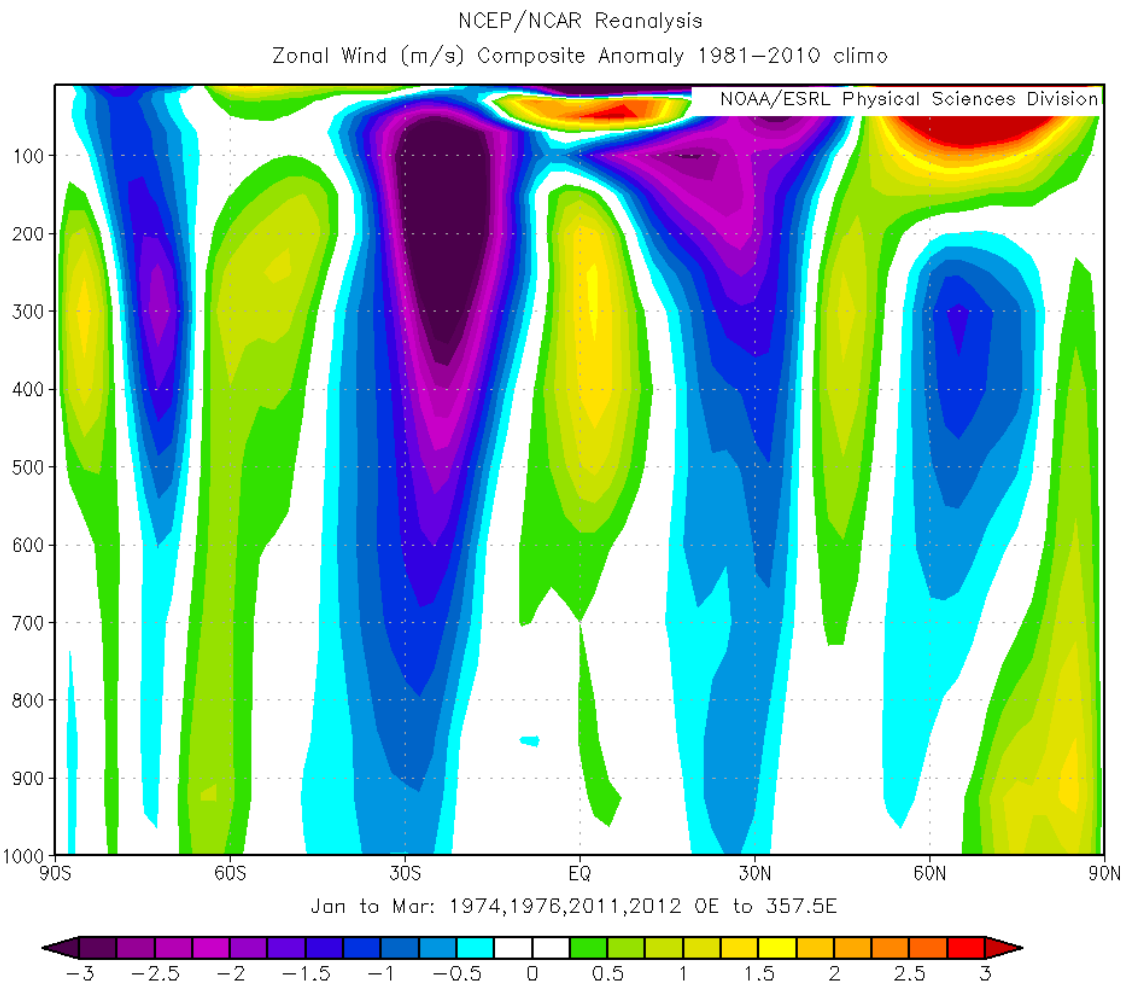

Figure 31. Cross section of anomalous JFM zonal wind from 1000 hPa to 100 hPa for warm/LN years. Note the negative anomalies from about 55N to 75N. These anomalies indicate a weakening of the polar vortex.

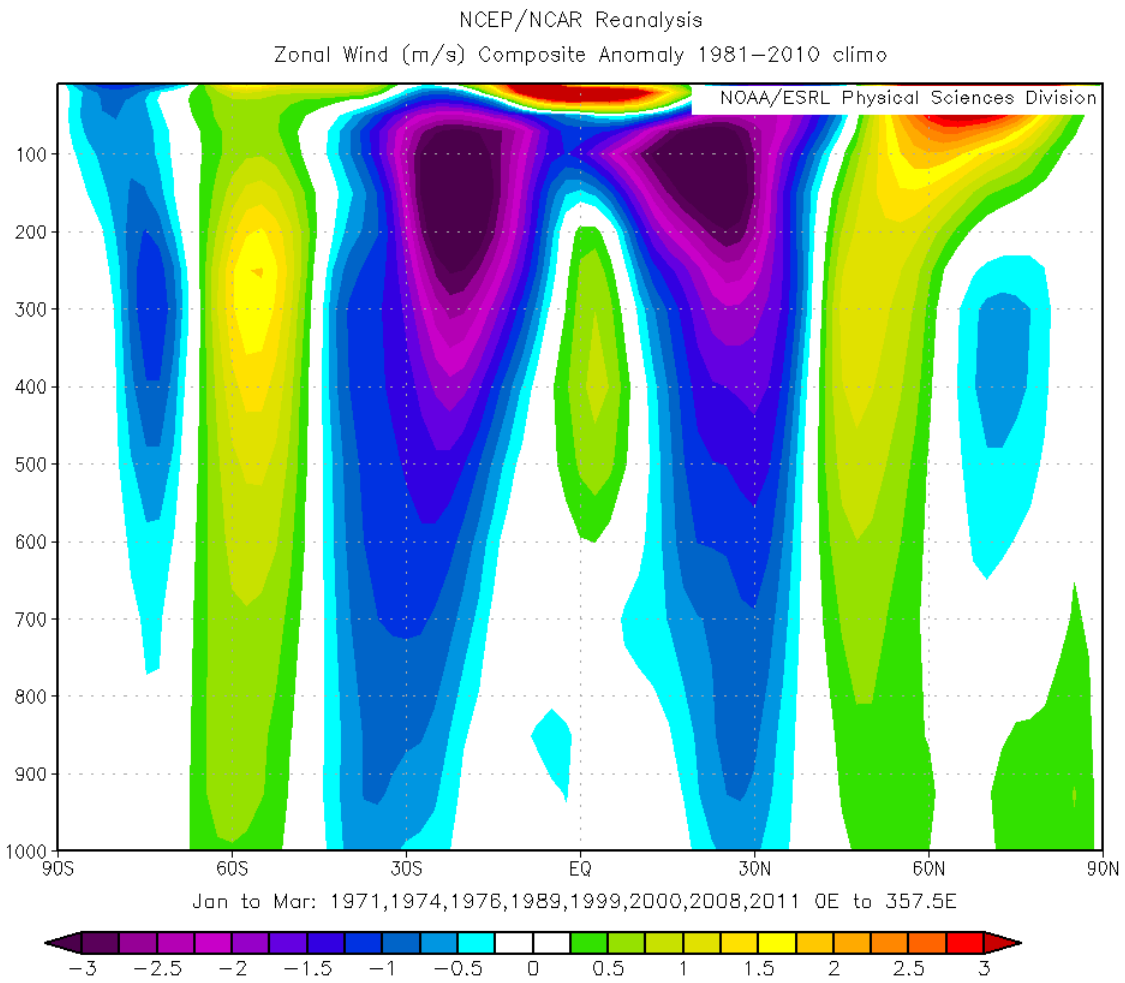

Figure 32. Cross section of anomalous JFM zonal wind from 1000 hPa to 100 hPa for the eight strongest LN years of our study period. Note the negative anomalies from about 65N to 80N. Though weak, these anomalies indicate a weakening of the polar vortex

In Figures 33 through 35, the large area of positive anomalies from about 60N-75N indicates a strengthening of the westerlies throughout the troposphere in this region, which suggests a strengthening of the polar vortex. Evidence of these strong westerlies was also shown in Figures 23 (24) in Chapter III, Sections D. It is important to note that this positive anomaly is strongest for the cold/EN composite in Figure 34, and suggests EN may play a role in strengthening the polar vortex during these four years of our study period. The combined results from Figures 30 through 35 suggest that ENLN may have

played a role in changing the normal conditions of the polar vortex. However, EN may have played a larger role during the cold/EN years than LN had in the warm/LN years. Further research is needed to quantify the effect of ENLN on the polar vortex.

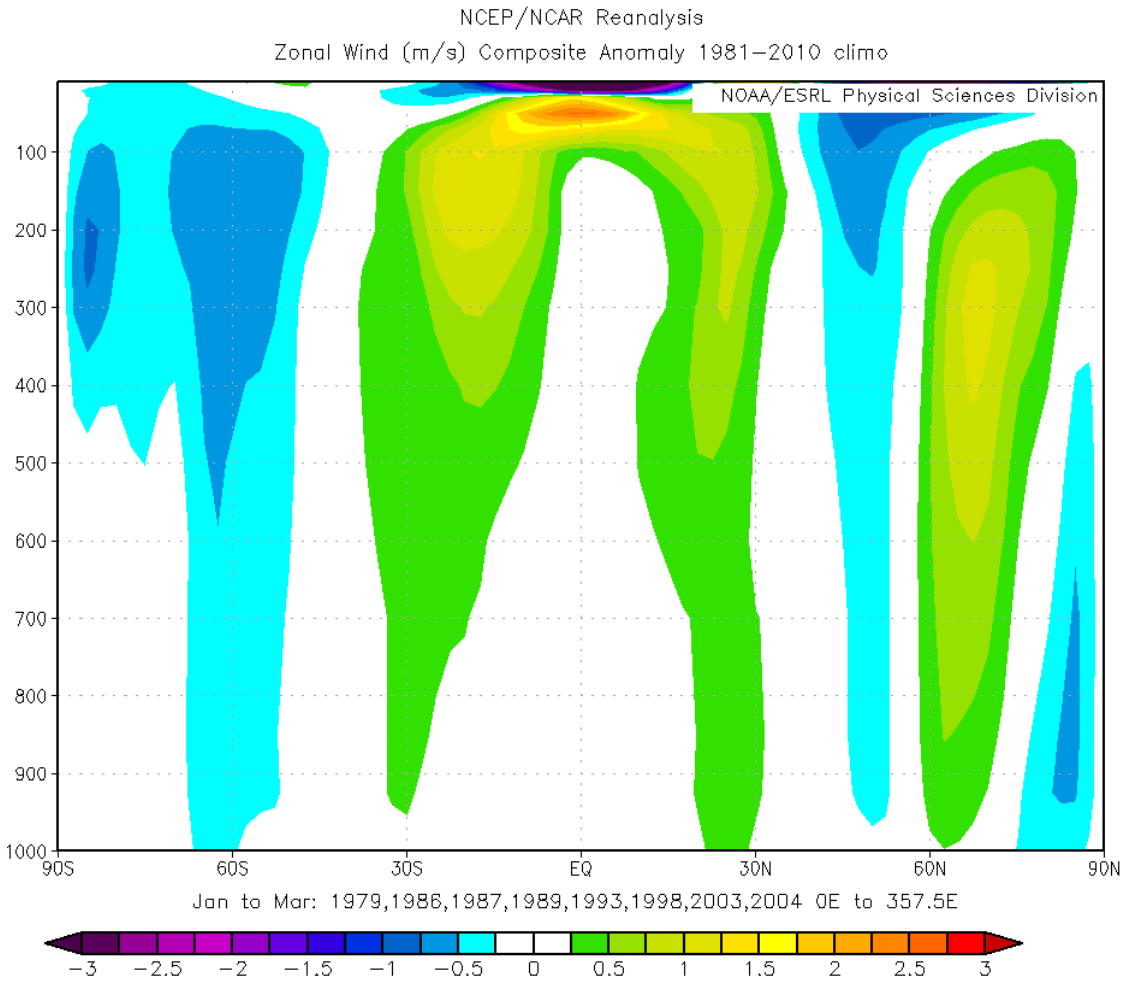

Figure 33. Cross section of anomalous JFM zonal wind from 1000 hPa to 100 hPa for cold years. Note the positive anomalies from about 60N to 75N. These anomalies indicate a strengthening of the polar vortex.

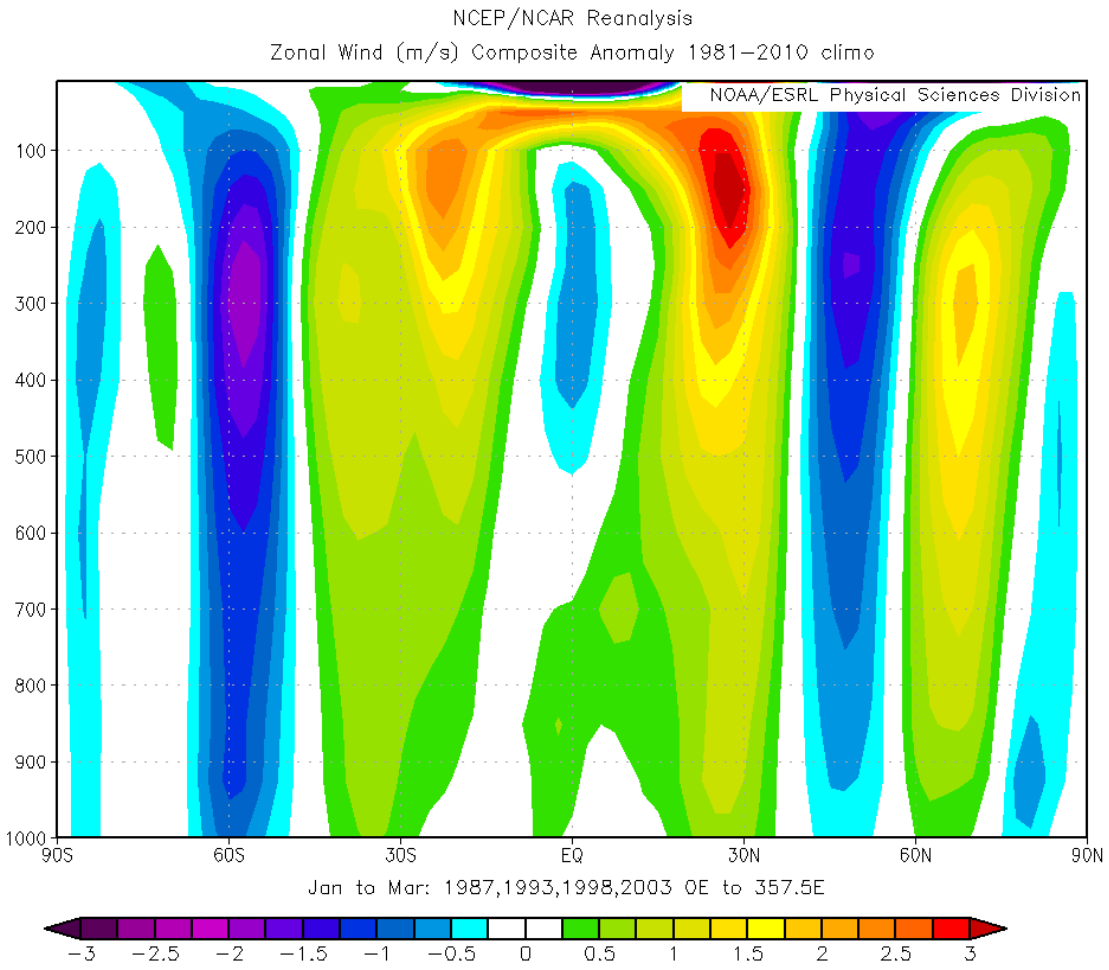

Figure 34. Cross section of anomalous JFM zonal wind from 1000 hPa to 100 hPa for cold/LN years. Note the strong positive anomalies from about 60N to 75N. These anomalies indicate a strengthening of the polar vortex.

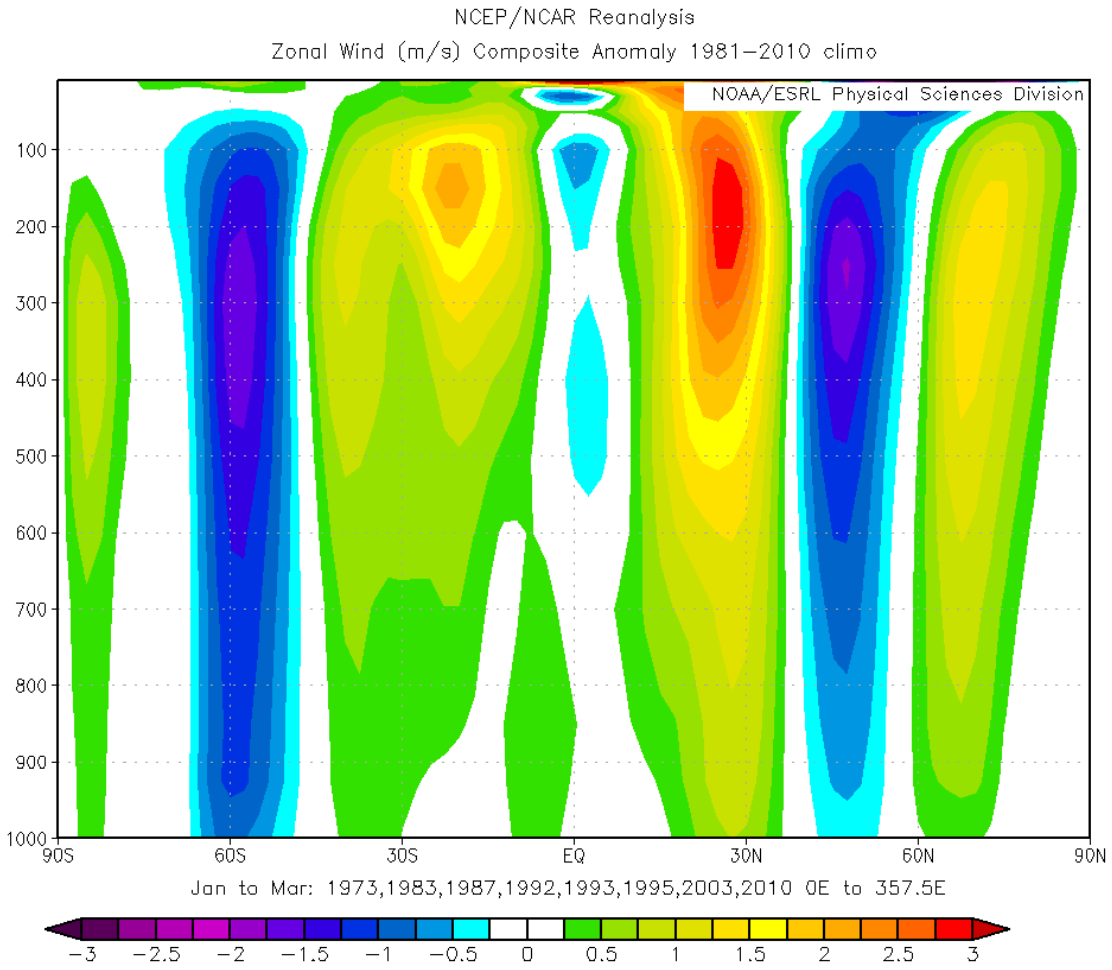

Figure 35. Cross section of anomalous JFM zonal wind from 1000 hPa to 100 hPa for the eight strongest EN years of our study period. Note the positive anomalies from about 60N to 80N. These anomalies indicate a strengthening of the polar vortex.

G. CORRELATIONS AND TELECONNECTIONS

We conducted correlation analyses to identify the relationships between winter Arctic T and T850, Z850, Z200, U850, U200, SST, and OLR (see Chapter II, Section C.2 for correlation methods), and to help verify the results of our warm and cold composite analysis. We treat Arctic T as our predictand (see time series for Arctic T in Figure 4 of Chapter III, Section A), and the other aforementioned variables as predictors. We also decided to calculate correlations between our predictand and the MEI, with the MEI as a predictor, since the composites in

previous sections revealed patterns associated with ENLN. To start this analysis, correlations between our predictand and the potential predictors were calculated at zero lag. The correlation values for our 45-year study period and their corresponding confidence levels are shown in Table 3.

Table 3. Correlation values and corresponding confidence levels for a 45-year period. Confidence levels were calculated using a two-tailed hypothesis test. (See ESRL 2015e, and Wilks 2006 for information on hypothesis testing methods.)

Correlation Values for 45 Years	Confidence Levels for 45 Years
0.20	0.81
0.22	0.85
.245	.90
0.294	0.95
0.345	0.975
0.379	0.99
0.41	0.995

Figure 36(a)–(h) shows a set of eight correlation maps, one for each of our potential predictors, at zero lag (e.g., JFM Arctic T correlated with JFM T850). Each correlation map in Figure 36 is consistent with its corresponding warm composite in Chapter III, Section C, and shows patterns associated with ENLN (Murphree 2014c).

Figure 36a shows the zero lag correlation map of Arctic T correlated with T850. Strong negative correlations well above the 0.95 confidence level (see Table 3) are seen in parts of the central-eastern tropical Pacific. Figure 36a shows that when temperatures are cold (warm) in the central-eastern tropical Pacific during JFM, temperatures in the Arctic are simultaneously likely to be warm (cold) during JFM. There are also strong positive correlations between Arctic T, and T850 in the western tropical Pacific. These results show that when

temperatures in the western tropical Pacific are warm (cold) during JFM, temperatures in the Arctic are simultaneously likely to be warm (cold). These combined results suggest the possible presence of LN (EN).

Figure 36a also shows negative correlations over central Asia and parts of North America. These correlations show that when the Arctic is warm (cold), central Asia and parts of North America are cold (warm). We know that when the Arctic is warmer than normal in the winter, the polar vortex has the tendency to weaken, allowing cold Arctic air to flow southward into the midlatitudes. It may be that the warming of the Arctic, weakening of the temperature gradient and polar vortex, and colder temperatures over Eurasia all had a tendency to occur simultaneously during JFM. We speculate that these conditions are related to ENLN based on the T850 patterns shown in Figure36a and the warm composite of T850 in Chapter III, Section C.

Figure 36b shows the zero lag correlation map of Arctic T correlated with SST. This figure shows similar correlations and SST patterns over the ocean to those seen in Figure 36a. We drew similar conclusions from Figure 36b because of the known relationships between T850 and SST (refer to Chapter II, Section B.3 for a discussion of these relationships).

Figure 36c shows the zero lag correlation map of Arctic T correlated with Z850. Strong positive correlations over northern Siberia show that when the Arctic is warm (cold), a broad region of high (low) heights may simultaneously occur over northern Siberia. These results are consistent with our results from Figure 12 (Chapter III, Section C), in which we speculated that the implied WAA from the anomalously high heights over northern Siberia may have aided in warming the Arctic during the eight warm winters of our study period. Similarly, the negative correlations over Canada, and positive correlations in the northern and northeastern Pacific, also resemble the anomalous patterns in Figure 12. Note the negative correlations throughout the tropics. These correlations tell us that when the Arctic is warm (cold), the tropics are simultaneously likely to be cold (warm), further suggesting the presence of LN (EN).

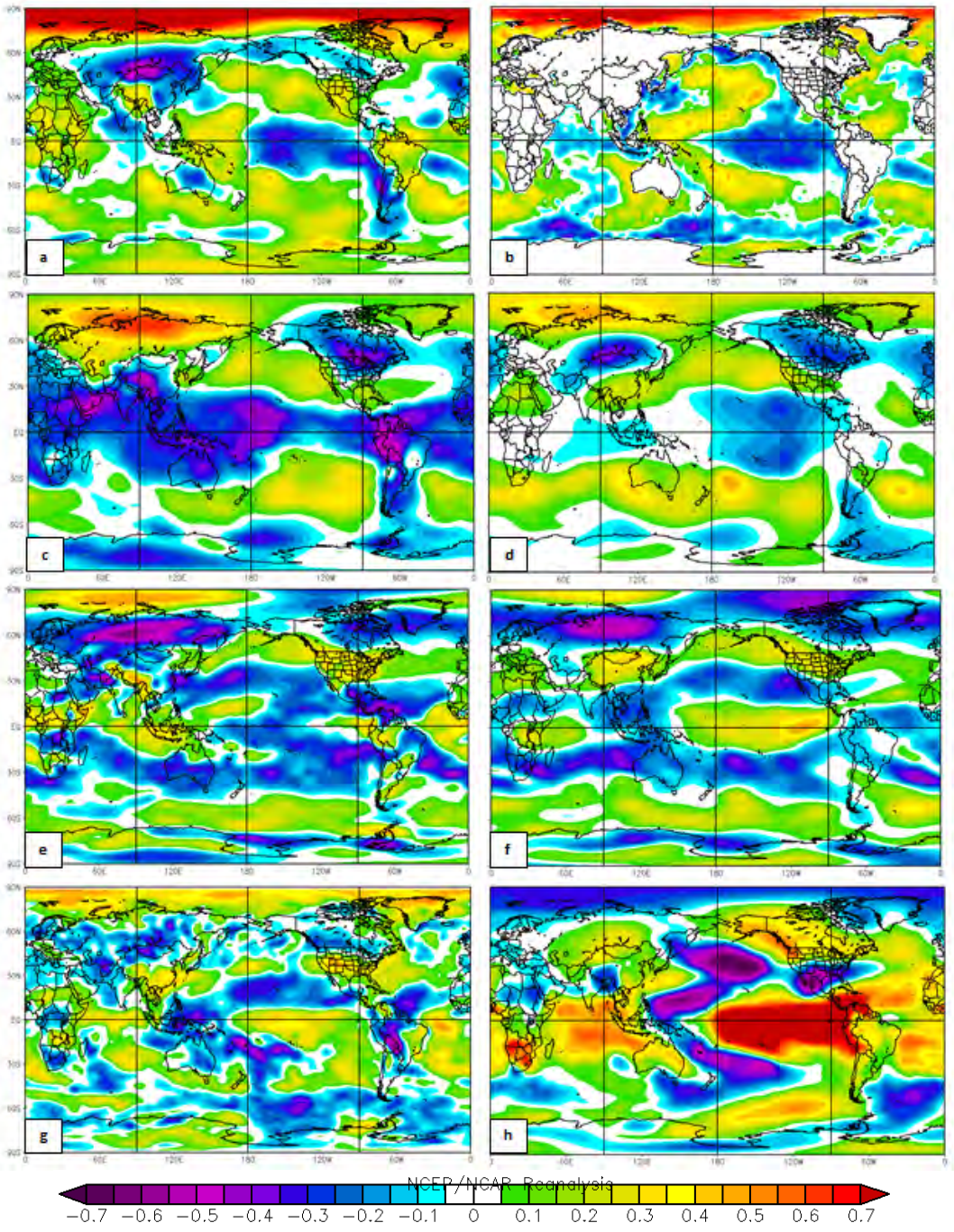

Figure 36. Zero lag correlation maps for Arctic T correlated with: (a) T850; (b) SST; (c) Z850; (d) Z200; (e) U850; (f) U200; (g) OLR and (h) the MEI. Correlations (a)–(h) reveal similar patterns to the corresponding warm composites in Chapter III Section C, and show relationships between Arctic T and ENLN. Figure 36h shows strong, positive (negative) correlations between ENLN and T850 in the tropics (Arctic).

Figure 36d shows the correlation map of Arctic T correlated with Z200, and evidence of the PNA-like patterns and stationary anomalous Rossby wave train in the warm Z200 composite (see Chapter III, Section C). The alternating negative and positive correlations suggest that when heights near: (a) Hawaii are low (high); (b) the northeastern Pacific are high (low); (c) eastern Canada are low (high) and (d) southern U.S. are high (low), that the Arctic is likely to be warm (cold). This pattern is consistent with results from the warm composite of Z200 that Arctic T may be associated with a negative (positive) PNA pattern and LN (EN). This result is also consistent with prior studies concerning the PNA pattern's possible influence on Arctic climate (cf. L'Heureux 2008). We can infer from Figure 36d that the positive correlations north of western Russia and the negative correlations over central Asia, may have helped to produce the negative correlations over northern Eurasia in Figures 36e(f). These results suggest that a weakening (strengthening) of the polar vortex may be associated with warm (cold) Arctic T, and are consistent with the results from the warm composites of U850 and U200 (see Figures 15 (16), Chapter III, Section C). The presence of the PNA pattern and Rossby wave train in Figure 36d show that ENLN and changes in the polar vortex may be associated with interannual variations in Arctic T.

The correlation patterns in Figure 36f show that when there is increased (decreased) convection in the western tropical Pacific, Arctic T tends to be warm (cold). Increased localized convection in the western (central-eastern) tropical Pacific on interannual time scales is indicative of LN (EN) conditions, which supports our results above and is consistent with prior studies (e.g., Lee et al., 2011a, 2011b, Lee 2012).

Thus far, the correlations maps support our speculation that Arctic T may be related to ENLN. We believe Arctic T tends to be warm (cold) when there is a LN (EN) present. To investigate this relationship further, we created a zero lag correlation map of T850 correlated with the MEI (Figure 27f). From 75N-90N, when the MEI is negative (positive), Arctic T tends to be warm (cold). As

expected, the correlation between T850 in the central-eastern tropical Pacific was positively correlated with the MEI and statistically significant above the .995 confidence level. This means that when the MEI is negative (positive) T850 in the central-eastern tropical Pacific is likely to be warm (cold).

Table 3 shows the correlation values for Arctic T correlated with the MEI during seven three-month seasons at zero lag. These three-month seasons include: October-December (OND); November-January (NDJ); December-February (DJF); JFM; February-April (FMA); March-May (MAM) and April-June (AMJ) The strongest correlation occurred during JFM, and was -0.30, which is statistically significant above the 0.95 confidence level. We also see significant correlations during December-February (DJF) and February-April (FMA). These findings tell us that there is a teleconnection between ENLN and Arctic T, especially during the winter. These correlations support our earlier findings from the warm and cold year composites presented in Chapter III, Sections C-E.

Table 4. Correlations of Arctic T during our study period 1970–2014, with the simultaneous MEI (lag equal to zero months). The correlations are shown for seven three-month periods (OND-AMJ). Note that the highest correlations, and those that are at or above an 85% confidence level (in red), occur during the winter periods (DJF-FMA).

	Seasons						
	OND	NDJ	DJF	JFM	FMA	MAM	AMJ
Correlations of Arctic T with MEI (1970-2014)	-0.02 OND Arctic T with OND MEI	-0.07 NDJ Arctic T with NDJ MEI	-0.25 DJF Arctic T with DJF MEI	-0.30 JFM Arctic T with JFM MEI	-0.27 FMA Arctic T with FMA MEI	-0.13 MAM Arctic T with MAM MEI	-0.12 AMJ Arctic T with AMJ MEI

Figures 37 through 43 are a series of correlation maps. In each figure, one of our potential predictors (e.g., T850, Z850) leads Arctic T by: (a) one; (b) three; and (c) five months. These maps helped us to identify which variables may be good predictors of Arctic T at leads of one to five months.

In Figure 37, the correlations between our predictand and T850 are positive (negative) in the western (central-eastern) tropical Pacific, with T850

leading at one and three months. However, at five months the correlation in the western tropical Pacific weakened, while the central and eastern tropical Pacific correlations remained strong, and appeared to shift westward. Positive correlations over the northern and southern Pacific and negative correlations along the west coast of South America also persisted from one to five months. This map shows that T850 in the central-eastern tropical Pacific may be a good predictor of Arctic T at leads up to five months. This map also shows that T850 in both the western and central-eastern tropical basins may be good predictors of Arctic T at leads up to three months. These patterns suggest that ENLN may have influenced Arctic T. The negative correlations over central Asia and parts of North America in (a) are either weak or not apparent in (b) and (c), which suggests that perhaps the possible ENLN-related Arctic warming only has a short-lived relationship to the weakening of the polar vortex.

Figure 38 shows negative correlations between our predictand and SST throughout much of the central-eastern tropical Pacific and along the west coasts of North and South America at each lag (a)–(c). The negative correlations in (c) appear stronger than in (a) and (b). Positive correlations in the northern, and southern Pacific, and in the western tropical Pacific also occurred from one to five months. These correlation maps show that at leads of one to five months, when SST is warm (cold) in the western (central-eastern) tropical Pacific, Arctic T is likely to be warm (cold). Likewise, when SST in the northern, southern, and western tropical Pacific are warm (cold), Arctic T is likely to be warm (cold). These patterns in SST resemble ENLN patterns and tell us that ENLN may be a good predictor of Arctic T as well.

Figure 39 shows Z850 leading Arctic T by: (a) one three, and five months. When Z850 leads Arctic T by one month, a large positive correlation exits over northern Siberia, however this correlation is not seen at leads of three and five months. A positive correlation in this region suggests that Z850 over northern Siberia may be a good predictor of Arctic T at a lead of one month, and further suggests that a weakening of the polar vortex may lead to warm Arctic T one

month later. At one to five months lead, Z850 over the Indian Ocean may be a good predictor of Arctic T; however the strongest correlations are at one month lead. The areas of positive correlations in the northeast Pacific and southeast Pacific in (a) appear to expand westward in (b) and (c), indicating that Z850 over the Pacific may be a good predictor of Arctic T at one to five months lead.

Figure 40 shows evidence of a negative PNA pattern and Rossby wave train. Alternating areas of negative and positive correlations from Hawaii northward and eastward to the central Atlantic, indicate that a negative PNA pattern may be a good predictor of Arctic T at a lead of one month. Evidence of this pattern can be seen at three and five months as well, but the correlations have shifted westward and the negative correlations have weakened. Negative (positive) PNA patterns are also associated with LN (EN) events; therefore we speculate that ENLN may be a good predictor of Arctic T at leads of one to five months as well. Figure 40 also shows evidence of a Rossby wave train, indicated by the areas of alternating positive and negative correlations from the northeast Pacific eastward and southward to Southeast Asia. Our results from Figure 40 suggest that Z200 may be a good predictor of Arctic T at leads of one to five months, and that ENLN may also be a good predictor of Arctic T at leads of one to five months.

Figure 41 (42) shows correlations between Arctic T and U850 (U200). In Figure 41a (42a), negative correlations over Eurasia and Canada show that weak (strong) westerlies over Eurasia and Canada may indicate a warm (cold) Arctic at a lead of one month, suggesting that a weak (strong) polar vortex may lead a warm (cold) Arctic by one month. The possible relationships between ENLN and the polar vortex found in the warm (cold) composites of Chapter III, Section C-F, led us to further investigate a relationship between ENLN and the polar vortex. Possible relationships between the polar vortex and Arctic T at leads greater than one month are unclear in Figures 41 and 42, and need to be investigated further.

Figure 43 shows correlations between Arctic T and OLR. In Figure 43(a)–(c) the negative correlations near the maritime continent and positive correlations

in the central-eastern tropical Pacific are seen at one to five months lead. These OLR patterns resemble inferred ENLN convection patterns, and are consistent with our results in Chapter III, Section C for OLR. The correlations in Figure 43 suggest that ENLN may be a good predictor of Arctic T at one to five months.

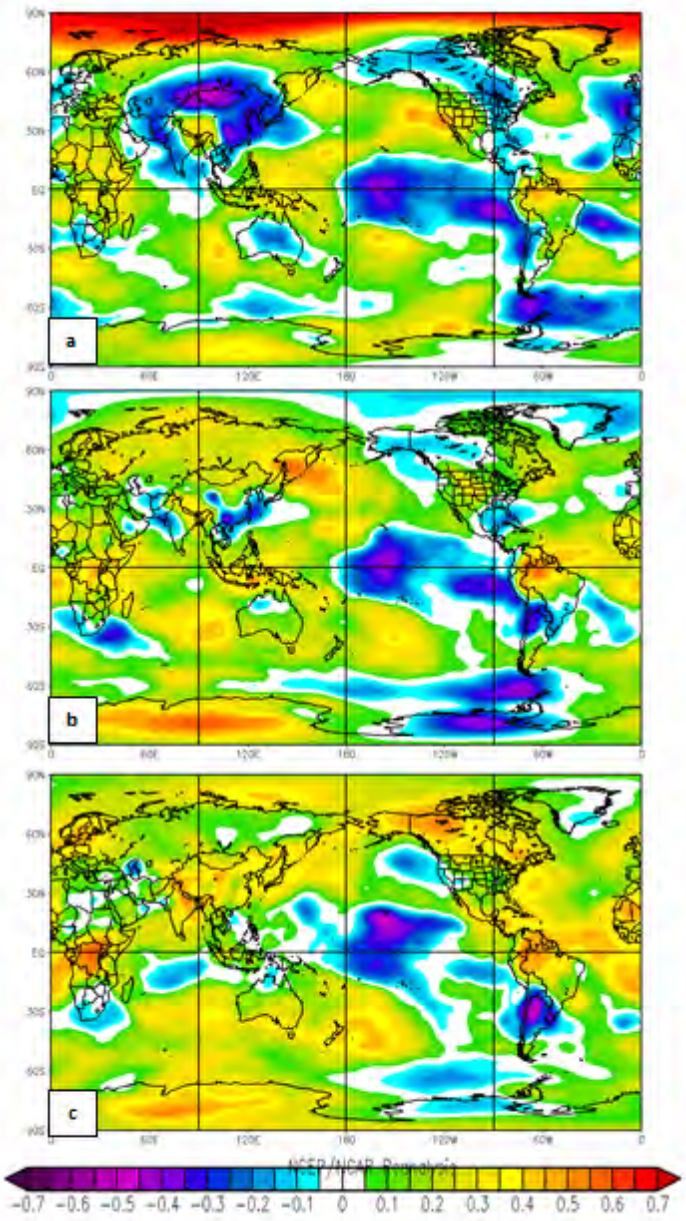

Figure 37. Set of correlation maps of our predictand lagging global T850 by: (a) one month; (b) three months; and (c) five months. Note the persistent negative correlations over the eastern tropical Pacific and the west coast of South America. T850 patterns throughout the Pacific resemble ENLN T850 patterns.

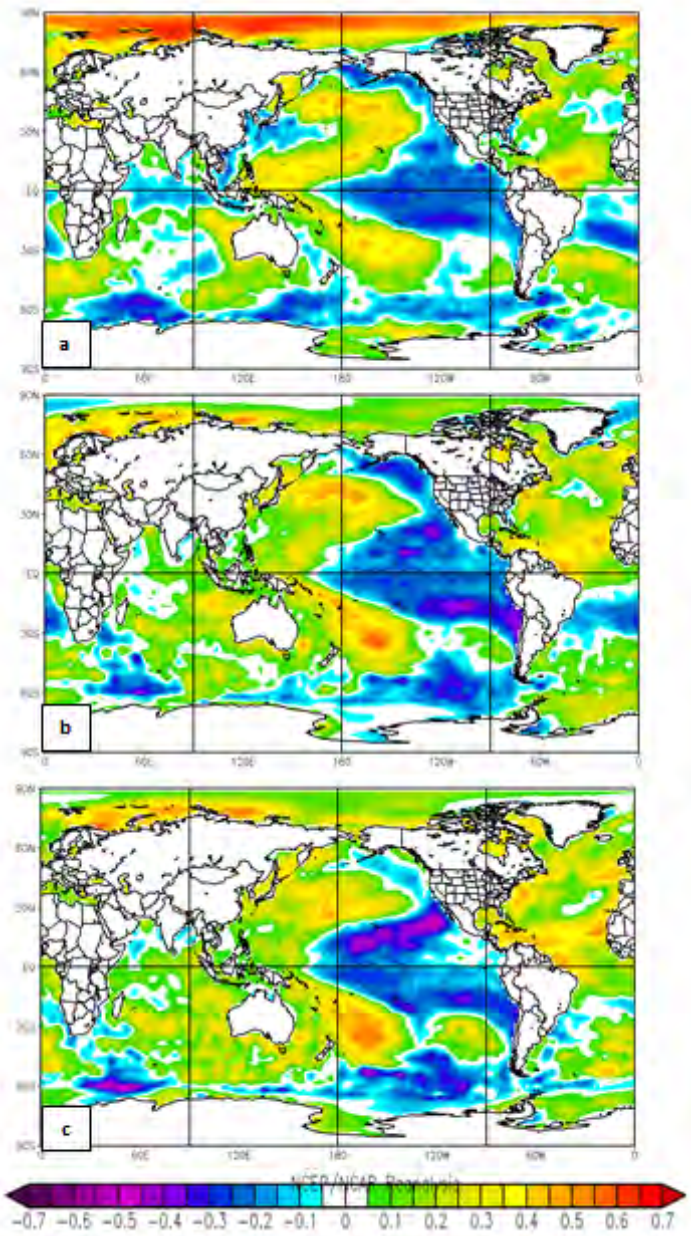

Figure 38. Set of correlation maps of our predictand lagging global SST by: (a) one month; (b) three months; and (c) five months. Note the persistent negative (positive) correlations over the central-eastern (western) tropical Pacific. SST patterns throughout the Pacific resemble ENLN SST patterns.

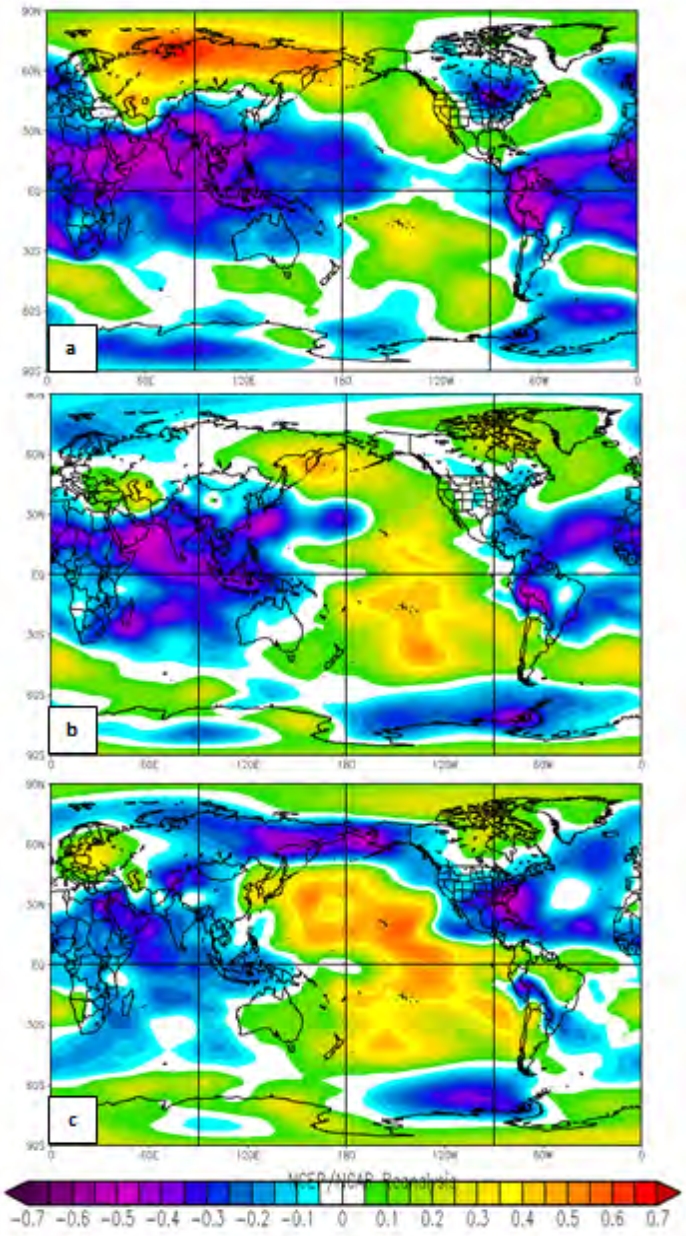

Figure 39. Set of correlation maps of our predictand lagging global Z850 by: (a) one month; (b) three months; and (c) five months. Note the strong, positive correlation over northern Siberia in (a), and the positive (negative) correlations over the Pacific (Indian) Ocean in (b) and (c). Negative correlations can also be inferred over the central-eastern Pacific at upper levels. Note possible relationships between Arctic T and ENLN.

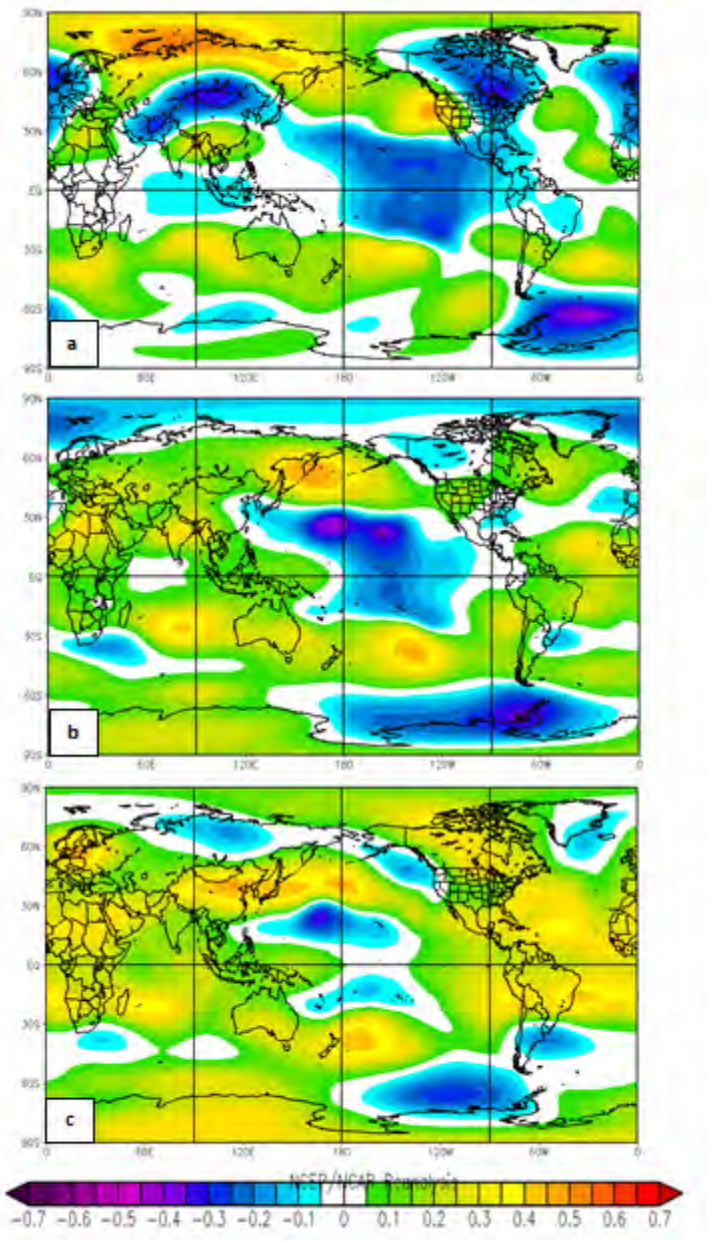

Figure 40. Set of correlation maps of our predictand lagging global Z200 by: (a) one month; (b) three months; and (c) five months. Note the persistence of the negative PNA-like pattern in (a)–(c). Also note evidence of the anomalous wave train in (a).

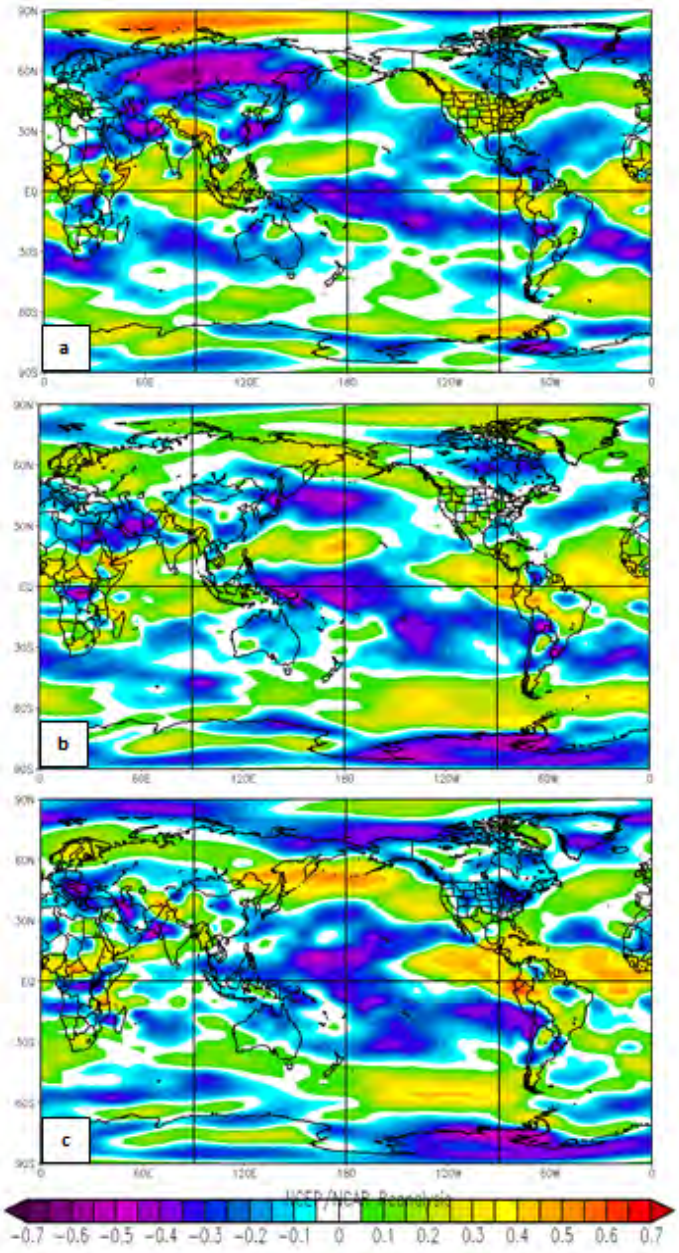

Figure 41. Set of correlation maps of our predictand lagging global U850 by: (a) one month; (b) three months; and (c) five months. Note the strong negative correlations over Eurasia and the negative correlations over Canada in (a). These correlations indicate a weakening of the polar vortex at one month lead.

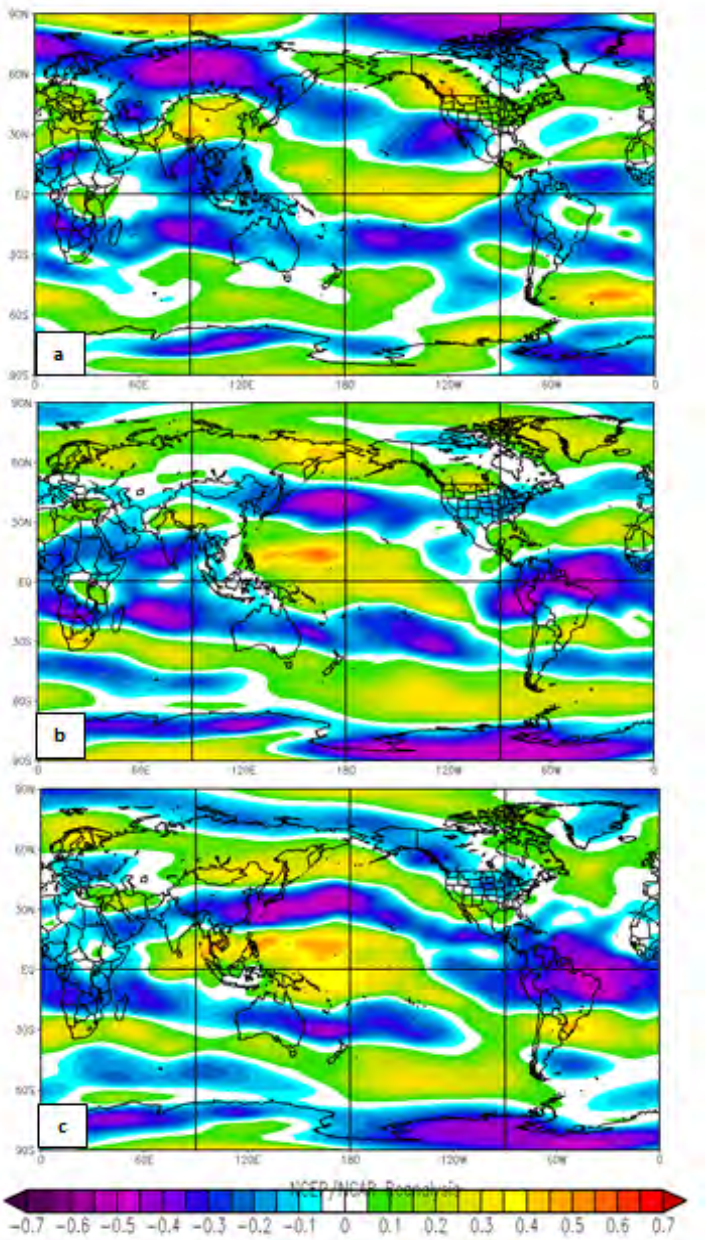

Figure 42. Set of correlation maps of our predictand lagging global U200 by: (a) one month; (b) three months; and (c) five months. Note the strong negative correlations over Eurasia. These correlations indicate a weakening of the polar vortex at one month lead

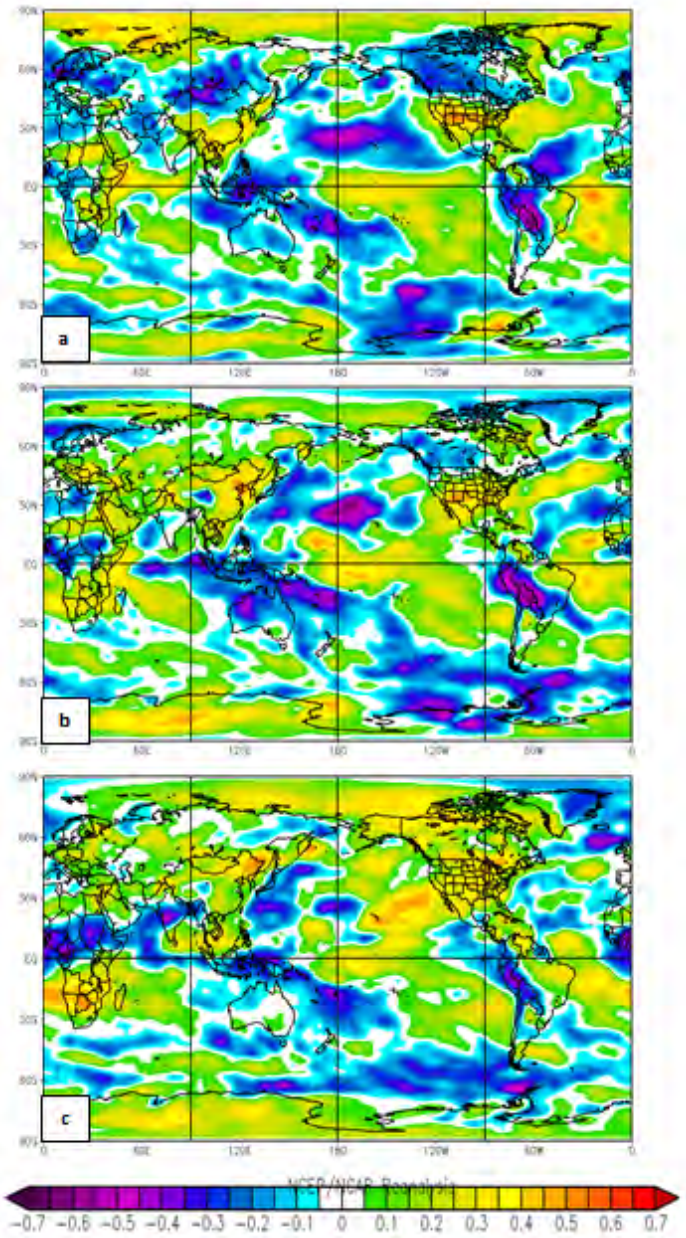

Figure 43. Correlation maps of our predictand lagging global 200 hPa OLR by: (a) one month; (b) three months; and (c) five months. Note the negative (positive) correlations over the western (central-eastern) tropical Pacific in (a)–(c).

We continued our correlation analysis by calculating correlations between our predictand and ENLN, via the MEI. Table 5 shows correlations between Arctic T during our study period and the MEI in seven different three-month periods from OND to AMJ. Our predictand (JFM Arctic T) lags the MEI in the first three columns (OND-DJF), and leads the MEI in the last three columns (FMA-AMJ). It is important to note that all correlations are significant above the 0.85 confidence level however the strongest correlation occurs when the MEI led Arctic T by one month. Correlations were stronger when the MEI led Arctic T; therefore we performed a series of additional correlations with the MEI leading Arctic T by zero to ten months (see Table 6). The three-month seasons in Table 6 include: MAM; AMJ; May-July (MJJ); June-August (JJA); July-September (JAS); August-October (ASO); September-November (SON); OND; NDJ; DJF and JFM. All correlations in Table 6 are statistically significant above the 0.81 confidence level. Correlations were significant above the 0.95 confidence level when the MEI led Arctic T by zero to three months (JFM-OND). These correlations indicate that: (a) there are intraseasonal to seasonal (S2S) teleconnections between ENLN conditions in the tropical Pacific and lower tropospheric T in the Arctic, especially during the Arctic winter; (b) ENLN may trigger Arctic T variations; and (c) ENLN may be useful as a predictor of Arctic T variations at intraseasonal to seasonal (S2S) lead times.

Table 5. Correlations of Arctic T during our study period, 1970–2014, with the MEI in seven three-month periods (OND-AMJ), with JFM Arctic T lagging three to zero months, and Arctic T leading by zero to three months.

	MEI Seasons						
	OND 1969-2013	NDJ 1969-70 to 2013-14	DJF 1969-70 to 2013-14	JFM 1970-2014	FMA 1970-2014	MAM 1970-2014	AMJ 1970-2014
Correlations of JFM Arctic T (1970-2014) with MEI	-0.3 MEI leads JFM Arctic T by 3 months	-0.31 MEI leads JFM Arctic T by 2 months	-0.33 MEI leads JFM Arctic T by 1 month	-0.30 Zero lag Zero lead	-0.29 JFM Arctic T leads MEI by 1 month	-0.28 JFM Arctic T leads MEI by 2 months	-0.23 JFM Arctic T leads MEI by 3 months

Table 6. Correlations of Arctic T850 (75-90N) during JFM 1970–2014 with the MEI in eleven three-month periods (MAM-JFM), with the MEI leading by zero to ten months. Note that the correlations are significant at the 0.81 confidence level or higher (in red) for MEI leading by ten to zero months (MAM-JFM), and are especially strong and significant at leads of two to zero months (NDJ-JFM). These correlations indicate that: (a) there are intraseasonal to seasonal (S2S) teleconnections between ENLN conditions in the tropical Pacific and lower tropospheric T in the Arctic, especially during the Arctic winter; (b) ENLN may trigger Arctic T changes; and (c) ENLN may be useful as a predictor of Arctic T changes at S2S lead times.

MEI Season	MAM 1969-2013	AMJ 1969-2013	MJJ 1969-2013	JJA 1969-2013	JAS 1969-2013	ASO 1969-2013
Correlations with JFM Arctic Temp (1970-2014)	-0.21 MEI leads JFM Arctic T by 10 months	-0.24 MEI leads JFM Arctic T by 9 months	-0.25 MEI leads JFM Arctic T by 8 months	-0.28 MEI leads JFM Arctic T by 7 months	-0.28 MEI leads JFM Arctic T by 6 months	-0.29 MEI leads JFM Arctic T by 5 months
MEI Season	SON 1969-2013	OND 1969-2013	NDJ 1969-70 to 2013-14	DJF 1969-70 to 2013-14	JFM 1970-2014	
Correlations with JFM Arctic Temp (1970-2014)	-0.28 MEI leads JFM Arctic T by 4 months	-0.3 MEI leads JFM Arctic T by 3 months	-0.31 MEI leads JFM Arctic T by 2 months	-0.33 MEI leads JFM Arctic T by 1 month	-0.30 Zero lag Zero lead	

IV. CONCLUSION

A. SUMMARY OF KEY RESULTS

This study investigated the possible teleconnections affecting winter Arctic climate. In doing so, we have exposed the potential for different oceanic and atmospheric variables, and known modes of climate variability, to be used as predictors of interannual variations in Arctic winter temperature. Our study is in line with the objectives put forth in the Arctic Roadmap, and attempts to improve climate support for U.S. Navy operations in the Arctic through an increased understanding of the factors influencing Arctic climate.

We used the methods outlined in Chapter II of this study, and applied them towards tercile categorical, composite, correlation and teleconnection analyses in order to investigate the interannual variations of Arctic T. From our tercile categorical analysis, we found that an anomalously cold (warm) Arctic tends to be associated with EN (LN) conditions during the winter. This lead us speculate that a possible relationship between Arctic T and ENLN may exist.

An analysis of LTM conditions gave us a sense of normal conditions during JFM for our focus variables. The warm and cold composite analyses helped us to identify anomalous atmospheric and oceanic patterns that were associated with Arctic T during our study period. We found that several of the patterns revealed by the warm (cold) composite analyses of global T850, Z850, Z200, U850, U200, SST, and OLR, strongly resembled patterns associated with LN (EN) events, and were consistent with our speculations and several of the prior studies discussed in Chapter I, Section B. It is important to note that the anomalies in the cold composites were opposite in sign, and in relatively the same location as the warm composite anomalies, however the cold composite anomalies were weaker. This result led us to speculate that LN may have more of an impact on Arctic T than EN. In this section, we will give our key results for the warm composites only. Please refer to Chapter III, Section D-E for further

discussion of the cold composite anomalies, and their comparisons to the warm composite anomalies.

Warm composite anomalies of T850 helped us to identify anomalous T850 patterns associated with a warm Arctic. The warm composites of Z850 revealed anomalous lower tropospheric height patterns that suggested there were plausible dynamic mechanisms associated with the anomalous T850 distribution. For example, subpolar height anomalies like the large positive anomaly over western Russia, and implied WAA, may have contributed to an anomalously warm Arctic T during our study period. Similarly, warm Z200 composites revealed upper tropospheric height patterns associated with Arctic T. We found that Z200 anomalies revealed a negative PNA pattern and a stationary anomalous Rossby wave train. Negative (positive) PNA patterns are normally associated with LN (EN) events; therefore we speculated that ENLN was associated with Arctic T during our study period. We found that the anomalous wave train from the northern Pacific to Southeast Asia may have been triggered by anomalous convection in the western tropical Pacific associated with ENLN. This result was consistent with the results of the warm OLR composite anomaly, which revealed that a warm Arctic may be associated with enhanced (decreased) convection in the western (central-eastern) tropical Pacific. An analysis of warm composites of U850 and U200 revealed regions of a possibly weakened polar vortex over Eurasia and North America, and led us to speculate that a weakened polar vortex may be associated with an anomalously warm Arctic. This made dynamic sense because a warm Arctic tends to weaken the pole-to-equator temperature gradient, which can weaken the polar vortex. Anomalous Z850 and Z200 also provided evidence of a weakened polar vortex over Eurasia and North America. Warm composite anomalies of SST revealed similar patterns to those of anomalous T850, which also resembled SST patterns closely associated with ENLN. We conclude that a warm Arctic was associated with LN SST patterns during our study period.

Through our correlation and teleconnection analyses, we showed that the dynamic plausibility gained from the composite analyses, was also statistically significant. A series of correlation maps showed correlations between Arctic T and the other focus variables (Figure 36), and revealed statistically significant correlations at zero lag. These maps revealed similar patterns to those found in the warm composites, confirming our speculation of a relationship between Arctic T and ENLN. We correlated Arctic T with the MEI at zero lag as well, and found that a warm (cold) Arctic may be associated with LN (EN) at zero lag. We then created correlation maps of Arctic T correlated with each of our focus variables leading Arctic T by one to five months. We found that ENLN signatures could be seen from one to five months in the correlations between Arctic T and: (a) T850; (b) SST; (c) Z850; (d) Z200 and (e) OLR. Correlation maps of Arctic T correlated with U850 (U200) revealed relationships between Arctic T and a weakening of the polar vortex at a lead of one month.

We also produced a series of correlation tables to show teleconnections between Arctic T and ENLN. We used the MEI to represent ENLN. Table 4 showed correlations between Arctic T and the MEI at zero lag for seven different three-month periods, with the MEI leading Arctic T during each period. We found that the strongest correlation between Arctic T and the MEI occurred during JFM. This correlation was -0.30, and was statistically significant above the 0.95 confidence level. This correlation prompted us to then correlate Arctic T with the MEI from zero to three months, with the MEI leading and lagging Arctic T. We found that all correlations were negative and statistically significant above the 0.85 confidence level, however the strongest correlations occurred when the MEI led Arctic T by zero to three months. We then calculated correlations from zero to ten months, with the MEI leading Arctic T, and found that all of the correlations were statistically significant at or above the 0.81 confidence level, and that correlations from zero to three months were significant above the 0.95 confidence level.

We created similar correlation tables for Arctic T and the AO, and found that the AO was not a good predictor of Arctic T, but that the reverse relationship may exist. We found evidence that Arctic T may be a good precursor to the AO at a lead time of three months. This could mean that a change in Arctic T during JFM may influence the AO during the late spring to early summer. We further speculate that the MEI may in fact influence the AO. Our results only touch on this relationship; therefore more research is needed to examine these possible relationships. Please see the Appendix for additional results regarding Arctic T and the AO. The combined results from our different analyses showed that ENLN may be a good predictor of Arctic T at zero to ten months lead.

These results may be useful in the future planning of military operations in the Arctic region. Our study helped to increase knowledge and awareness of the Arctic climate, and the relationships it may have with ENLN during the NH winter. Though we may not yet be able to predict the exact timing of anomalous Arctic winter temperature, our results may prompt future research to head in that direction. With further study in this area, and the further development of advanced climate data sets, perhaps in the next year we may come closer to being able to accurately predict anomalous conditions in the Arctic. We have provided evidence linking interannual variations in Arctic winter temperature to ENLN, however this evidence is in no way suggests that ENLN is the only teleconnection linked to Arctic T. Our study also shows evidence that there may be several other climate variations at work which help to produce anomalous Arctic T, on varying time scales.

B. RECOMMENDATIONS FOR FUTURE RESEARCH

Our study and others have shown that the application of advanced climate data sets may be useful in the long-lead climate support and planning of operations in the Arctic. However, more research is needed to further our understanding of the Arctic climate and the factors that influence it on

intraseasonal to multi-decadal time scales. We have listed some areas of further research below.

(1) This study focused on interannual variations in Arctic T during JFM between 75N-90N, and at 850 hPa. Studies of the interannual variations in Arctic T during other seasons, latitude bands, and atmospheric levels are needed to increase our understanding of the conditions that influence Arctic warming, and to what extent Arctic warming contributes to global climate change (GCC).

(2) This study focused on relationships between Arctic T and ENLN, and only touched on possible relationships between Arctic T and the AO. In addition to the results provided in the Appendix (see Tables 8 through 12 of the Appendix), more research is needed to understand the relationships between Arctic T and the AO, as well as relationships between Arctic T and other climate variations.

(3) Relationships between the AO and the ENLN should be investigated to help with forecasting changes in the AO, and perhaps subsequent changes in Arctic and/or midlatitude climate.

(4) This study investigated relationships between the polar vortex and ENLN in Chapter III, Section F. Additional correlations between U200 and the MEI revealed further evidence of these relationships (see Figures 62 through 64 of the Appendix). Further research is needed in relating ENLN to changes in the polar vortex.

(5) Figures 65 and 66 of the Appendix show relationships between the AO and polar vortex via U850 (U200). The results in Chapter III, Section F, and Figures 65 (66), suggest that the MEI has a stronger impact on the polar vortex than does the AO. Additional research is needed to explain these relationships.

(6) This study focused on the atmospheric and oceanic changes influencing Arctic warming. It would be interesting to investigate the

influence Arctic warming has on changes elsewhere (e.g., tropics, midlatitudes).

(7) The significance of relationships found in this study could be further investigated via the development of linear regression models to test our predictors.

APPENDIX. ADDITIONAL RESULTS

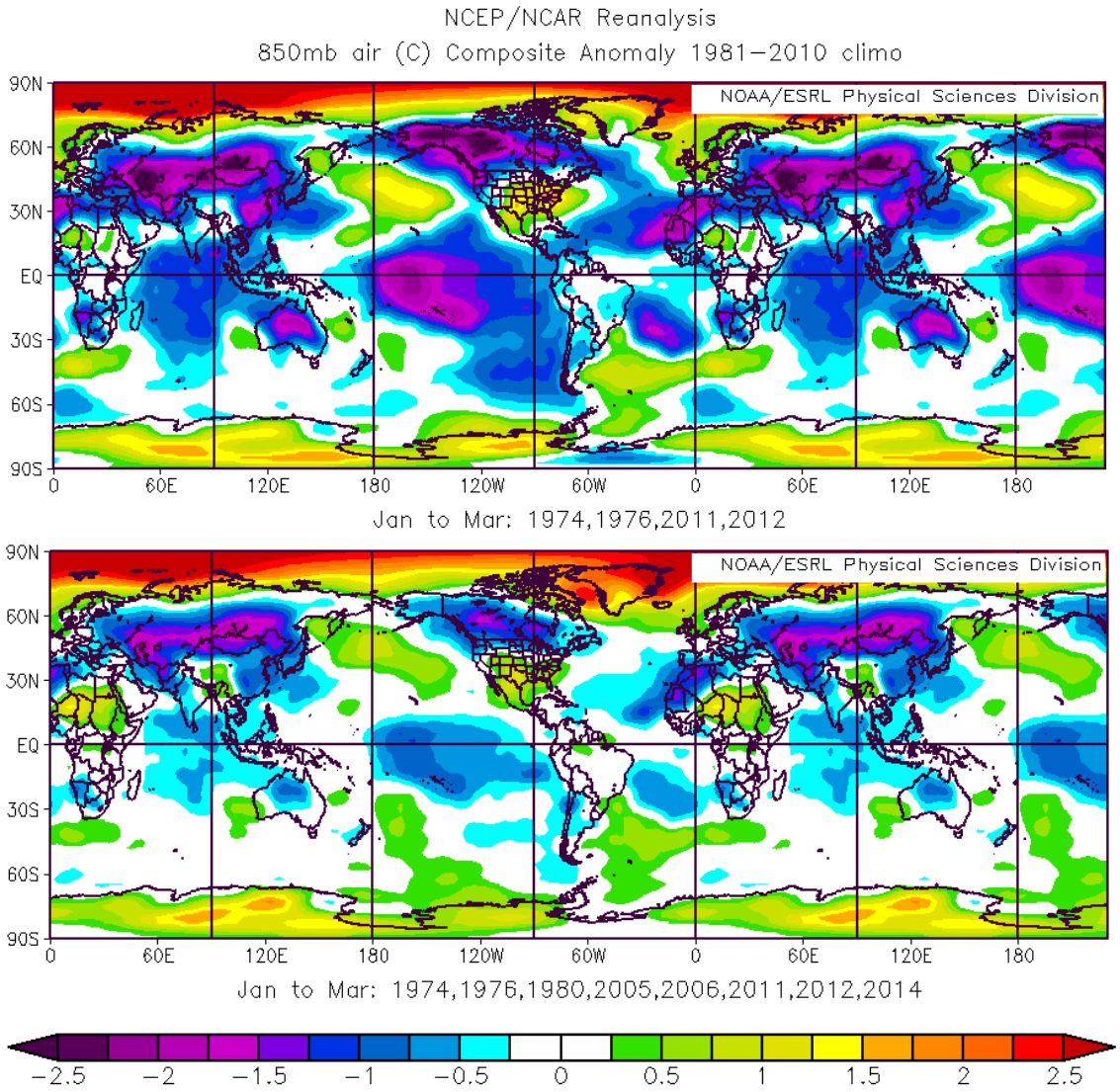

Figure 44. Anomalous JFM T850 for 1970–2014 for: (top panel) four of the eight warm years in which LN events occurred; (bottom panel) eight warmest years of our study period.

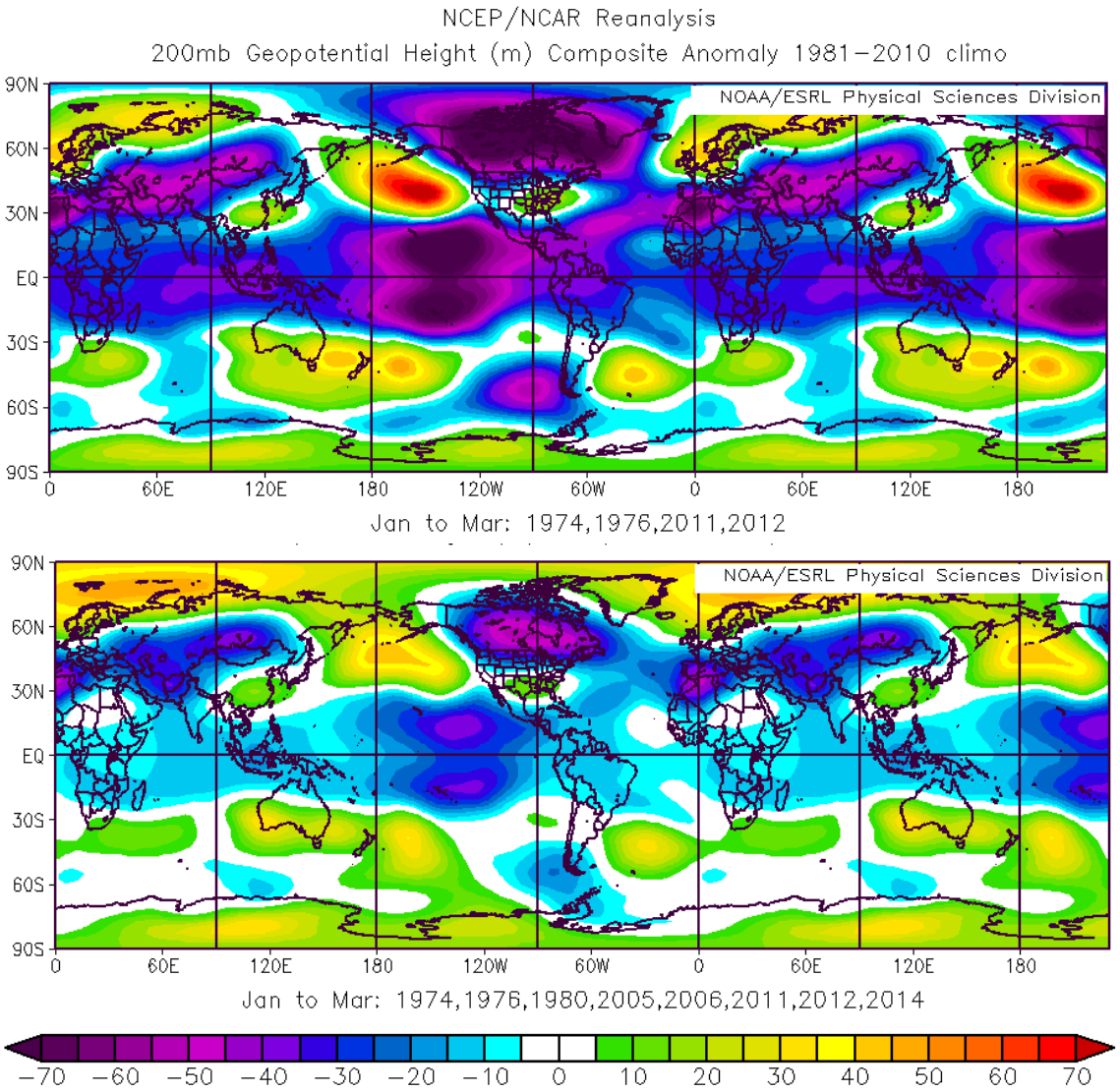

Figure 45. Anomalous JFM Z200 for 1970–2014 for: (top panel) four of the eight warm years in which LN events occurred; (bottom panel) eight warmest years of our study period.

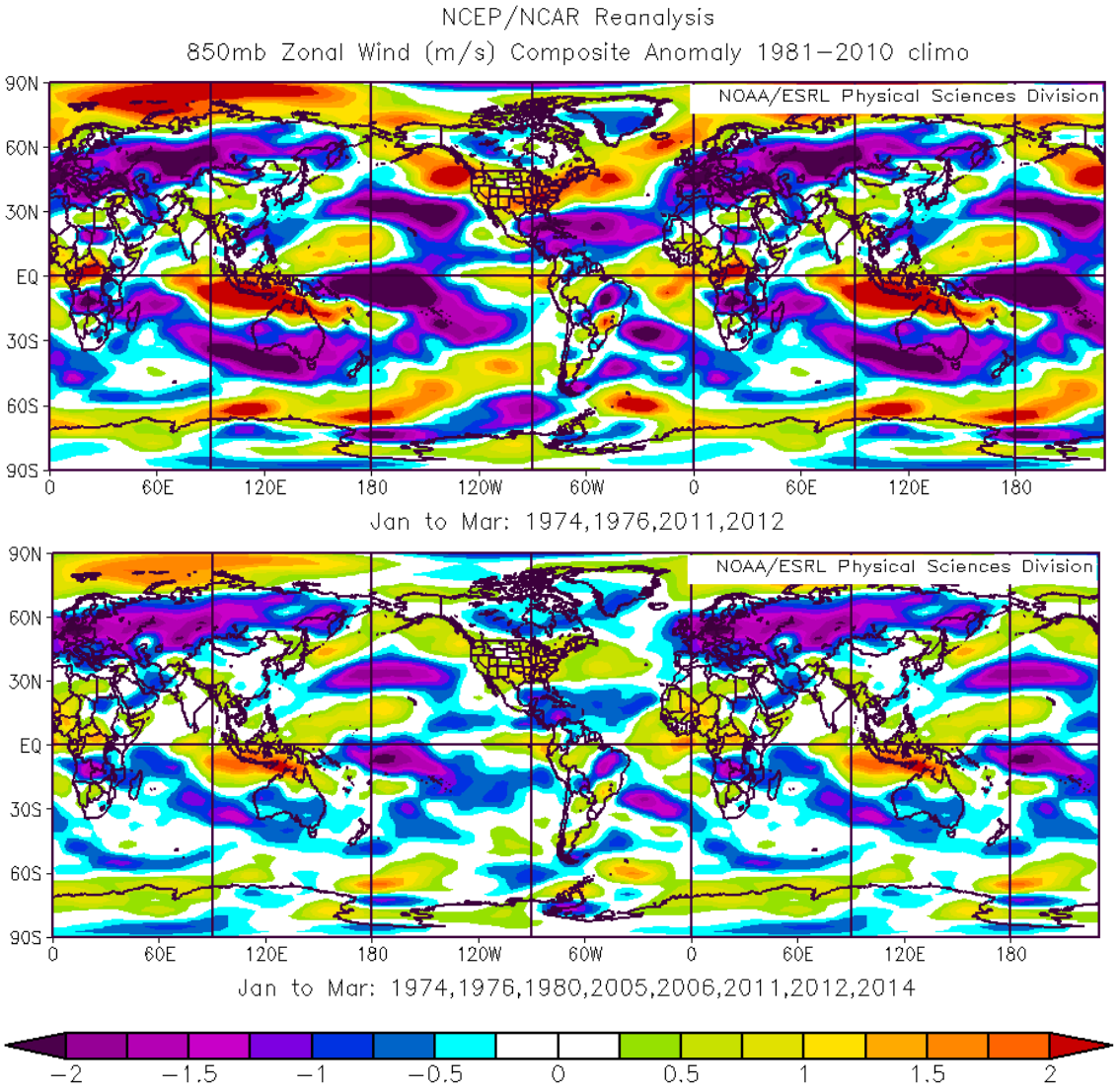

Figure 46. Anomalous JFM U850 for 1970–2014 for: (top panel) four of the eight warm years in which LN events occurred; (bottom panel) eight warmest years of our study period.

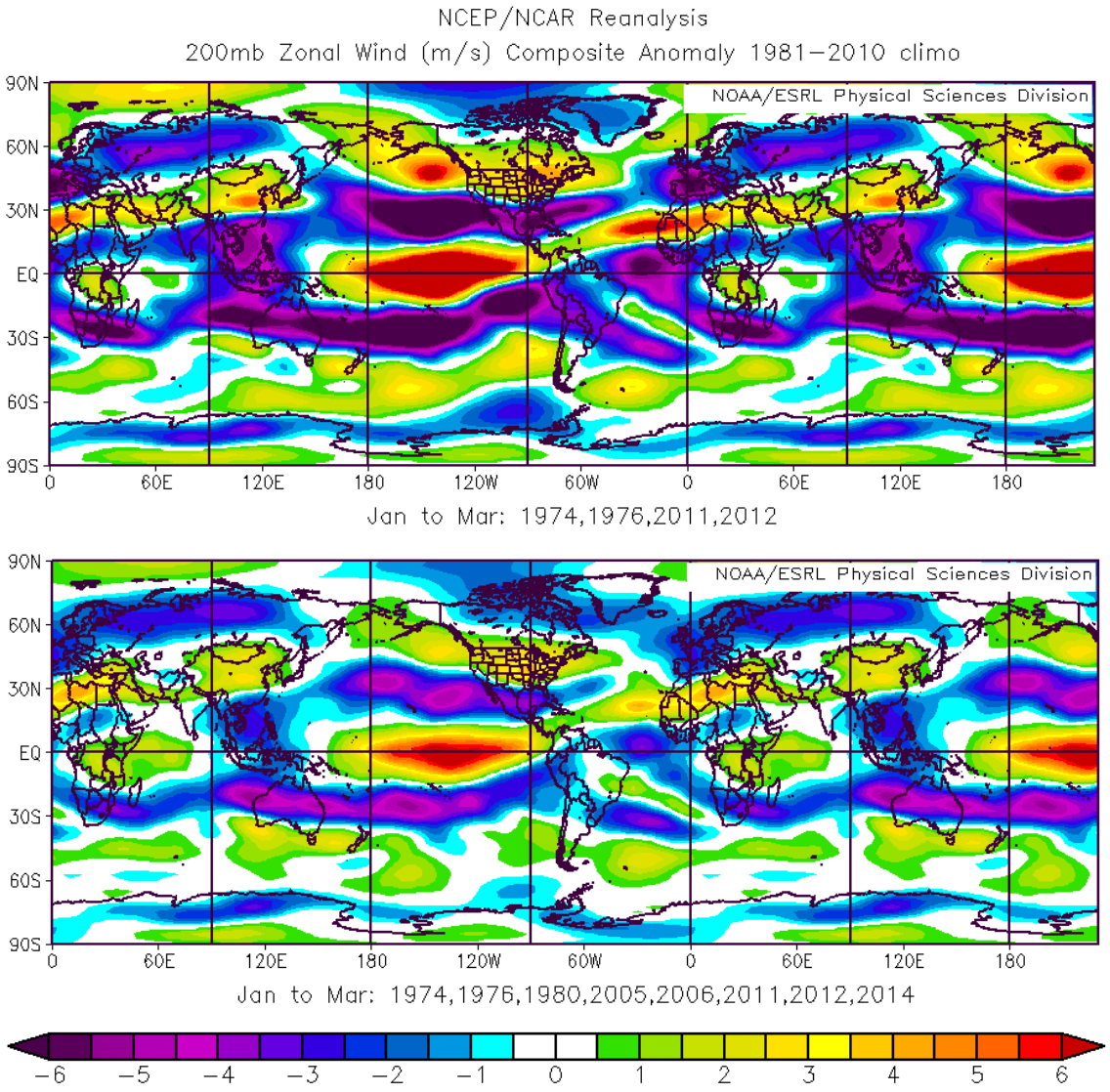

Figure 47. Anomalous JFM U200 for 1970–2014 for: (top panel) four of the eight warm years in which LN events occurred; (bottom panel) eight warmest years of our study period.

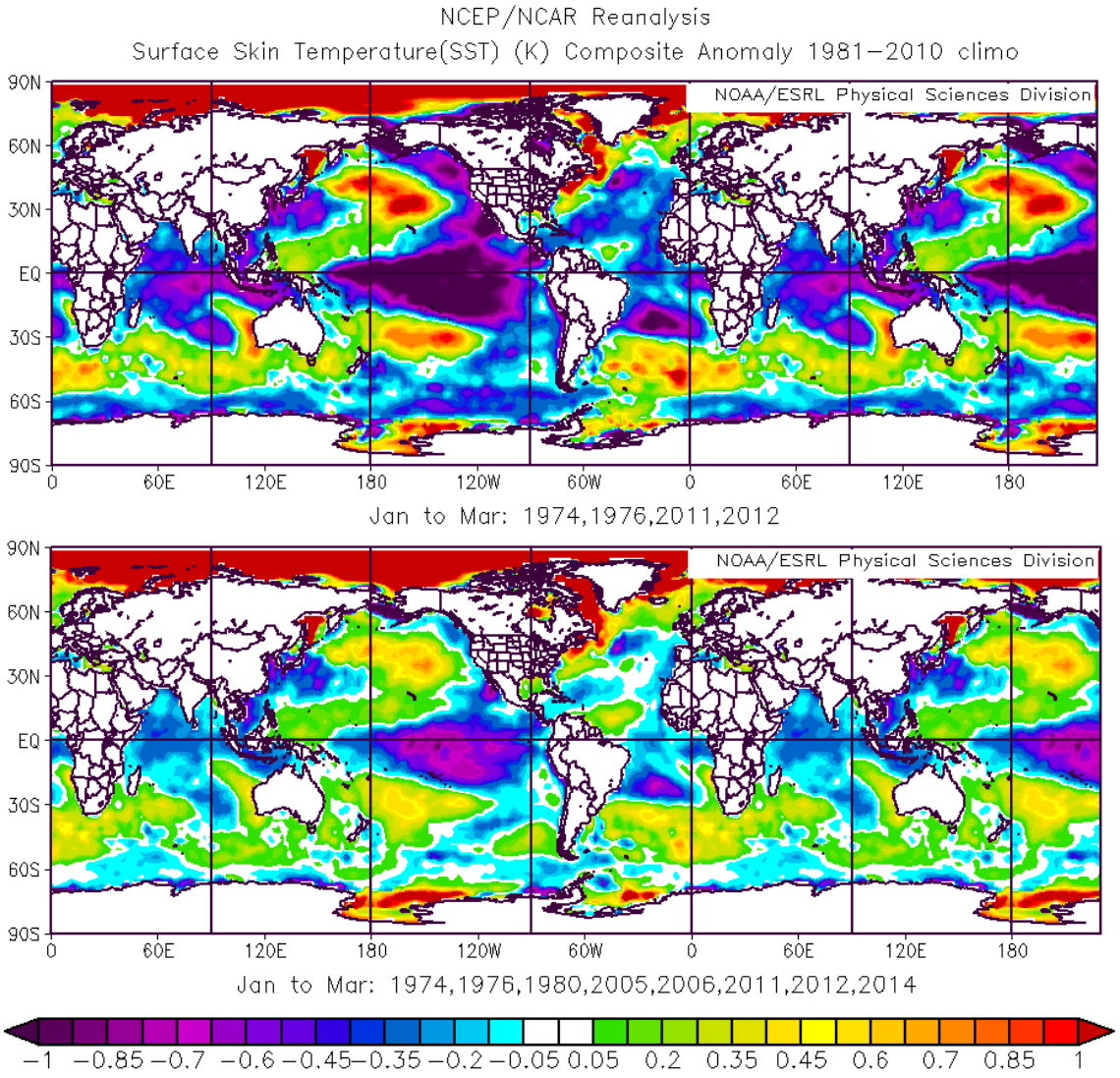

Figure 48. Anomalous JFM SST for 1970–2014 for: (top panel) four of the eight warm years in which LN events occurred; (bottom panel) eight warmest years of our study period.

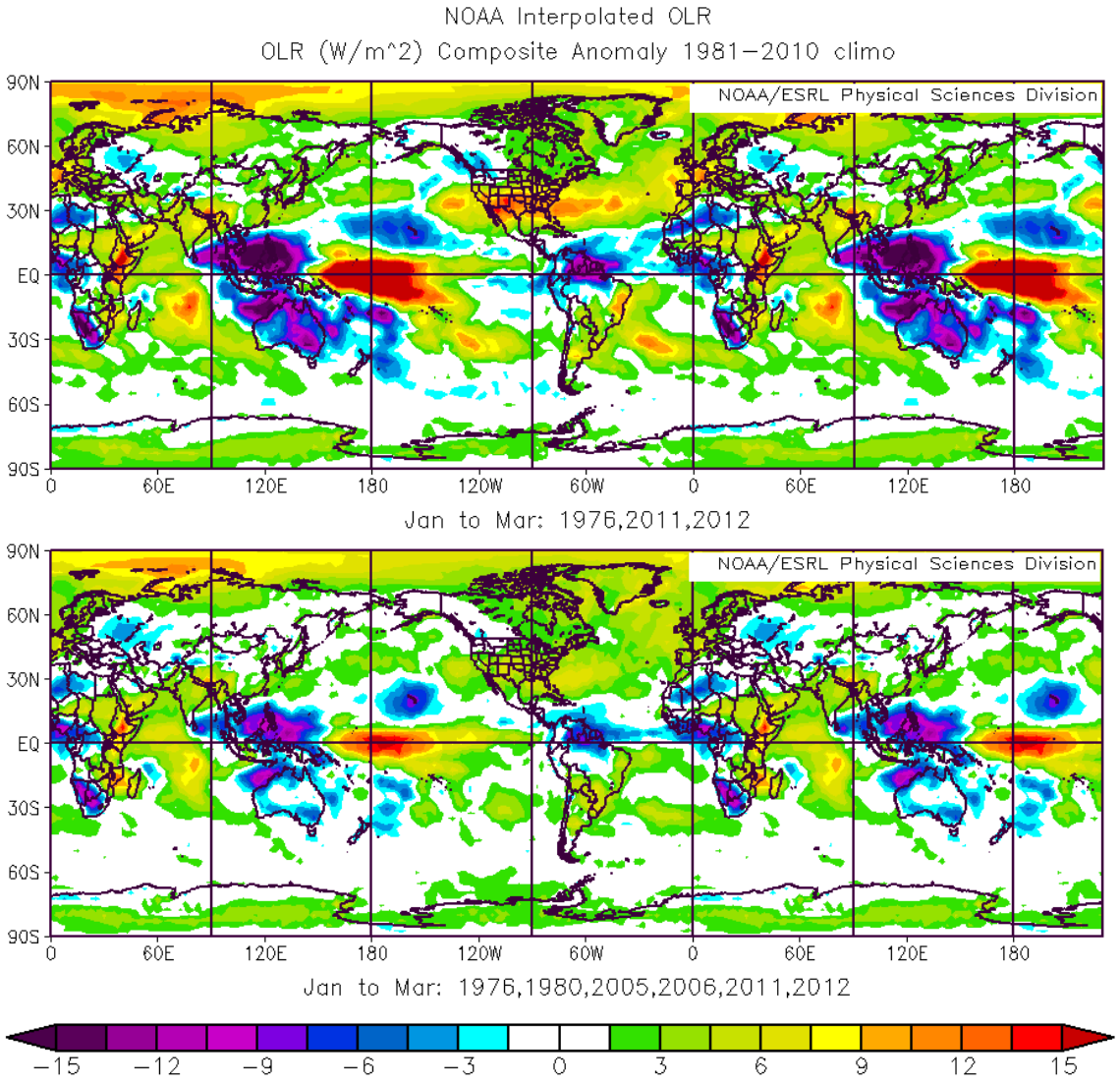

Figure 49. Anomalous JFM OLR for 1970–2014 for: (top panel) four of the eight warm years in which LN events occurred; (bottom panel) eight warmest years of our study period.

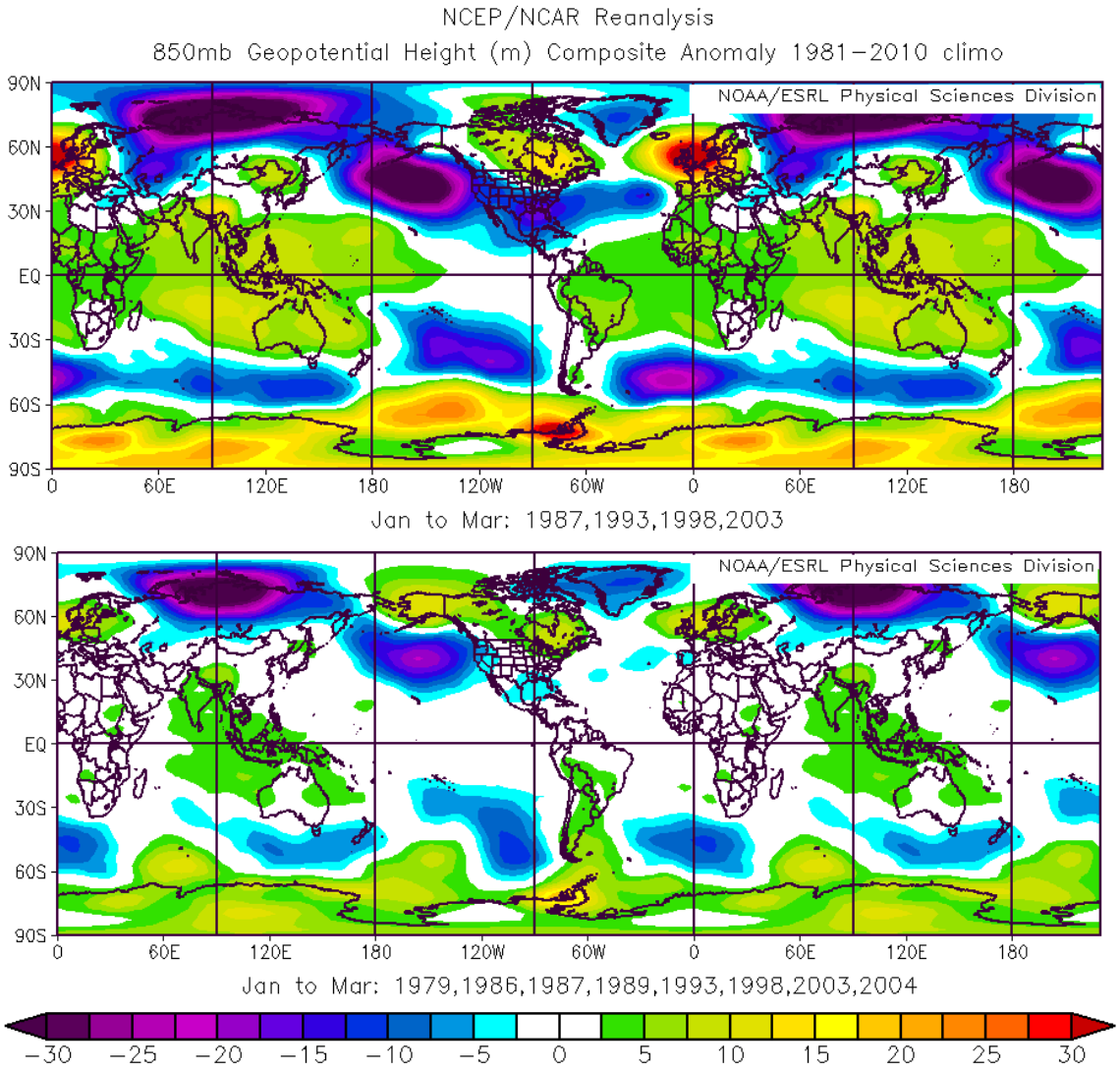

Figure 50. Anomalous JFM Z850 for 1970–2014 for: (top panel) four of the eight cold years in which EN events occurred; (bottom panel) eight coldest years of our study period.

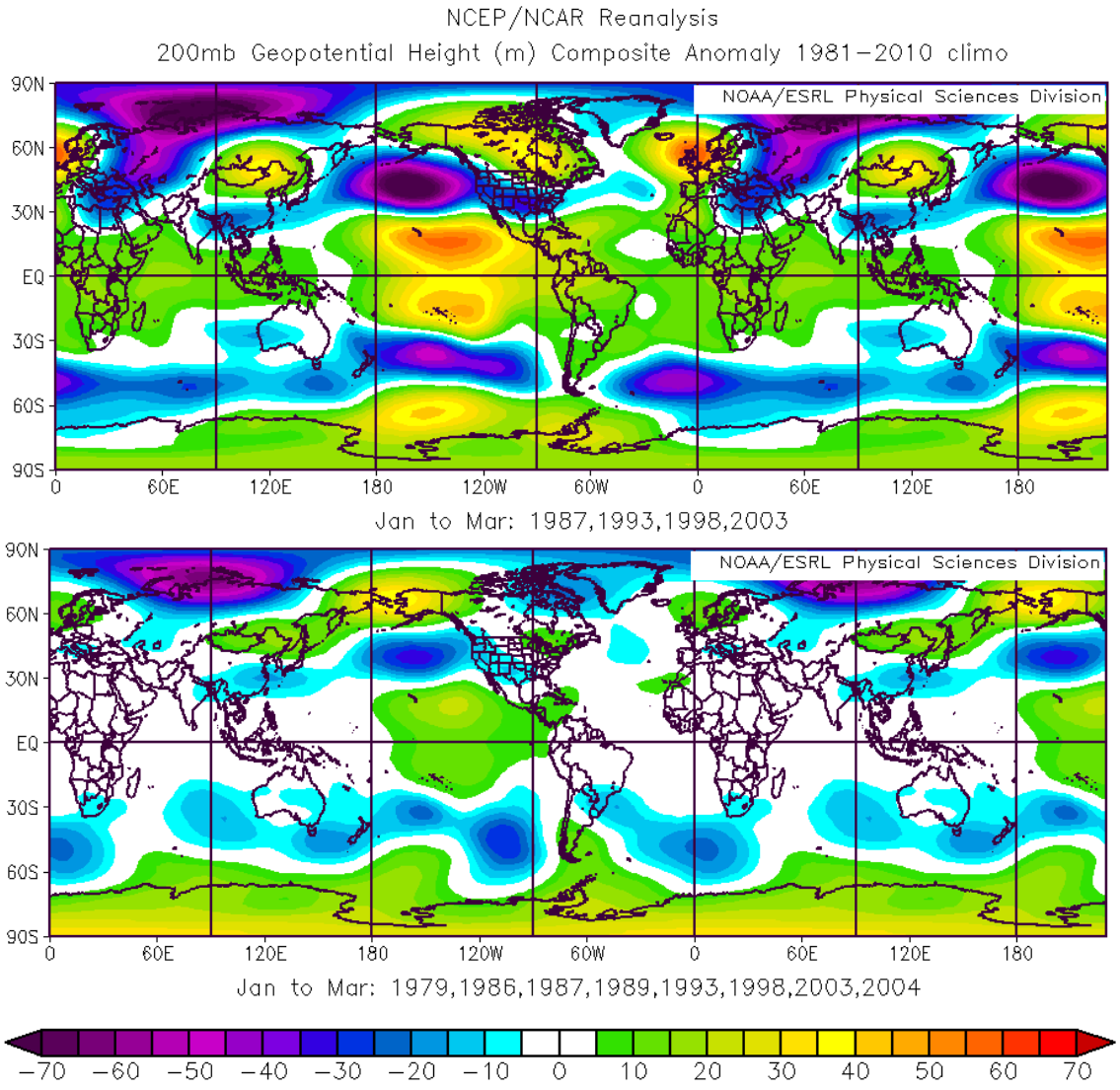

Figure 51. Anomalous JFM Z200 for 1970–2014 for: (top panel) four of the eight cold years in which EN events occurred; (bottom panel) eight coldest years of our study period.

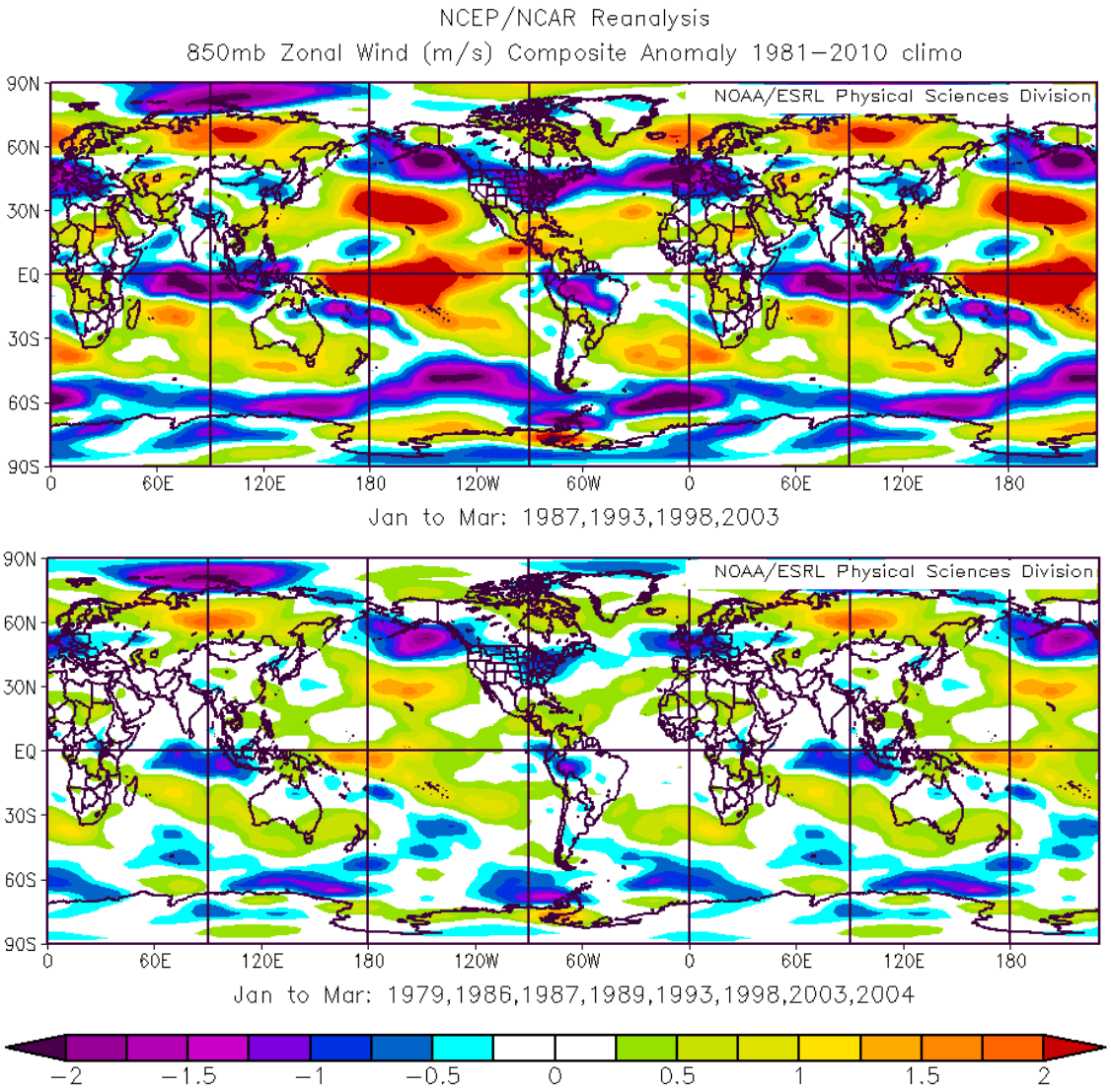

Figure 52. Anomalous JFM U850 for 1970–2014 for: (top panel) four of the eight cold years in which EN events occurred; (bottom panel) eight coldest years of our study period.

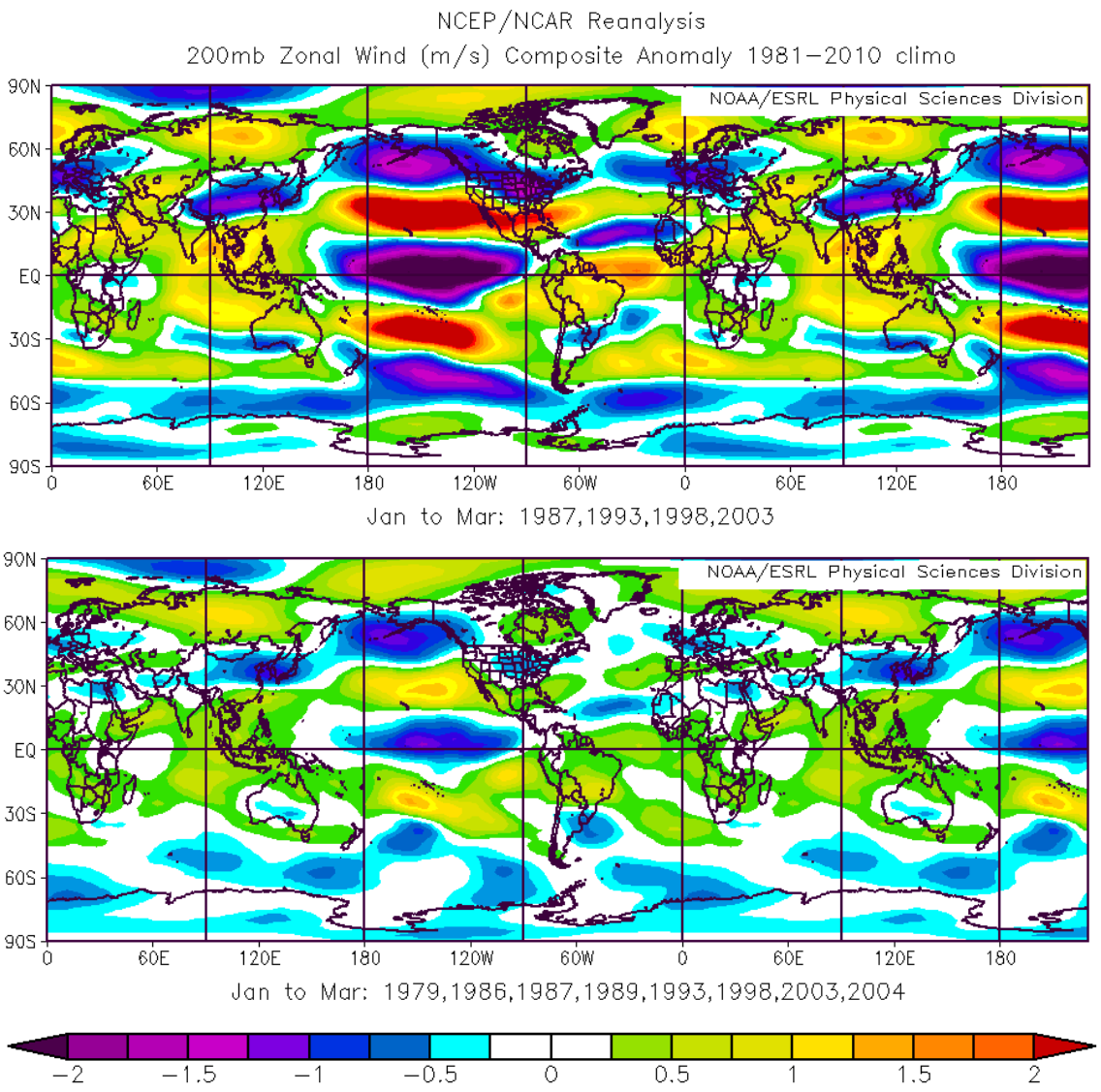

Figure 53. Anomalous JFM U200 for 1970–2014 for: (top panel) four of the eight cold years in which EN events occurred; (bottom panel) eight coldest years of our study period.

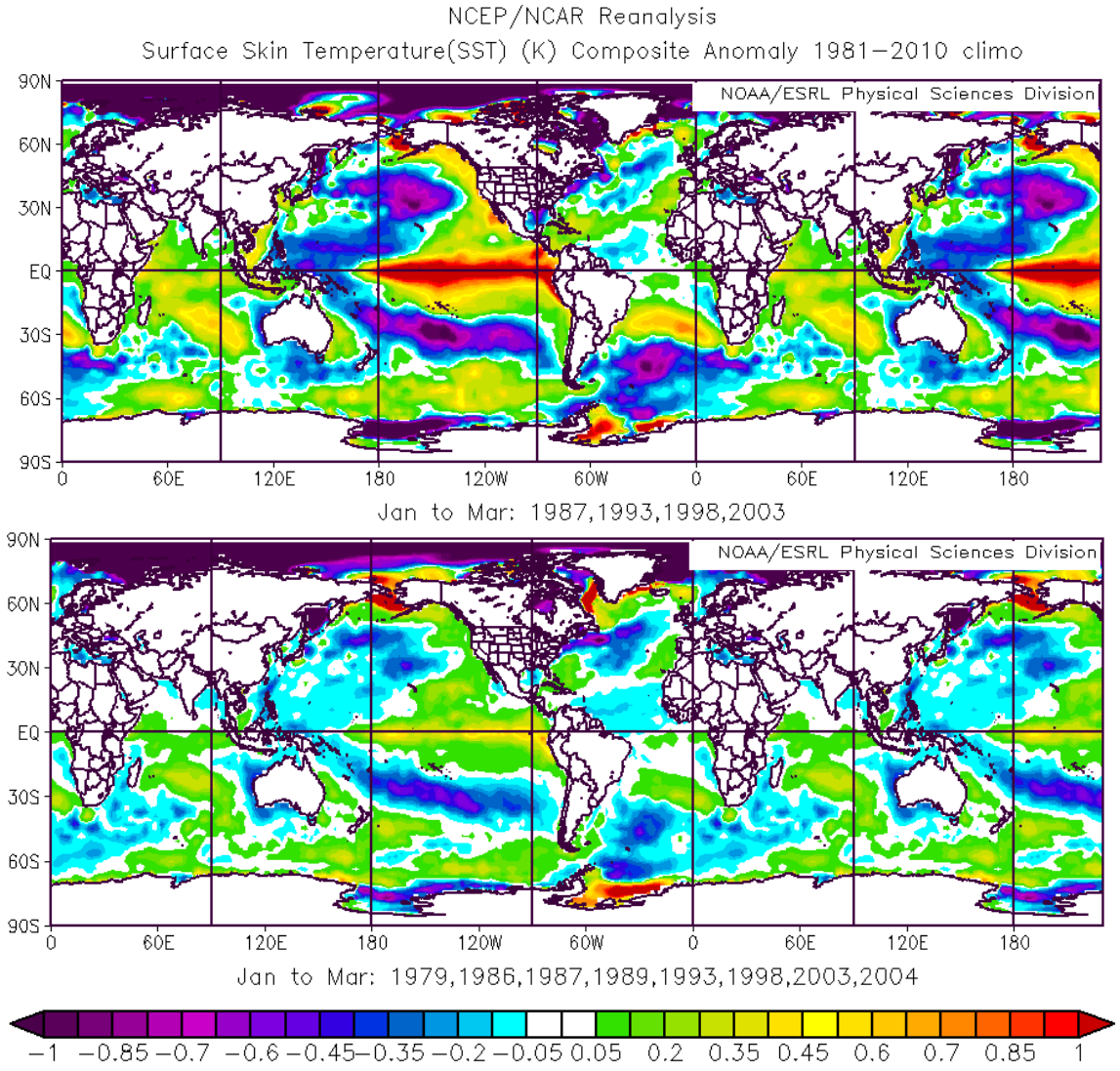

Figure 54. Anomalous JFM SST for 1970–2014 for: (top panel) four of the eight cold years in which EN events occurred; (bottom panel) eight coldest years of our study period.

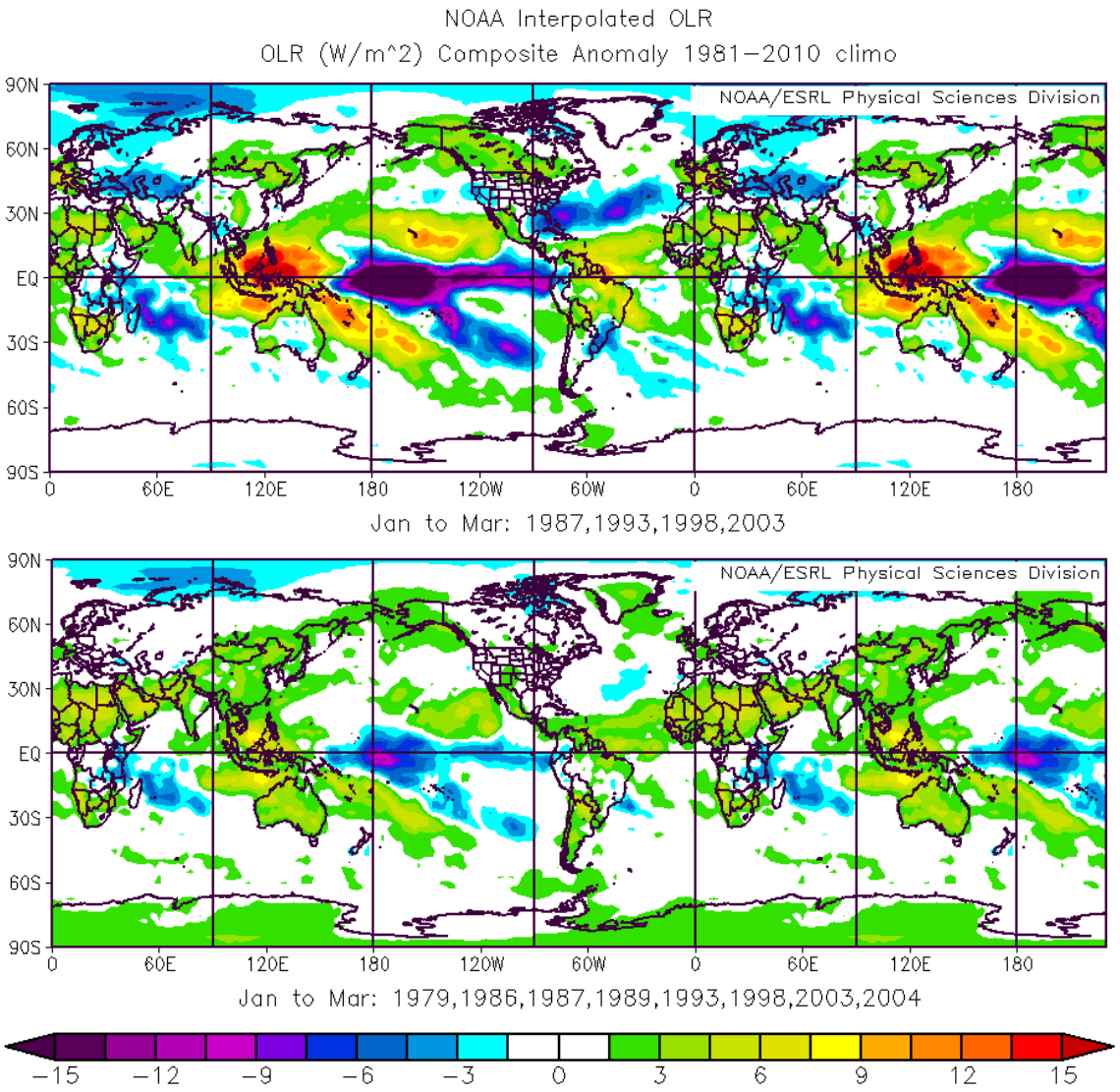

Figure 55. Anomalous JFM OLR for 1970–2014 for: (top panel) four of the eight cold years in which EN events occurred; (bottom panel) eight coldest years of our study period.

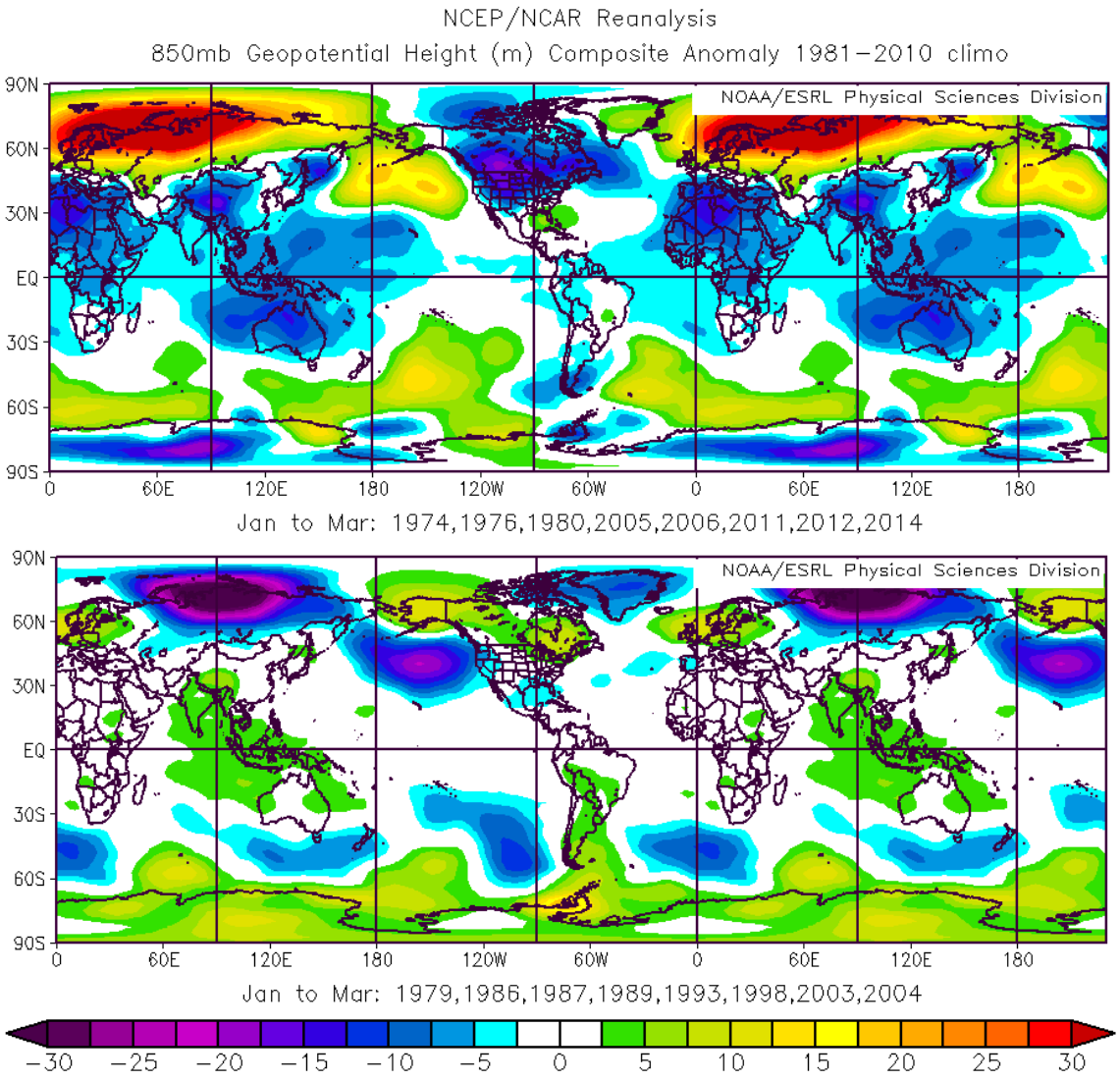

Figure 56. Comparison anomalous JFM Z850 for warm and cold years. The top panel shows the anomalies in Z850 that occurred during our eight warm years. The bottom panel shows the anomalies in Z850 that occurred during our eight cold years.

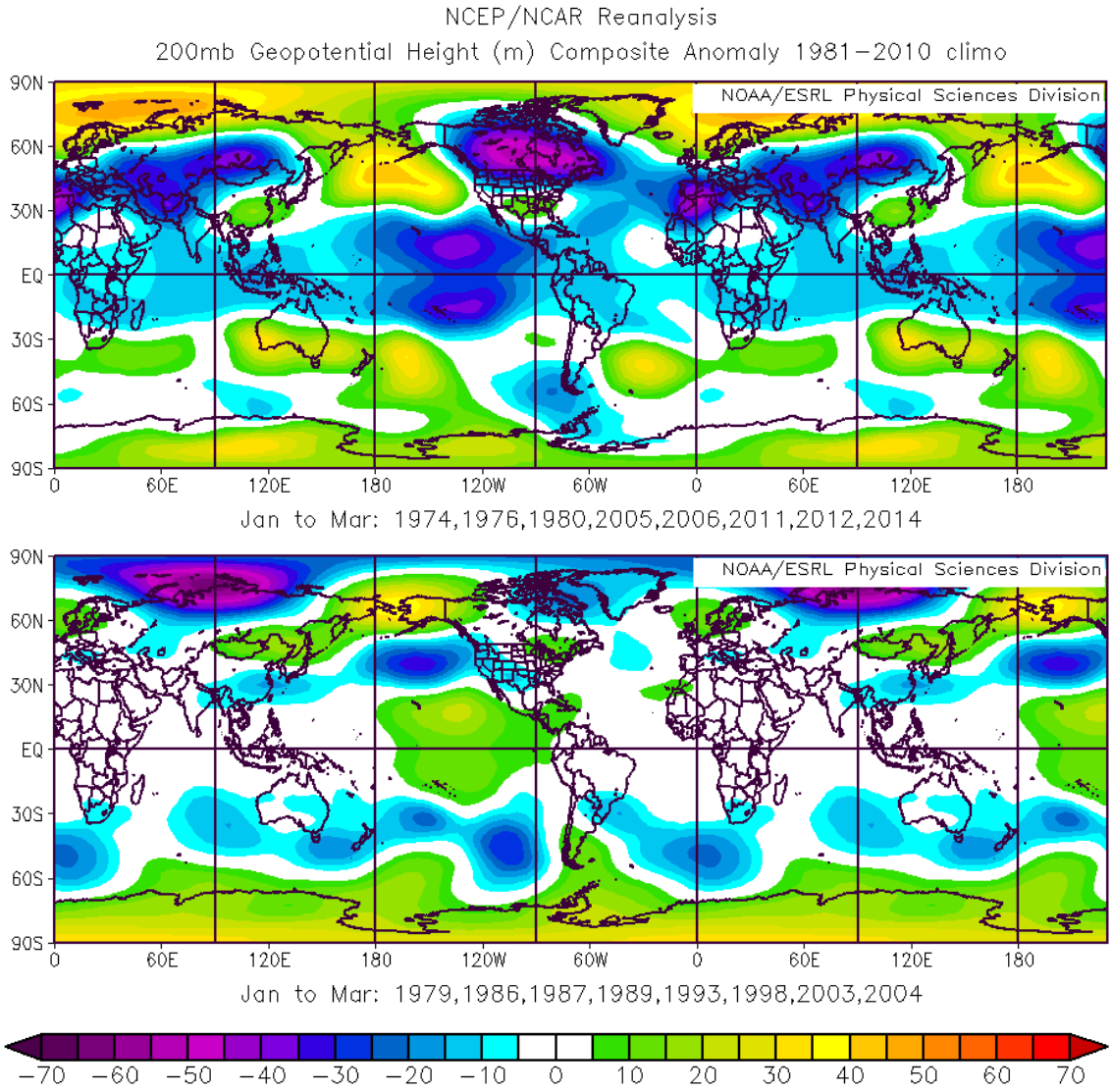

Figure 57. Comparison anomalous JFM Z200 for warm and cold years. The top panel shows the anomalies in Z200 that occurred during our eight warm years. The bottom panel shows the anomalies in Z200 that occurred during our eight cold years.

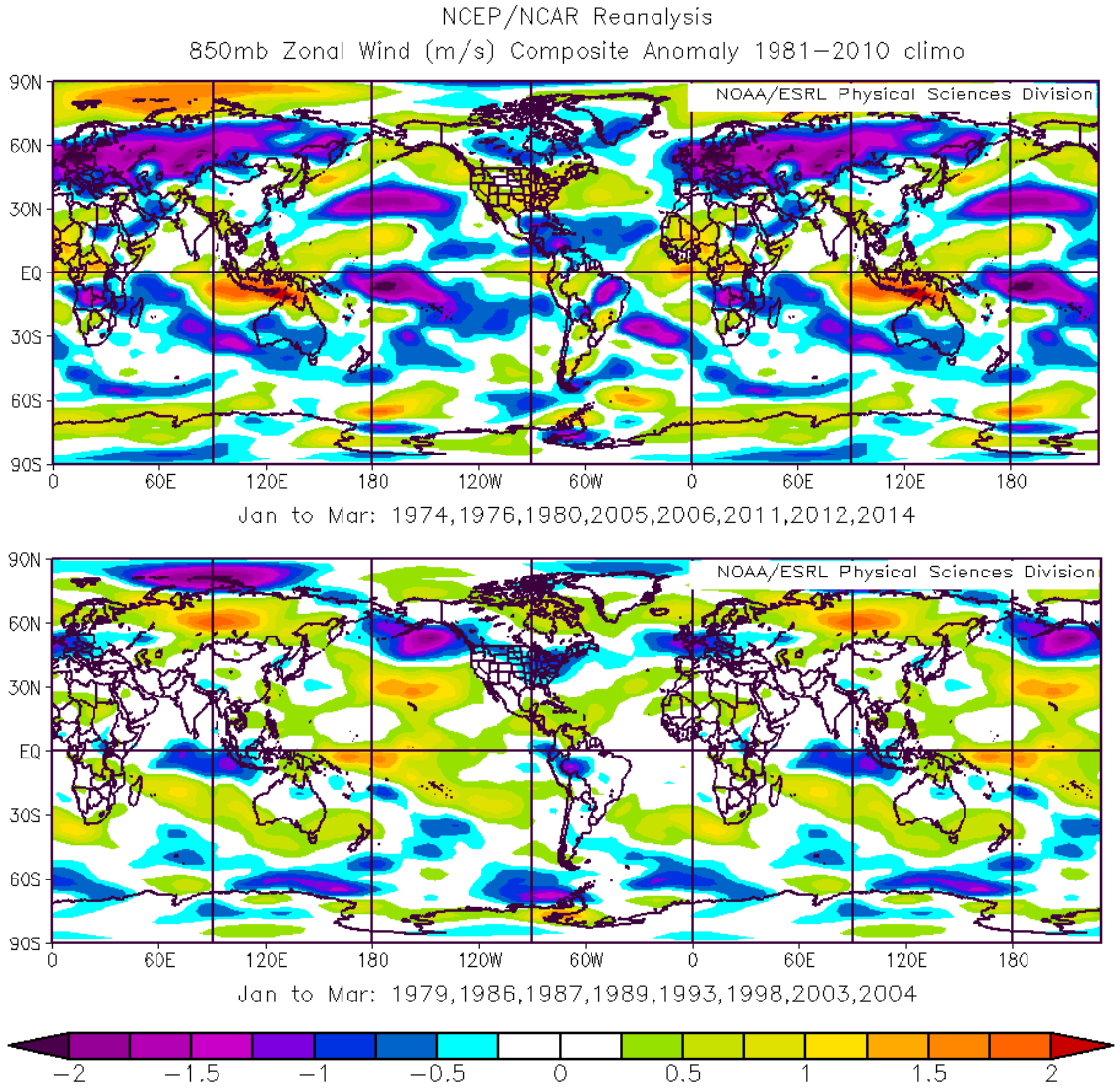

Figure 58. Comparison anomalous JFM U850 for warm and cold years. The top panel shows the anomalies in U850 that occurred during our eight warm years. The bottom panel shows the anomalies in U850 that occurred during our eight cold years.

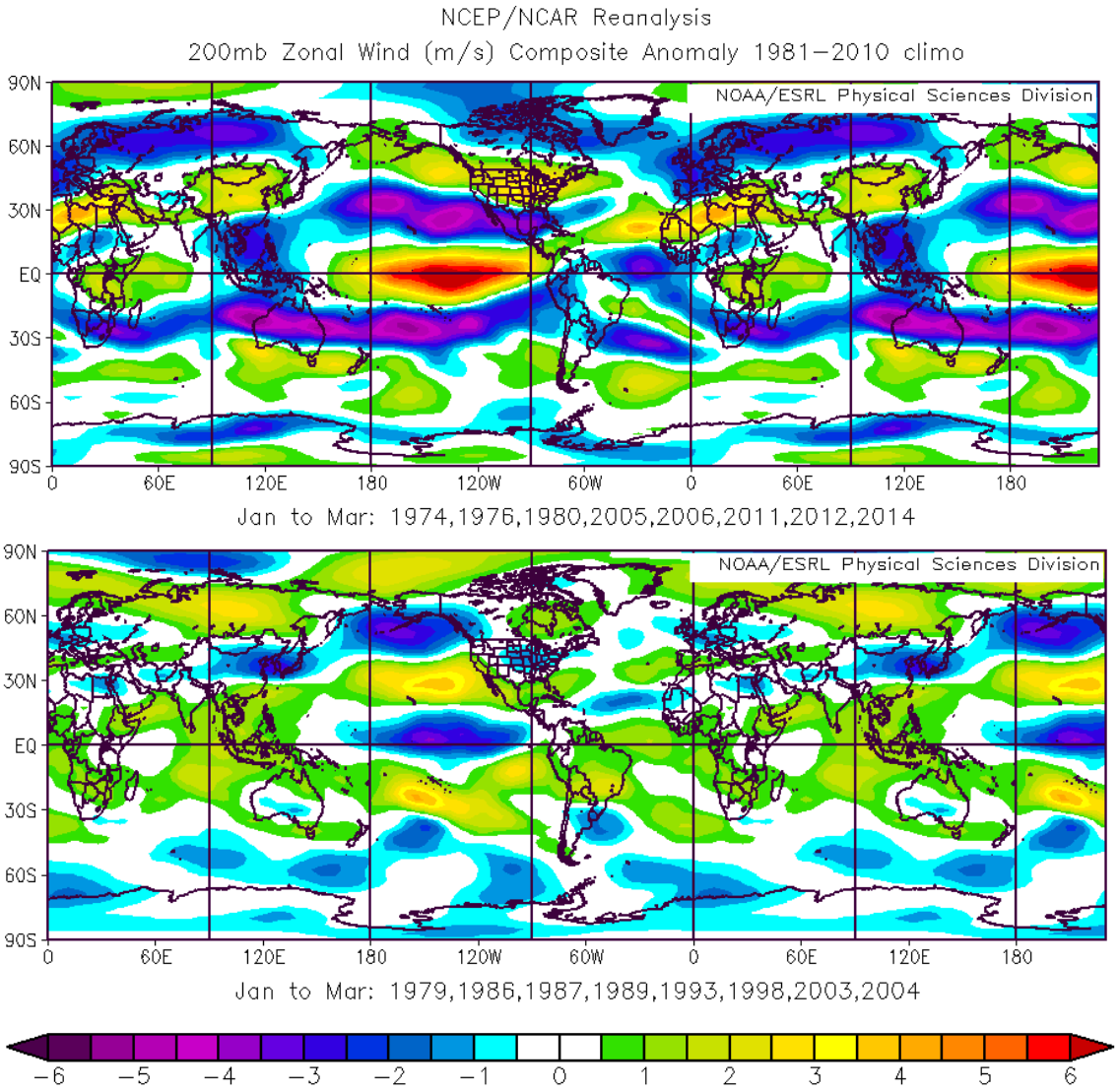

Figure 59. Comparison anomalous JFM U200 for warm and cold years. The top panel shows the anomalies in U200 that occurred during our eight warm years. The bottom panel shows the anomalies in U200 that occurred during our eight cold years.

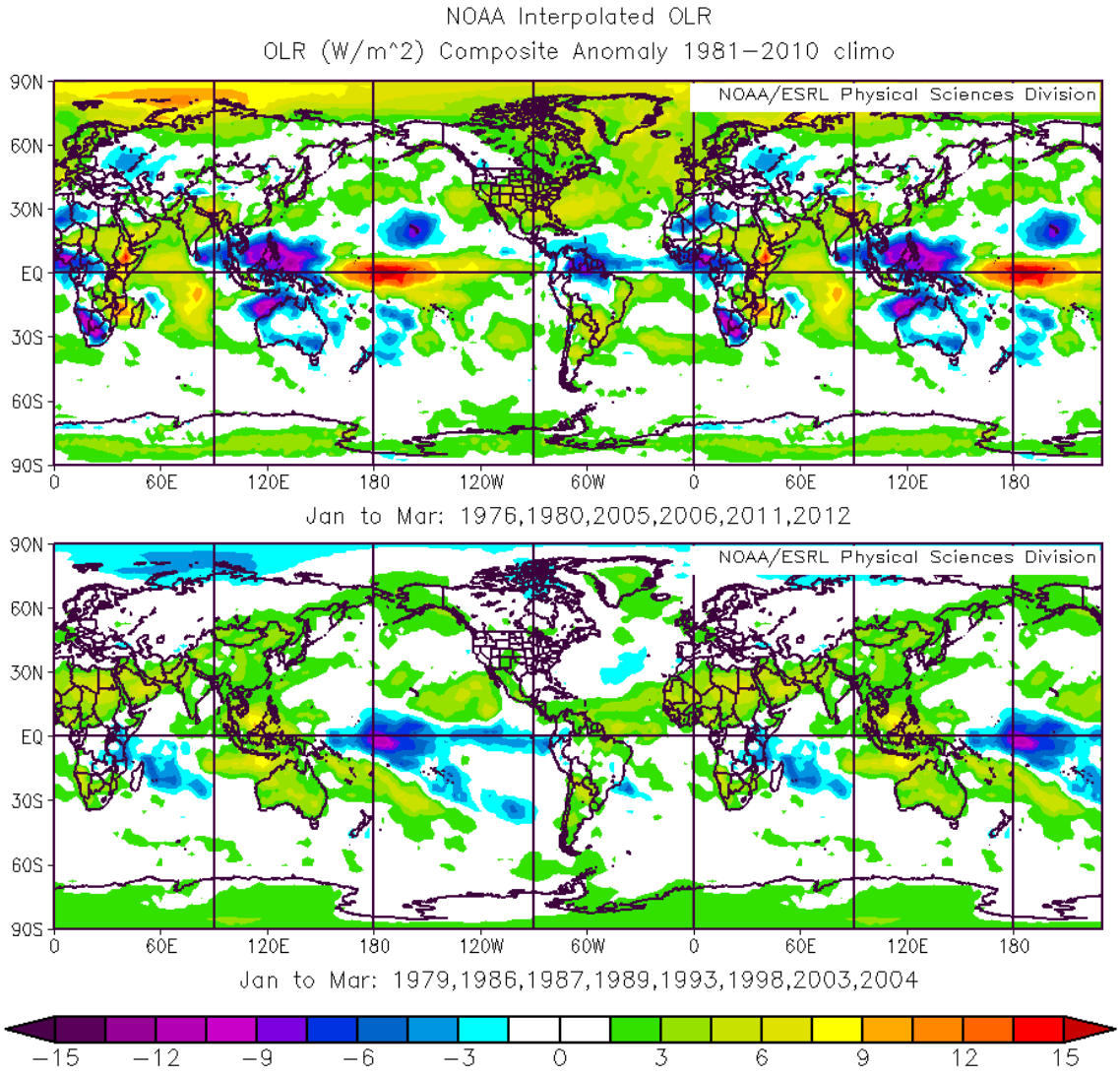

Figure 60. Comparison anomalous JFM OLR for warm and cold years. The top panel shows the anomalies in OLR that occurred during our eight warm years. The bottom panel shows the anomalies in OLR that occurred during our eight cold years.

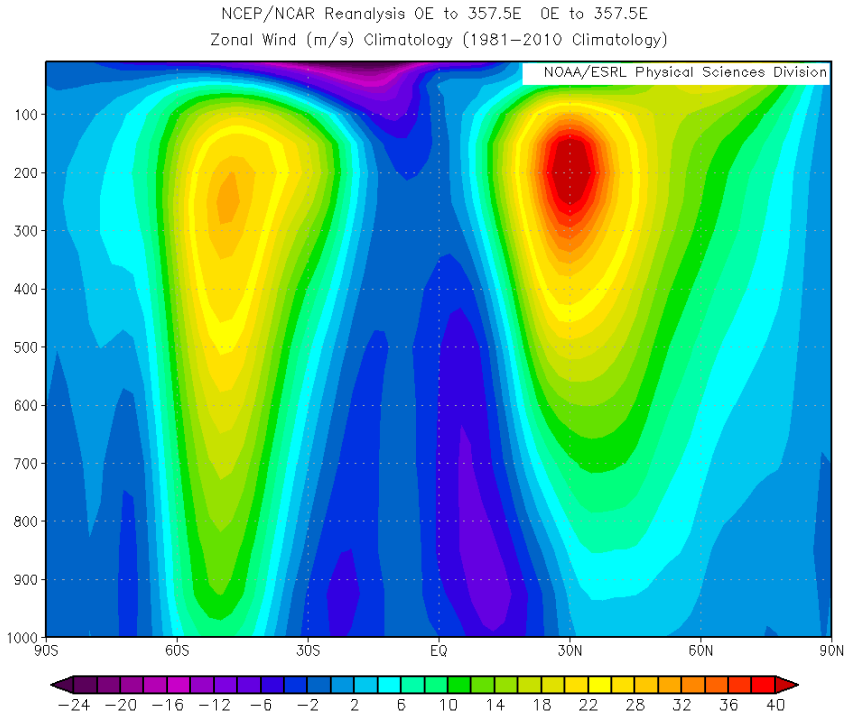

Figure 61. LTM of zonal wind from the surface to less than 100 hPa.

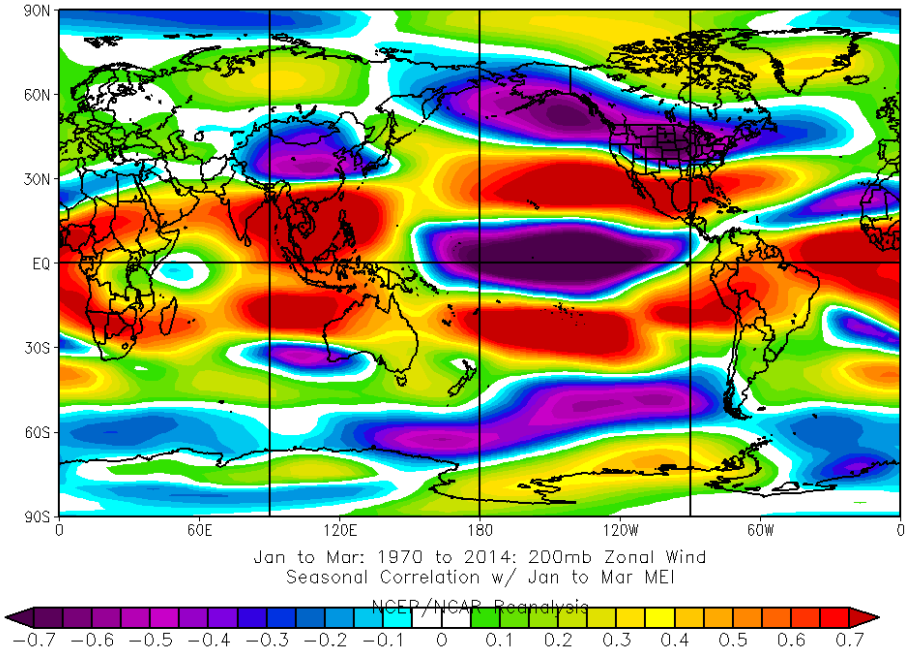

Figure 62. Zero lag correlation between U200 and the MEI.

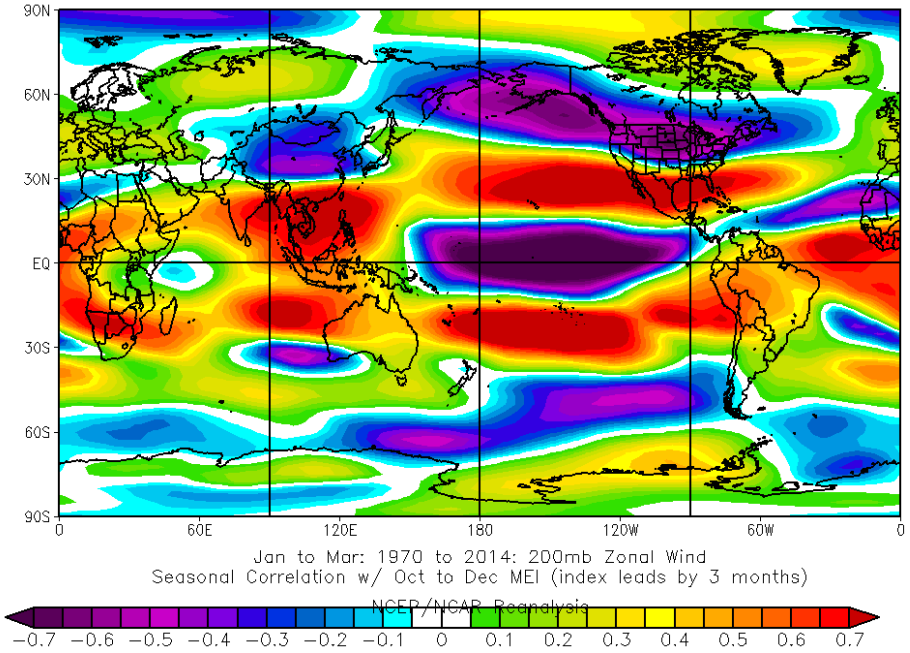

Figure 63. Correlation between U200 and MEI; MEI leads U200 by 3 months.

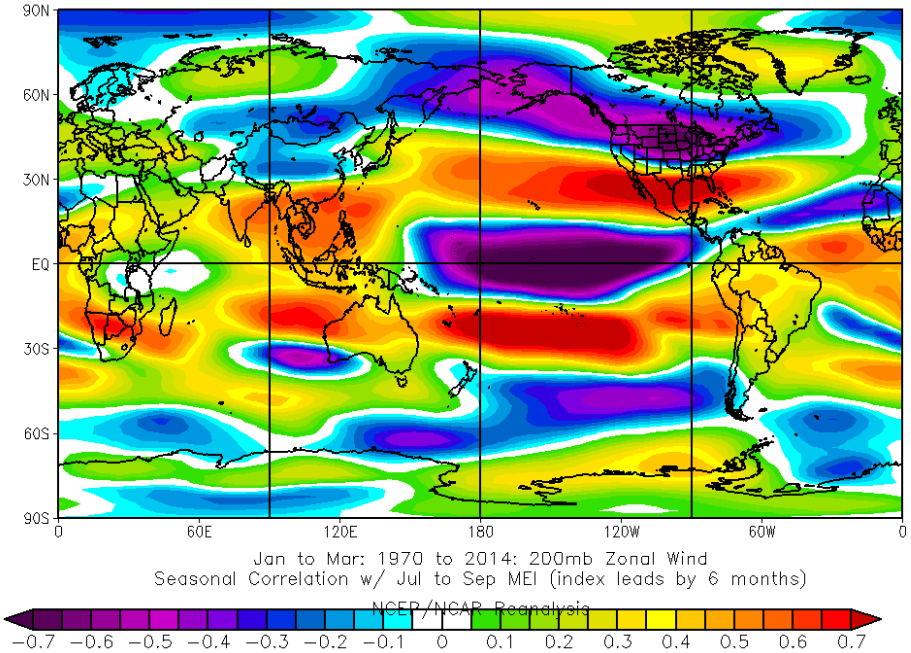

Figure 64. Correlation between U200 and MEI; MEI leads U200 by 6 months

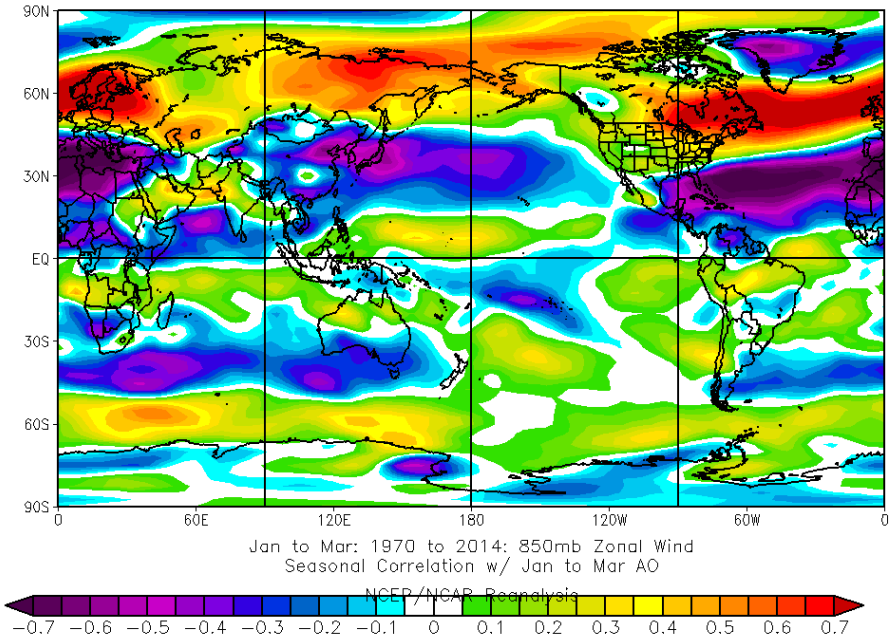

Figure 65. Zero lag correlation between U850 and the AO.

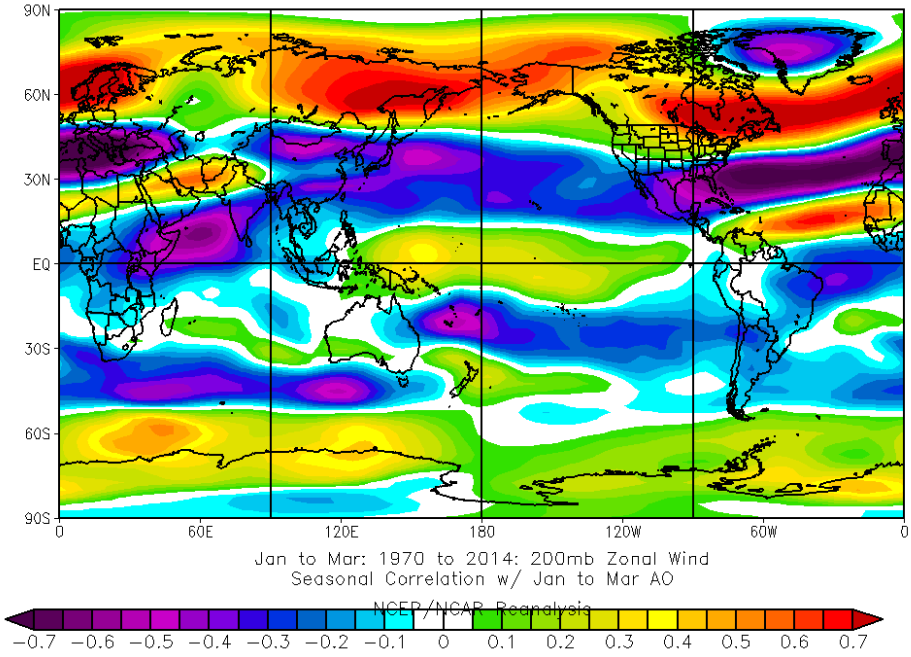

Figure 66. Zero lag correlation between U200 and the AO.

Table 7. Zero to six month lag correlations between AMJ Arctic T and the MEI. MEI leads AMJ Arctic T.

MEI Season	OND 1969-2013	NDJ 1969-70 to 2013-14	DJF 1969-70 to 2013-14	JFM 1970-2014	FMA 1970-2014	MAM 1970-2014	AMJ 1970-2014
Correlations with AMJ Arctic Temp (1970-2014)	+0.08 AMJ Arctic T lags MEI by 6 months	+0.07 AMJ Arctic T lags MEI by 5 months	+0.05 AMJ Arctic T lags MEI by 4 months	+0.03 AMJ Arctic T lags MEI by 3 months	-0.02 AMJ Arctic T lags MEI by 2 months	-0.06 AMJ Arctic T lags MEI by 1 month	-0.12 Zero lag Zero lead

Table 8. Zero lag correlations between Arctic T and the AO. Red indicates values at or above the .81 confidence level.

Seasons	OND	NDJ	DJF	JFM	FMA	MAM	AMJ
Correlations of Arctic T with AO (1970-2014)	-0.11 OND Arctic T with OND AO	-0.41 NDJ Arctic T with NDJ AO	-0.19 DJF Arctic T with DJF AO	-0.10 JFM Arctic T with JFM AO	+0.14 FMA Arctic T with FMA AO	-0.06 MAM Arctic T with MAM AO	-0.21 AMJ Arctic T with AMJ AO

Table 9. Zero to three-month lag, and zero to three-month lead correlations between JFM Arctic T and the AO. Red indicates values at or above the .81 confidence level.

AO Season	OND 1969-2013	NDJ 1969-70 to 2013-14	DJF 1969-70 to 2013-14	JFM 1970-2014	FMA 1970-2014	MAM 1970-2014	AMJ 1970-2014
Correlations with JFM Arctic Temp (1970-2014)	+0.09 JFM Arctic T lags AO by 3 months	-0.02 JFM Arctic T lags AO by 2 months	-0.07 JFM Arctic T lags AO by 1 month	-0.1 Zero lag Zero lead	+0.1 JFM Arctic T leads AO by 1 month	+0.13 JFM Arctic T leads AO by 2 months	+0.27 JFM Arctic T leads AO by 3 months

Table 10. Zero to ten month lag correlations between JFM Arctic T and the AO. AO leads JFM Arctic T. Red indicates values at or above the .81 confidence level.

AO Season	MAM 1969-2013	AMJ 1969-2013	MJJ 1969-2013	JJA 1969-2013	JAS 1969-2013	ASO 1969-2013
Correlations with JFM Arctic Temp (1970-2014)	-0.21 JFM Arctic T lags AO by 10 months	-0.07 JFM Arctic T lags AO by 9 months	-0.07 JFM Arctic T lags AO by 8 months	-0.02 JFM Arctic T lags AO by 7 months	+0.18 JFM Arctic T lags AO by 6 months	+0.07 JFM Arctic T lags AO by 5 months
AO Season	**SON 1969-2013**	**OND 1969-2013**	**NDJ 1969-70 to 2013-14**	**DJF 1969-70 to 2013-14**	**JFM 1970-2014**	
Correlations with JFM Arctic Temp (1970-2014)	+0.22 JFM Arctic T lags AO by 4 months	+0.09 JFM Arctic T lags AO by 3 months	-0.02 JFM Arctic T lags AO by 2 months	-0.07 JFM Arctic T lags AO by 1 month	-0.1 Zero lag Zero lead	

Table 11. Zero to eleven month lag correlations between JFM Arctic T and the AO. JFM Arctic T leads the AO. Red indicates values at or above the .81 confidence level.

AO Season	JFM 1970-2014	FMA 1970-2014	MAM 1970-2014	AMJ 1970-2014	MJJ 1970-2014	JJA 1970-2014
Correlations with JFM Arctic Temp (1970-2014)	-0.10 Zero lag Zero lead	+0.10 JFM Arctic T leads AO by 1 month	+0.13 JFM Arctic T leads AO by 2 2 months	+0.27 JFM Arctic T leads AO by 3 months	+0.02 JFM Arctic T leads AO by 4 months	-0.04 JFM Arctic T leads AO by 5 months
AO Season	**JAS 1970-2014**	**ASO 1970-2014**	**SON 1970-2014**	**OND 1970-2014**	**NDJ 1970-2014**	**DJF 1970-2014**
Correlations with JFM Arctic Temp (1970-2014)	-0.04 JFM Arctic T leads AO by 6 months	-0.16 JFM Arctic T leads AO by 7 months	-0.19 JFM Arctic T leads AO by 8 months	-0.17 JFM Arctic T leads AO by 9 months	-0.02 JFM Arctic T leads AO by 10 months	-0.07 JFM Arctic T leads AO by 11 months

Table 12. Zero to three-month lag, and zero to three-month lead correlations between OND Arctic T and the AO. Red indicates values at or above the .81 confidence level.

AO Season	OND 1969-2013	NDJ 1969-70 to 2013-14	DJF 1969-70 to 2013-14	JFM 1970-2014	FMA 1970-2014	MAM 1970-2014	AMJ 1970-2014
Correlations with OND Arctic Temp (1969-2013)	-0.39 Zero lag Zero lead	-0.43 OND Arctic T leads AO by 1 month	-0.4 OND Arctic T leads AO by 2 months	-0.23 OND Arctic T leads AO by 3 months	-0.12 OND Arctic T leads AO by 4 months	+0.03 OND Arctic T leads AO by 5 months	+0.04 OND Arctic T leads AO by 6 months

LIST OF REFERENCES

Aguado, E., and Burt J.E., 2004: *Understanding Weather and Climate,* Pearson Education, Inc., 560pp.

American Meteorological Society, cited 2015: Polar vortex. Glossary of Meteorology. [Available online at http://glossary.ametsoc.org/wiki/Polar_vortex.]

DeHart, J.A., 2011: Long-range Forecasting in Support of Operations in Pakistan. M.S. thesis, Dept. of Meteorology, Naval Postgraduate School, 107pp.

Department of Defense, 2013: Arctic Strategy. November 2013, 14pp. [Available online at http://www.defense.gov/pubs/2013_Arctic_Strategy.pdf.]

Earth Systems Research Laboratory, Physical Science Division, 2015a: *El Nino/Southern Oscillation (ENSO).* [Available online at http://www.esrl.noaa.gov/psd/enso/.]

Earth Systems Research Laboratory, Physical Science Division, 2015b: *Create a monthly or seasonal time series of climate variables.* [Available online at http://www.esrl.noaa.gov/psd/data/timeseries/.]

Earth Systems Research Laboratory, Physical Science Division, 2015c: *Monthly/Seasonal Climate Composites.* [Available online at http://www.esrl.noaa.gov/psd/cgi-bin/data/composites/printpage.pl.]

Earth Systems Research Laboratory, Physical Science Division, 2015d: *Linear Correlations in Atmospheric Seasonal/Monthly Averages.* [Available online at http://www.esrl.noaa.gov/psd/data/correlation/.]

Earth Systems Research Laboratory, Physical Science Division, 2015e: *Significance of Correlations.* [Available online at http://www.esrl.noaa.gov/psd/data/correlation/significance.html.]

Francis, J.A. and S.J. Vavrus, 2012: Evidence linking Arctic amplification to extreme weather in mid-latitudes, *Geophys. Res. Lett.,* **39,** L06801, doi:10.1029/2012GL051000.

Francis, J.A**.,** 2013: Rapid Arctic warming and wacky weather: Are they linked? *Amer. Assoc. for Women in Science Magazine*, **44,** Winter 2013.

Hoskins, B.J., and D.J. Karoly, 1981: The steady linear response of a spherical atmosphere to thermal and orographic forcing. *J. Atmos. Sci.,* **38,** 1179-1196.

Kalnay, E., and Coauthors, 1996: The NCEP/NCAR 40-year reanalysis project, *Bull. Amer. Meteor. Soc*, **77,** 437–471.

Kistler, R., and Coauthors, 2001: The NCEP–NCAR 50-Year Reanalysis: Monthly means CD-ROM and documentation. *Bull. Amer. Meteor. Soc.,* **82,** 247–268.

Lee, S., S.B. Feldstein, D. Pollard, and T.S. White, 2011a: Do planetary wave dynamics contribute to equable climates? *J. Climate,* **24,** 2391–2404.

Lee, S., T. Gong, N. Johnson, S.B. Feldstein, and D. Pollard, 2011b: on the possible link between tropical convection and the Northern Hemisphere Arctic surface air temperature change between 1958 and 2001. *J. Climate,* **24,** 3450–4367.

Lee, S., 2012: Testing of the tropically excited Arctic warming mechanisms (TEAM) with traditional El Niño and La Niña. *J. Climate,* **25,** 4015–4022.

L'Heureux, M.L., and R.W. Higgins, 2007: Boreal winter links between the Madden-Julian Oscillation and the Arctic Oscillation. *J. Climate,* **21,** 3040–3050.

L'Heureux, M.L., A. Kumar, G. D. Bell, M. S. Halpert, and R. W. Higgins, 2008: Role of the Pacific-North American (PNA) pattern in the 2007 Arctic sea ice decline. *Geophys. Res. Lett.,* **35,** L20701, doi:10.1029/2008GL035205.

L'Heureux, M.L., and D.W.J. Thompson, 2005: Observed relationships between the El Nino-Southern Oscillation and the extratropical zonal-mean climate. *J. Climate,* **19,** 276–287.

Murphree, T., 2012a: MR3610 Course Module 7: *Seasonal Cycles, Part 1*. Dept. of Meteorology, Naval Postgraduate School, Monterey, California.

Murphree, T., 2012b: MR3610 Course Module 16: *El Niño, La Niña, and the Southern Oscillation, Part1*. Dept. of Meteorology, Naval Postgraduate School, Monterey, California.

Murphree, T., 2012c: MR3610 Course Module 9: *Seasonal Cycles, Part 3*. Dept. of Meteorology, Naval Postgraduate School, Monterey, California.

Murphree, T., 2014a: MR3610 Course Module 6: *Introduction to Advanced Climate Support for National Security*. Dept. of Meteorology, Naval Postgraduate School, Monterey, California.

Murphree, T., 2014b: MR3610 Course Module 8: *Seasonal Cycles, Part 2*. Dept. of Meteorology, Naval Postgraduate School, Monterey, California.

Murphree, T., 2014c: MR3610 Course Module 17: *El Niño, La Niña, and the Southern Oscillation, Part2*. Dept. of Meteorology, Naval Postgraduate School, Monterey, California.

National Research Council, 2014: *The Arctic in the Anthropocene: Emerging Research Question: A study by the Committee on Emerging Research Questions in the Arctic, Polar Research Board, Division on Earth and Life Studies,* The National Academies Press, 220pp.

The National Weather Service (NWS) Climate Prediction Center (CPC), 2015: Arctic Oscillation (AO). [Available online at http://www.cpc.ncep.noaa.gov/products/precip/CWlink/daily_ao_index/ao.shtml#publication.]

Quadrelli, R., and J.M. Wallace, 2002: Dependence of the structure of the Northern Hemisphere annular mode on the polarity of ENSO. *Geophys. Res. Lett.,* **29,** NO. 23, 2132, doi:10.1029/2002GL015807.

Serreze, M.C., and Coauthors, 2000: Observational evidence of recent change in the northern high-latitude environment. *Climate Change,* **46,** 159–207.

Slingo, J., and R. Sutton, 2007: Sea-ice decline due to more than warming alone, *Nature,* **450,** 27.

Stepanek, A.J., 2006: North Pacific-North American Circulation and Precipitation Anomalies Associated with the Madden-Julian Oscillation. M.S. thesis, Dept. of Meteorology, Naval Postgraduate School, 143pp.

Stone, M.M., 2010: Long-range Forecasting of Arctic Sea Ice. M.S. thesis, Dept. of Meteorology, Naval Postgraduate School, 117pp.

Tang, Q., X. Zhang, X. Yang, and J.A. Francis, 2013: Cold winter extremes in northern continents linked to Arctic sea ice loss. *Environ. Res. Lett.,* **8,** doi:10/1088/1748-9326/8/1/014036.

Thompson, D. W. J, and J. M. Wallace, 1998: The Arctic Oscillation signature in the wintertime geopotential height and temperature fields. *Geophys. Res. Lett.,* **25,** 1297–1300.

Titley, RADM J., 2012: Assured Access to the Maritime Battlespace: Warfighting Requirements. 2012 Naval Science and Technology Partnership Conference, presentation. [Available online at http://www.onr.navy.mil/conference-event-onr/science-technology-partnership/~/media/Files/Conferences/Science-Technology-Partnership/2012/Oct22/RADM-White-Oct22.ashx.]

United States Navy, 2014: U.S. Navy Arctic Roadmap, Washington D.C., U.S. Department of the Navy Task Force Climate Change (TFCC), February 2014, 43pp.

The White House. “The National Strategy for the Arctic Region.” May 10, 2013. [Available online at https://www.whitehouse.gov/sites/default/files/docs/nat_arctic_strategy.pdf.]

Wilks, D., 2006: *Statistical Methods in the Atmospheric Science*, Academic Press, 627pp.

Wolter, K., and M.S. Timlin, 1993: Monitoring ENSO in COADS with a seasonally adjusted principal component index. *Proc. of the 17th Climate Diagnostics Workshop,* Norman, OK, NOAA/NMC/CAC, NSSL, Oklahoma Clim. Survey, CIMMS and the School of Meteor., Univ. of Oklahoma, 52–57.

Wolter, K., and M.S. Timlin, 1998: Measuring the strength of ENSO events—how does 1997/98 rank? *Weather,* **53,** 315–324.

Wolter, K., and M.S. Timlin, 2011: El Niño/Southern Oscillation behavior since 1871 as diagnosed in an extended multivariate ENSO index (MEI.ext). *Intl. J. Climatology,* **31,** 14pp.

Yoo, C., S. Feldstein, and S. Lee, 2011: Impact of the Madden–Julian Oscillation trend on the Arctic amplification of surface air temperature during the 1979-2008 boreal winter. *Geophys. Res. Lett.,* **38,** L24804, doi:10.1029/2011GL049881.

INITIAL DISTRIBUTION LIST

1. Defense Technical Information Center
   Ft. Belvoir, Virginia

2. Dudley Knox Library
   Naval Postgraduate School
   Monterey, California